UNIVERSITÀ DEGLI STUDI DI ROMA "LA SAPIENZA"

FACOLTÀ DI INGEGNERIA

CORSO DI LAUREA IN INGEGNERIA DELLE TELECOMUNICAZIONI

ANNO ACCADEMICO 2007/2008

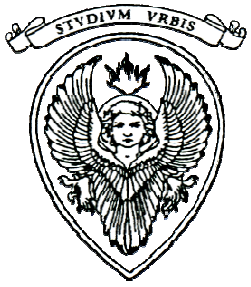

LA SAPIENZA

OVERVIEW OF THE CASSINI PROCESSING ALTIMETRIC DATA SYSTEM

Relatore

Prof. Roberto Seu

Laureando

Oriol Martín Isanda

"better results are always achieved through teamwork"

GENERAL INDEX

1) INTRODUCTION TO THE CASSINI-HUYGENS INTERPLANETARY MISSION TO TITAN

Although the *Cassini-Huygens* interplanetary mission is a project that covers Saturn, its rings and most of its multiple satellites, in this introduction attention will be focused mainly in the biggest moon of Saturn: Titan, since *Cassini* Radar, from which *Cassini* Processing Altimetric Data (PAD) system (on which is based this work) receives science data, has been built especially to study Titan.

1.1) Titan

Saturn, being the second outer planet of the solar system has a large number of satellites. The largest saturnine satellites known before the start of space research were: Mimas, Encélado, Tethys, Dione, Rea, Titan, Hyperion, Jápeto and Febe.

Titan is the largest of them and the second largest satellite in the whole Solar System, after Jupiter's moon Ganymede. It was discovered on March 25, 1655 by Dutch astronomer Christiaan Huygens, and was the first satellite in the Solar System to be discovered after Jupiter's Galilean moons. Titan has a 5.150 km diameter, and is larger than planets Mercury (although only half as massive) and Pluto. It orbits Saturn at a distance of 1,222,000 km and it takes 15.9 days to complete an entire revolution.

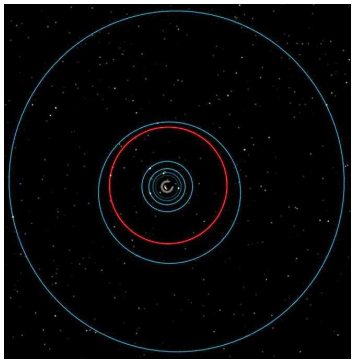

Image 1. Titan's orbit (highlighted in red) among the other large inner moons of Saturn.

Moreover Titan is the only moon in the solar system that has a significant atmosphere. The presence of this atmosphere was proposed by the Catalan astronomer Jose Comas and Solá in 1908 based on his observations of Titan's darkening towards the edge of its disc. Before the arrival of *Voyager 1* in 1980, Titan was thought to be slightly larger than Ganymede (diameter 5,262 km) and thus the largest moon in the Solar System; this was an overestimation caused by Titan's dense, opaque atmosphere which extends many miles above its surface and increases its apparent diameter.

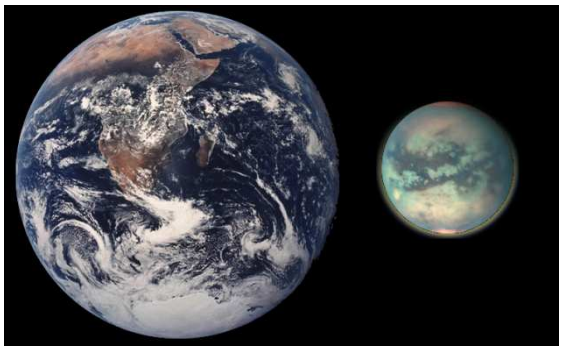

Image 2. Titan compared to Earth

The atmosphere of Titan dense, orange, and rich in methane and other hydrocarbons (1.6%), is other than that of Earth, the only which is mainly composed of nitrogen (98.4%). It is opaque at many wavelengths and a complete reflectance spectrum of the surface is impossible to acquire from the outside and that made that

before the *Cassini* mission, information and maps from Titan's surface were inaccurate. Its chemical composition seems to be very similar to the primitive atmosphere of the Earth in prebiotic times. Temperatures of about 90K should have preserved a very similar environment to that of the primitive Earth although at a much lower temperature. The atmosphere of Titan is denser than that of the Earth, with a surface pressure about one and a half times higher than that of our planet and with an opaque cloud layer formed by hydrocarbon aerosols that hide the features of Titan's surface.

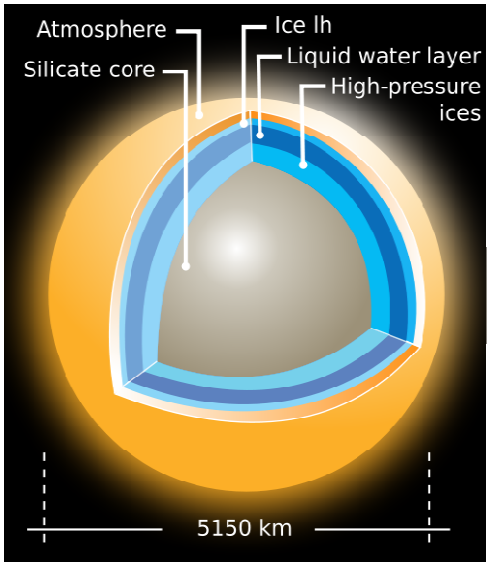

Image 3. Titan's internal structure

Titan is primarily composed of water ice and rocky material and is probably differentiated into several layers with a 3,400 km rocky center surrounded by several layers composed of different crystal forms of ice. Its interior may still be hot and there may be a liquid layer consisting of water and ammonia between the ice crust and deeper ice layers made of high-pressure forms of ice. Evidence for such an ocean has recently been uncovered by the *Cassini* probe in the form of natural extremely low frequency (ELF) radio waves in Titan's atmosphere. Titan's surface is thought to be a poor reflector of ELF waves, so they may instead be reflecting off the liquid-ice boundary of a subsurface ocean.

The surface is geologically young; although mountains and several possible cryovolcanoes have been discovered. Through images obtained with the Hubble Space Telescope a strange region, unofficially named Xanadu was discovered in 1994, with an area about the size of Australia, there are other dark areas of similar size elsewhere on the moon and it had been speculated that these are methane or ethane seas. The *Cassini* mission affirmed the former hypothesis: at Titan's south pole, an enigmatic dark feature named Ontario Lacus was the first suspected lake identified. Following a flyby on July 22, 2006, in which the *Cassini* spacecraft's radar imaged the northern latitudes, a number of large, smooth (and thus dark to radar) patches were seen dotting the surface near the pole. Based on the observations, scientists announced "definitive evidence of lakes filled with methane on Saturn's moon Titan" in January 2007.

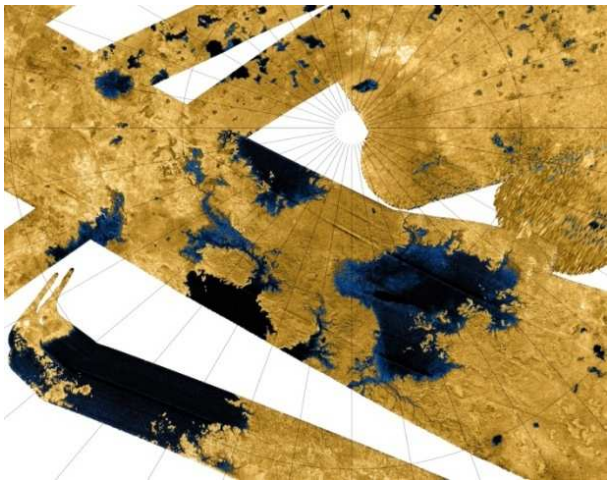

Image 4. False-color Cassini synthetic-aperture radar mosaic of Titan's north polar region, showing evidence for hydrocarbon seas, lakes and tributary networks.

In Titan, methane plays the role of water on Earth; it produces clouds in its atmosphere that, when they condense on the aerosols, produce a methane rain with particles that fill the streams with a dark flowing material. Therefore rain, along with wind, creates surface features that are similar to those on Earth, such as sand dunes, shorelines, seas, lakes and rivers and, like Earth, is dominated by seasonal weather. Thus Titan is the only known object other than Earth in the Solar System where it rains on the surface and for which clear evidence of stable bodies of surface liquid has been found.

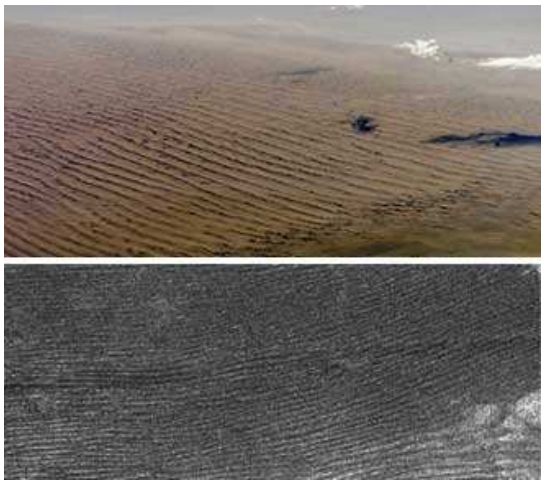

Image 5. Sand dunes on Earth (top), compared with dunes on Titan's surface.

Titan's surface temperature is about 94 K (−179 °C, or −290 °F). At this temperature water ice does not sublimate from solid to gas, so the atmosphere is nearly free of water vapor. The haze in Titan's atmosphere contributes to the moon's anti-greenhouse effect by reflecting sunlight away from the satellite, making its surface significantly colder than its upper atmosphere.

The clouds on Titan, composed of methane, ethane or other simple organics, are scattered and variable, punctuating the overall haze. This atmospheric methane conversely creates a greenhouse effect on Titan's surface, without which Titan would be far colder. The findings of the *Huygens* probe indicate that Titan's atmosphere periodically rains liquid methane and other organic compounds onto the moon's surface.

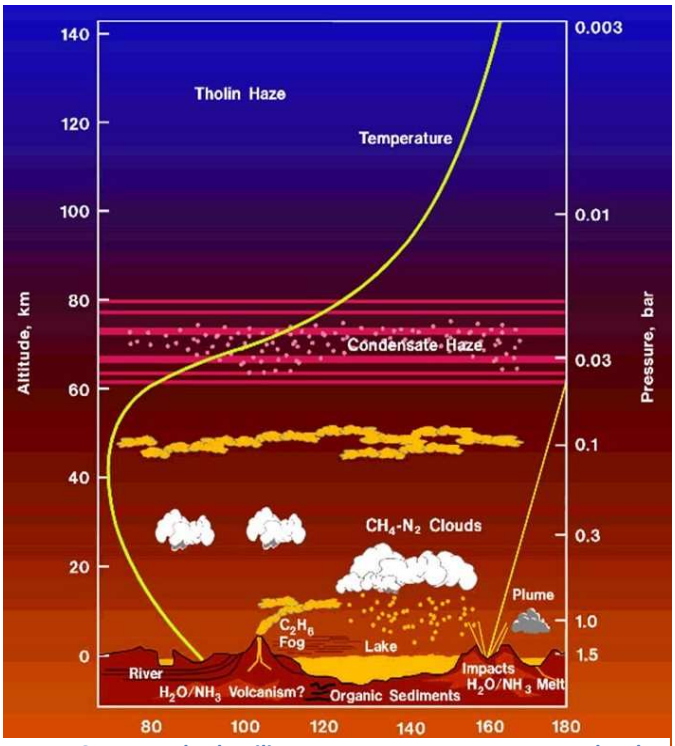

Image 6. A graph detailing temperature, pressure, and other aspects of Titan's atmosphere.

With *Cassini-Huygens* interplanetary mission, scientists hope to reach a better understanding of the surface, atmosphere and chemical composition of Titan to perhaps shed some light on how Earth might have been before life, as we know it, began to pump oxygen into the earth's atmosphere.

1.2) Overview of the mission

The *Cassini-Huygens* is a joint NASA, European Space Agency (ESA), and Italian Space Agency (ASI) spacecraft interplanetary mission. The total cost of the mission is about US$3,2 billion, NASA contributed with $2,6 billion, ESA with $500 million and $160 million came from the ASI. The project proceeded politically smoothly after 1994, although, citizens' groups concerned about its potential environmental impact attempted to derail it through protests and lawsuits until and past its 1997 launch. A few years after being approved by the United States Congress and after an intensive work of design, development and seek of international cooperation the spacecraft was ready for its launch from the Kennedy Space Center on October 15th, 1997.

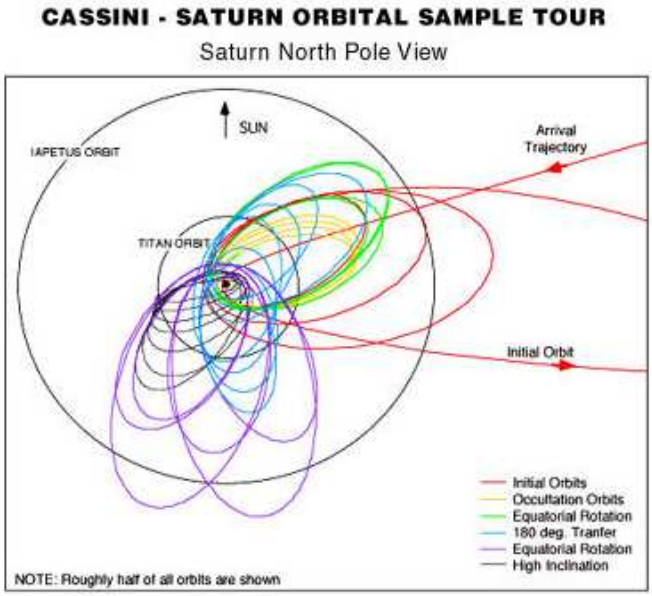

Image 7. Orbital motion of Cassini–Huygens on and after arrival at Saturn.

The spacecraft entered into orbit around Saturn on July 1, 2004 after giving two laps around the Sun and having taken advantage of the gravitational field of Venus, Earth and Jupiter to achieve enough momentum to reach the outer Solar System, using a new technique known as "gravity assists" whereby the spacecraft "steals" a small part of the planet's orbital energy. This technique came about in response to the fact that no existing launcher could have sent, with enough power, the 6000 kg. spacecraft directly to Saturn.

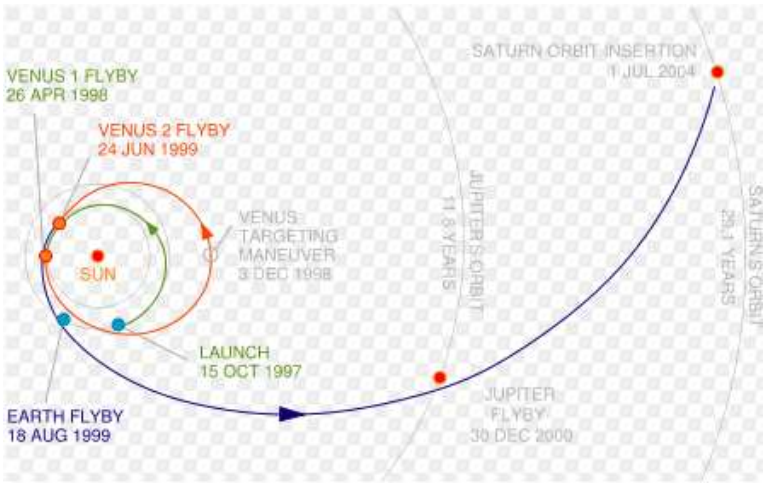

Image 8. Initial gravity-assist trajectory of Cassini–Huygens.

The *Cassini-Huygens* spacecraft was composed of the *Cassini* orbiter, designed to orbit Saturn and its moons for four years and which is doing so since the July 1, 2004, and the *Huygens* probe that was separated from the orbiter on December 25, 2004 and arrived at the surface of Titan on 14 January 2005, successfully fulfilling its mission to descend over Titan's atmosphere collecting all kind of information along the way, and finally to land on Titan's surface, analyzing it and then sending the data to the *Cassini* orbiter.

The *Cassini* orbiter was built and managed by NASA/Caltech's Jet Propulsion Laboratory. The *Huygens* probe was built by the European Space Agency (ESA). The Italian Space Agency (ASI) provided *Cassini*'s high-gain communication antenna, and a revolutionary compact and light-weight multimode radar (synthetic aperture radar, radar altimeter, radiometer).

During the 4 years the *Cassini* is orbiting Saturn is expected to submit enough information to understand and study in detail the planet and its magnetosphere, its rings and its numerous natural satellites. The nominal end of the mission is in 2008 but an extension to the mission is being planned which will end in 2010, although this has yet to be formally announced.

1.3) Main Objectives

The main objectives of the mission are:

- For Saturn:

- Determine the temperature field, cloud properties and composition of Saturn's atmosphere.
    - Image Saturn's atmosphere over a large range of latitudes and longitudes.
    - Determine the 2-cm wavelength radiometer thermal emission from the subcloud atmosphere.
    - Study belt/zone structure variations in ammonia concentration.
- Measure the planet's global wind field, including its waves; make long-term observations of cloud features to see how they grow, evolve, and dissipate.
- Determine the internal structure and rotation of the deep atmosphere.
    - Explore the unknown dynamical properties of the atmosphere.
    - Examine ammonia as a tracer for atmospheric circulations.
    - Determine the equator-to-pole temperature gradient and unknown subcloud longitudinal structures.
- Study daily variations and relationship between the ionosphere and the planet's magnetic field.
- Determine the composition, heat flux, and radiation environment present during Saturn's formation and evolution.
- Investigate sources and nature of Saturn's lightning.

- For the Rings:

- Study configuration of the rings and dynamic processes responsible for ring structure.
- Map the composition and size distribution of ring material.

- Investigate the interrelation of Saturn's rings and moons, including imbedded moons.
- Determine the distribution of dust and meteoroid distribution in the vicinity of the rings.
- Study the interactions between the rings and Saturn's magnetosphere, ionosphere and atmosphere.

- For Titan:

- Determine the most abundant elements, and most likely scenarios for the formation and evolution of Titan and its atmosphere.
- Determine the relative amounts of different components of the atmosphere
- Observe vertical and horizontal distributions of trace gases; search for complex molecules; investigate energy sources for atmospheric chemistry; determine the effects of sunlight on chemicals in the stratosphere; study formation and composition of aerosols (particles suspended in the atmosphere).
- Measure winds and global temperatures; investigate cloud physics, general circulation and seasonal effects in Titan's atmosphere; search for lightning.
- Determine the physical state, topography and composition of Titan's surface; characterize its internal structure.
- Investigate Titan's upper atmosphere, its ionization and its role as a source of neutral and ionized material for the magnetosphere of Saturn.
- Determine whether Titan's surface is liquid or solid; analyze the evidence of a bright continent as indicated in Hubble images taken in 1994.

1.4) Spacecraft

Cassini-Huygens is one of the most ambitious missions ever launched into space. Loaded with an array of powerful instruments and cameras, the spacecraft is capable of taking accurate measurements and detailed images in a variety of atmospheric conditions and light spectra.

The spacecraft, including the orbiter and the probe, is the largest and most complex interplanetary spacecraft built to date. The orbiter has a mass of 2,150 kg, the probe 350 kg. With the launch vehicle adapter and 3,132 kg of propellants at launch, the spacecraft had a mass of about 5,600 kg. Only the two Phobos spacecraft sent to Mars by the Soviet Union were heavier. The *Cassini* spacecraft was more than 6.8 meters (22.3 ft) high and more than 4 meters (13.1 ft) wide. The complexity of the spacecraft is necessitated both by its trajectory (flight path) to Saturn, and by the ambitious program of scientific observations once the spacecraft reaches its destination.

Image 9. Cassini Spacecraft

Cassini-Huygens is a three-axis stabilized spacecraft equipped for 27 diverse science investigations. The *Cassini* orbiter has 12 instruments and the Huygens probe had six. The instruments often have multiple functions, equipped to thoroughly investigate all the important elements that the Saturn system may uncover. The spacecraft communicates through one high-gain and two-low gain antennas. It is only in the event of a power failure or other such emergency situation, however, that the spacecraft will communicate through one of its low-gain antennas, known as LGA-1.

Three Radioisotope Thermoelectric Generators (commonly referred to as RTGs) provide power for the spacecraft, including the instruments, computers, and radio transmitters on board, attitude thrusters, and reaction wheels.

- *Cassini orbiter instruments*:

- **Optical Remote sensing.** Mounted on the remote sensing pallet, these instruments study Saturn and its rings and moons in the electromagnetic spectrum.
    - *Composite Infrared Spectrometer (CIRS).* the Composite Infrared Spectrometer consists of a dual interferometer, which measures the infrared emission from atmospheres, rings and surfaces at wavelengths between 7 and 1000 microns to determine their composition and temperatures.
    - *Imaging Science Subsystem (ISS).* the scientific imaging subsystem is a remote sensor that captures images in visible light, infrared and ultraviolet. The science objectives include studying the atmospheres of Saturn and Titan, Saturn's rings and their interactions with the satellites of the planet and the characteristics of the satellites, including Titan.
    - *Ultraviolet Imaging Spectrograph (UVIS).* is a set of detectors designed to measure ultraviolet light reflected or emitted by atmospheres, rings and surfaces to determine its composition, distribution, aerosol content and temperatures.
    - *Visible and Infrared Mapping Spectrometer (VIMS).* is a remote sensor consisting of two cameras in one: one is used for measurements in the visible spectrum and the other infrared.
    - The VIMS obtains images using infrared light and visible to learn more about the composition of the lunar surface, rings and atmospheres of Saturn and Titan.

- **Fields, Particles and Waves.** These instruments study the dust, plasma and magnetic fields around Saturn. While most don't produce actual "pictures," the information they collect is critical to scientists' understanding of this rich environment.
    - *Cassini Plasma Spectrometer (CAPS).* It measures the energy and electric charge of particles such as electrons and protons that the instrument founds around the ship. The instrument is used to study the composition, density, flow, velocity and temperature of ions and electrons in the magnetosphere of Saturn.
    - *Cosmic Dust Analyzer (CDA).* The Cosmic Dust Analyzer is a direct instrument sensor that measures the size, speed and direction of dust particles near Saturn. Some of these particles are orbiting Saturn while others may come from other solar systems. The CDA on board the *Cassini* is designed to help discover more about these mysterious particles.
    - *Ion and Neutral Mass Spectrometer (INMS).* It is a direct sensor that analyzes the charged particles (protons and heavy ions) and neutral particles (atoms) near Titan and Saturn to learn more about their atmospheres. One of its main aims will be to investigate the interaction between the upper atmosphere of Titan with the magnetosphere and the solar wind.
    - *Magnetometer (MAG).* It is a direct sensor that measures the strength and direction of the magnetic field around Saturn. The information collected by MAG can be used to explain the fact that despite the magnetic field of Saturn is similar to that of the Earth; the geographic north pole coincides exactly with the magnetic north pole, which only happens on this planet throughout the solar system.
    - *Magnetospheric Imaging Instrument (MIMI).* It is a remote and direct sensor that gets images and other data about the particles trapped in the large magnetic field of Saturn, and in its magnetosphere. This information will be used to study the overall configuration and the dynamics of the magnetosphere and its interactions with the solar wind, the atmosphere of Saturn, Titan, the rings and the icy satellites.
    - *Radio and Plasma Wave Science (RPWS).* The main functions of the scientific instrument Wave Radio and Plasma (RWPS) are measuring electrical and magnetic fields and the electron density and temperature in the interplanetary medium and planetary magnetospheres. The scientific instrument of radio waves and plasma (RPWS) will be used to investigate electric and magnetic waves in space plasma in Saturn.
- **Microwave Remote Sensing**. Using radio waves, these instruments map atmospheres, determine the mass of moons, collect data on ring particle size, and unveil the surface of Titan.
    - *Radio Science (RSS).* It is a remote sensor that uses radio antennas on Earth to explore how the radio signals from the spacecraft change when

they are sent through objects such as Titan's atmosphere and the rings of Saturn.

- *Radar*. It is both active and passive remote sensor that will produce maps of the surface of Titan and will measure the height of surface objects (such as mountains and canyons). In the following paragraphs it will be described with more detail.

1.5) The Cassini Radar

The main objective of the *Cassini* Radar Mission is Titan coverage. In order to study the inaccessible surface of Titan, its proprieties and processes, the spacecraft is making a number of close flybys, during which, the *Cassini* Radar conduct intense observations, in order to achieve its scientific goals. The first targeted fly-by of Titan (Ta) occurred on Tuesday, October 26, 2004 at 15:30 UTC.

- **RADAR Scientific Objectives:**
  - To determine whether oceans exist on Titan, and, if so, to determine their distribution.
  - To investigate the geologic features and topography of the solid surface of Titan.
  - To acquire data on non-Titan targets (rings, icy satellites) as conditions permit.
- **RADAR Sensing Instruments:**
  - Synthetic Aperture Radar Imager [SAR] (13.78 GHz Ku-band; 0.35 to 1.7 km resolution).
  - Altimeter (13.78 GHz Ku-band; 24 to 27 km horizontal, 90 to 150 m vertical resolution).
  - Radiometer (13.78 GHz passive Ku-band; 7 to 310 km resolution).
- **RADAR Instrument Characteristics:**
  - Mass (current best estimate) = 41.43 kg.
  - Peak Operating Power (current best estimate) = 108.40 W.
  - Peak Data Rate (current best estimate) = 364.800 kilobits/sec.

The *Cassini* Radar is a multimode microwave instrument that uses the 4 m high gain antenna (HGA) onboard the *Cassini* orbiter. The instrument operates at Ku-band (13.78 GHz or 2.2 cm wavelength) and is designed to operate in four observational modes (Imaging, Altimetry, Backscatter and Radiometry) at spacecraft altitude below 100.000 Km, on both inbound and outbound tracks of each hyperbolic Titan flyby, and to operate over a wide range of geometries and conditions. The instrument has been designed to have a wide range of capabilities in order to encompass a variety of possible surface proprieties.

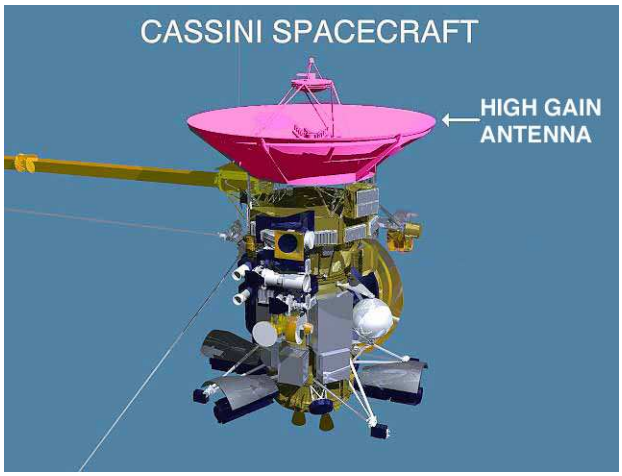

Image 10. Spacecraft's High Gain Antenna

Between 100.000km and 25.000km the RADAR will operate exclusively in the radiometry mode. In this mode, the RADAR will operate as a passive instrument, simply recording the energy emanating from the surface of Titan. This information will tell scientists the amount of latent heat (i.e. moisture) in the moon's atmosphere, a factor that has an impact on the precision of the other measurements taken by the instrument.

Between 25.000km and 9.000km the radar will operate alternatively as a radiometer and as a scatterometer (backscatter mode). In the backscatter mode it will bounce pulses off Titan's surface and then measure the intensity of the energy returning. This returning energy or backscatter is always less than the original pulse, because surface features inevitably reflect the pulse in more than one direction. From the backscatter measurements, scientists can infer the backscattering coefficient σ^0 of the surface of Titan.

For altitudes less than 4.000km the radar will operate in the imaging mode and secondarily as a radiometer. In the imaging mode of operation, the RADAR instrument will bounce pulses of microwave energy off the surface of Titan from different incidence angles and record the time it takes the pulses to return to the spacecraft. These measurements, when converted to distances (by dividing by the speed of light), will allow the construction of visual images of the target surface.

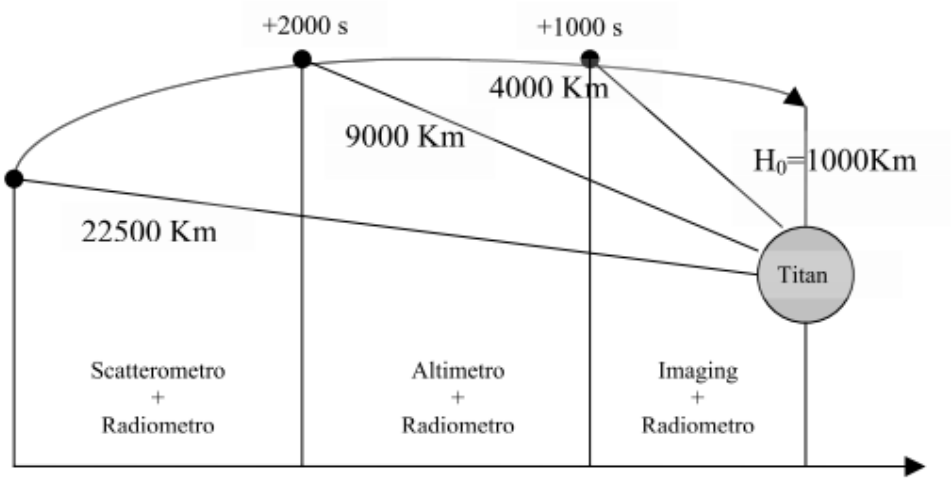

Figure 1.1 Modes of operation of the Cassini Radar for the different S/C altitudes during each fly-by

For altitudes between 9000km and 4000km the radar will operate as a radiometer and as an altimeter. The Altimeter Mode (ALT) is intended to study the relative topographic change of Titan's surface along sub-satellite tracks. The topography is a key characteristic of planetary surfaces and its quantitative evaluation is essential to understand flow such as occurs in volcanic and fluvial processes as well as for

geophysical probing of the interior of planets. Up to now, the only information about Titan's topography were from the Voyager-1 radio occultation experiment and ground based observations. Radar is presently the primary means of determining topography on Titan, since a smoggy haze completely obscures the satellite's surface.

The ALT mode is planned to operate at S/C altitudes between 4000 and 9000 Km, approximately from 16 minutes before the closest Titan approach of each Titan flyby until 16 minutes after the closest encounter. The Altimeter operates on "burst mode", similar to the imaging mode. When the ALT mode is executed, bursts of frequency modulated pulse signals (chirp pulses) of 150 μs time duration and at 5 MHz bandwidth will be transmitted in a Burst Period (the Burst Repetition Interval is 3333 ms). The transmit time varies from 1.4 to 1.8 μs. The number of pulses transmitted in each burst will vary throughout a single flyby pass.

During such operation, the radar utilizes the central, nadir-pointing antenna beam (Beam 3, a circular beam 0.350° across) for transmission and reception of chirp pulse. The collected altimeter measurements are expected to have horizontal resolutions ranging between 24 and 27 Km, while the accuracy in estimating the relative surface elevation (that is, the change in local surface elevation relative to a reference datum) depends also on the topographic relief of the surface as well as on the knowledge of the spacecraft's ephemeris and attitude, but is expected to be between 100-150 m.

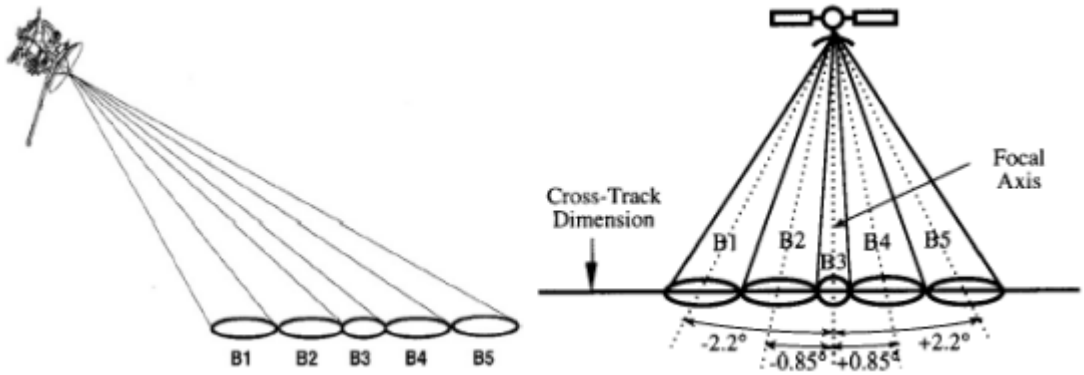

Figure 1.2 Representation of the different Cassini Radar beams for the active mode

The *Cassini* radar has three major functional components, namely:

- **The Radio Frequency Electronics Subsystem (RFES)** processes the microwave signals used by the instruments. We can divide the functions of this subsystem into three categories: the transmission of high-power, linearly frequency-modulated impulses and unmodulated impulses, the reception of the reflected energy and radiometric data, and the routing of calibration signals. It is composed of seven different units:
    - The **frequency generator (FG)** contains an ultra-stable oscillator that is the system timing source for the RADAR instrument.
    - The **digital chirp generator (DCG)** generates the low-power, baseband frequency, modulated pulse upon request from the RADAR Digital Subsystem.

  - The **chirp up-converter and amplifier (CUCA)** converts the baseband chirp pulse to Ku band.
  - The **high-power amplifier (HPA)** receives a low-power Ku-band chirp pulse from the CUCA and amplifies that pulse to the required power level for transmission.
  - The purpose of the **front-end electronics (FEE)** is to route the high-power transmission pulses, the returning low-energy echoes and radiometric signals, and the calibration signals.
  - The **microwave receiver (MR)** receives signals at Ku band and down-converts these to baseband so that they can be properly sampled. The sources of these signals are the echo returns, radiometric signals, and calibration signals routed through the FEE.
  - The **RFES power supply** converts the (approximately) 30-volt d.c. input from the Power and Pyrotechnic Subsystem to the required voltages for the RFES.

- The RADAR **Digital Subsystem (DSS)** is a central control unit for the RADAR operations. It manages the switches between the different operation modes and controls the chirp generation. It receives and transmits the RADAR commands to the Command and Data Subsystem (CDS), it generates and controls the properties of the transmitted impulse and manages the transfer of data and scientific information to the CDS. The DSS consists of the following units:
  - The **bus interface unit (BUI)** is the interface between RADAR and the CDS.
  - The **flight computer unit (FCU)** receives and routes the commands, it controls the RADAR configuration and the CTU information, etc….
  - The purpose of the **control and timing unit (CTU)** is to control the hardware configuration and the timing of control signals within RADAR.
  - The **signal conditioner unit (SCU)** consists of a science data buffer and high- and low-speed analog-to-digital (A/D) converters.
  - The **DSS power supply** converts the (approximately) 30-volt d.c. input from the Power and Pyrotechnic Subsystem to the voltages required for the DSS.
- The RADAR **Energy Storage Subsystem (ESS)** converts the (approximately) 30-volt d.c. input from the PPS to a higher voltage, stores energy in a capacitor bank, and provides a regulated voltage to the high-power amplifier (HPA) of the RFES. It is composed by:
  - The **boost circuitry** increases the (approximately) 30-volt d.c. input power to approximately 85 volts d.c. for more efficient energy storage by the capacitor bank.
  - The **capacitor bank** stores energy to supply to the buck regulator (and the HPA) during RADAR pulse bursts.

- The **buck regulator** regulates the varying capacitor bank voltage for the HPA.

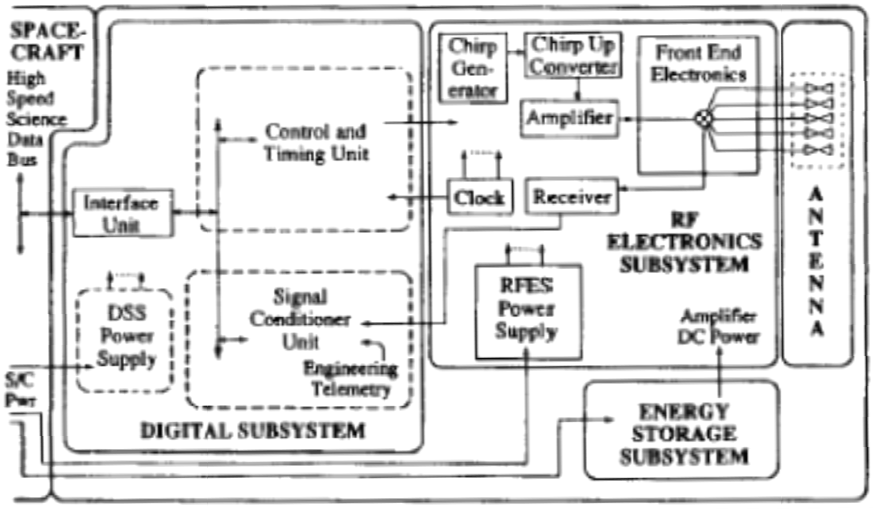

Figure 1.3 Block diagram of the Cassini Titan Radar Mapper

2) THE CASSINI PROCESSING ALTIMETRIC DATA SYSTEM

2.1) Introduction

In the frame of CASSINI-HUYGENS interplanetary mission, the *Cassini* PAD System contains the HW and SW tools necessary to:

- process the LBDR data (given by JPL → Jet Propulsion Laboratory in Pasadena, California) in order to produce ABDR science data (*a complete overview of the Cassini PAD data is presented in the following section*).
- evaluate the performance of RADAR altimeter.
- produce digital maps of Titan by using data acquired by all *Cassini* passes.

The *Cassini* Radar PAD system is conceived to receive science data acquired from the *Cassini* Radar while operating in high-resolution altimeter mode (ALTH/AHAG), to process this data at different levels, archive them, and visualize the obtained products. The *Cassini PAD System* shall provide a set of three tools for data processing and visualization together with the necessary archiving facility. The following *Cassini PAD* tools are foreseen:

- *ABDR Production Tool (PT)*: this tool shall be for produce altimetry data by processing the BODP coming from the *Cassini* RADAR. It shall take the LBDR files as input, returning the ABDR files as output.

- *PAD Science Look Tool (SLT)*: this tool shall allow users to interact with processed data. This tool shall be able to read and to manipulate the *Cassini* data.

- *PAD Map Tool (MT)*: this tool shall be able to visualize Titan-referenced altimetry data, with related satellite ground tracks for each Titan fly-by, inferred surface parameters and all those information which could be of interest through interaction with a high-resolution Titan map, available in a user-defined projection.

This work will be focused mainly in PT and SLT tools.

Each tool, developed in a Matlab® environment, is provided with a user-friendly graphical interface (GUI → Graphical User Interface), which allows users to exploit all implemented functionalities.

2.2) Data Product Identification

Three different types of data products are used by the *Cassini* Radar:

- Basic Image Data Records (BIDRs).
- Burst Ordered Data Products (BODPs).
- Digital Map Products (DMPs).

The interest of the *Cassini Radar PAD system* is for Burst Ordered Data Products (BODPs) which are comprehensive data files that include engineering telemetry, radar

operational parameters, raw echo data, instrument viewing geometry, and calibrated science data.

The BODP files contain time-ordered fixed length records. Each record corresponds to the full set of relevant data for an individual radar burst. The *Cassini* Radar is operated in "burst mode", which means the radar transmits a number of pulses in sequence then waits to receive the return signals. "Burst" is a descriptive term for the train of pulses transmitted by the radar.

The term "burst" (somewhat unconventionally) is used to refer to an entire measurement cycle including transmit, receipt of echo, and radiometric (passive) measurements of the naturally occurring radiation emitted from the surface. Burst Ordered Data Products are fixed header length, fixed record length files. The header is an attached PDS label.

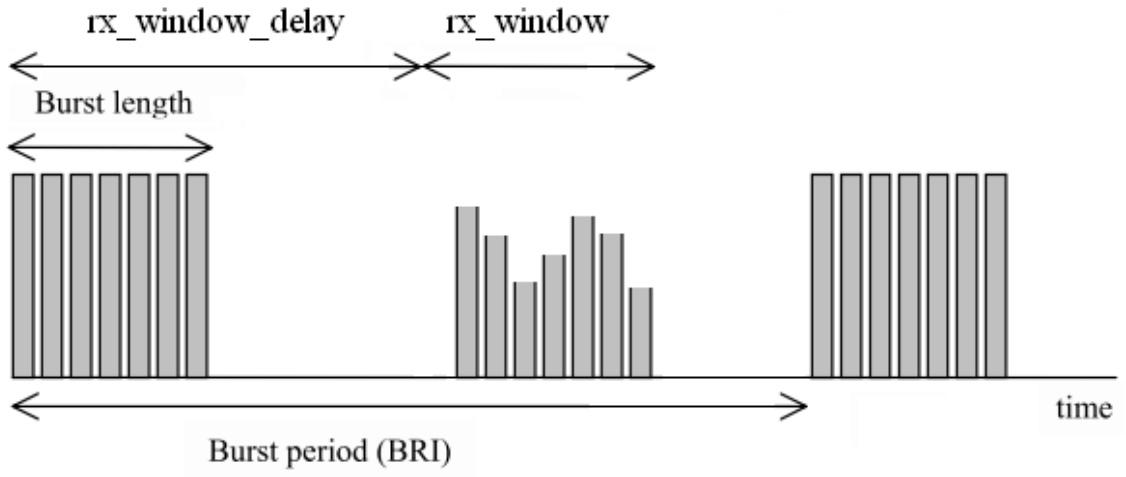

Figure 2.1 Example of burst cycle time

The BODP comprise three separate data sets:

- Short Burst Data Record (SBDR).
- Long Burst Data Record (LBDR).
- Altimeter Burst Data Record (ABDR).

The only difference between the three formats is whether or not two data fields are included: the sampled echo data, and the altimeter profile. The altimeter profile is an intermediate processing result between sampled echo data and a final altitude estimate. LBDRs include the echo data but not the altimeter profile. ABDRs include the altimeter profile but not the echo data. SBDRs include neither.

The SBDR data record is divided into three consecutive segments from three different levels of processing:

1) The engineering data segment includes a copy of the radar telemetry contained in the Engineering Ground Support Equipment (EGSE) files obtained from the spacecraft data downlinks. This data is stored to allow investigators to access as much of the information obtained by the spacecraft as possible.

2) The intermediate level data segment containing timing and spacecraft geometry information. The data fields in this segment include time at start of burst,

spacecraft position and velocity, the direction vectors of the axes of the spacecraft coordinate system, and the angular velocity vector of the spacecraft.

3) The science data segment: three primary estimates of geophysical quantities are available in the science data segment:

- the normalized backscatter cross-section σ_0 obtained from the scatterometer measurement.
- the antenna temperature determined from the radiometer measurement.
- the range to target (RTT = distance between the sensor and the closest surface point) computed from the altimeter measurement.

In addition to these primary values additional ancillary parameters are also computed. The ancillary parameters include intermediate values, (e.g., receiver temperature, total echo energy, system gain, etc.) analytical estimates of the standard deviation of the residual error in each of the three primary measurements, and measurement geometry. Synthetic Aperture Radar (SAR) ancillary data is also included in the science data segment when available.

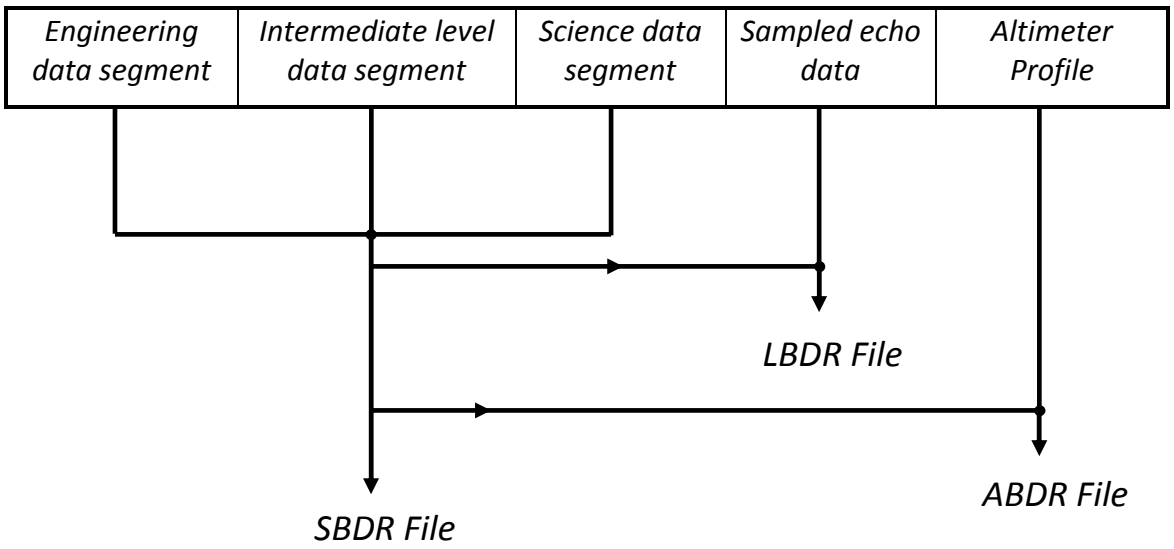

Figure 2.2 Structure of the Cassini BODP's files

- Sampled Echo Data:

The sampled echo data array is located at the end of each record in the LBDR data files. It constitutes the only difference between SBDR records and LBDR records.

The array consists of 32,768 4-byte floating point values. It contains the active mode time-sampled data obtained during the receive window. The data was encoded prior to downlinking from the spacecraft in order to minimize the data transfer rate, and then decoded during the ground processing (the data stored in the array has already been decoded).

The length of the array corresponds to the maximum amount of echo data that can ever be obtained from a single burst. Only the first N elements in the array are valid data. These data are N floating point values in the range [-127.5, 127.5] sampled

consecutively at a rate of B Hz. N is stored in the raw_active_mode_length data field in the engineering data segment. B is in the adc_rate field in the same segment. The raw_active_mode_rms field (also in the engineering data segment) contains the root mean square of the N sampled echo data values:

$$RMS = \sqrt{\frac{1}{N}\sum_{i=1}^{N} x_i^2} = \sqrt{\frac{x_1^2 + x_2^2 + \cdots + x_N^2}{N}}$$

- *Altimeter Profile:*

The altimeter profile is the range compressed active mode data obtained while the radar is in altimeter mode. It is located at the end of each record in the ABDR files. It is an array of floating point values the length of which is stored in the altimeter_profile_length data field in the science data segment.

During range compression the active mode data is decompressed and segmented by pulse. Each pulse is then separately correlated with the real -valued chirped transmit waveform, in order to distribute the energy within each returned pulse into range bins. The range for the first sample of each pulse in the altimeter profile and the range step are data fields in the science data segment. The number of pulses received is stored in the science data segment.

The JPL *Cassini* RADAR science data products will be produced by the radar processing group. The pre-processor (part of the radar analysis software (RAS)) creates SBDR and LBDR files for each radar observation (i.e., each Titan pass). Initially these files only contain valid data in the engineering and intermediate level data segments. These files will then be used as inputs for the various science processing routines (SP), such as *Cassini* Radar PAD system.

In the following pages will be described the general architecture of the Detailed Processing Model chain for ABDR Production Tool (PT) and PAD Science Look Tool (SLT).

2.3) ABDR Production Tool (PT)

The main functionalities of PT Tool are:

- Input Data Retrieving & Reading
- Range Compression
- ABDR Production

This tool first reads the LBDR file selected interactively, and immediately starts the creation of subsets of the input LBDR file (intermediate PT Files) containing only the data records belonging to the ALTH/AHAG radar operational modes. The tool also fills the end of each record in the intermediate PT file with the results from the range

compression of the sampled echo data. This intermediate files are created in order to be accessed by the SLT and MT tools.

Then the PT tool starts the creation of the ABDR file starting from the selected LBDR file. The ABDR file contains only the records pertinent to the two (inbound and outbound) periods in which the radar was in altimeter mode. In order to produce the ABDR file, the appropriate data fields of the Science Data Segment are automatically filled with values coming from SLT processing, the end of each record is also filled with the values obtained from range compression (i.e. the altimeter profile).

Once this process is done the ABDR PT stores the file into the local archive along with a report file and updates the list of the processed LBDR files. Using the Configuration File the tool also allows user to specify the default processing parameters and the I/O path for reading and saving files.

The general set of input/output variables of the ABDR Production Tool is showed in the following table:

Input	
Name	***Format***
LBDR file	*Binary format data file*
SLT file results	*Binary format data file*
Output	
Range compressed data	*Floating point double precision*
ABDR file	*Binary format data file*
Intermediate data file	*Binary format data file* *ASCII Format Data File*

Table 2.1 Input and Output variables of the ABDR PT

A diagram that contains the main PT functionalities is presented in the following:

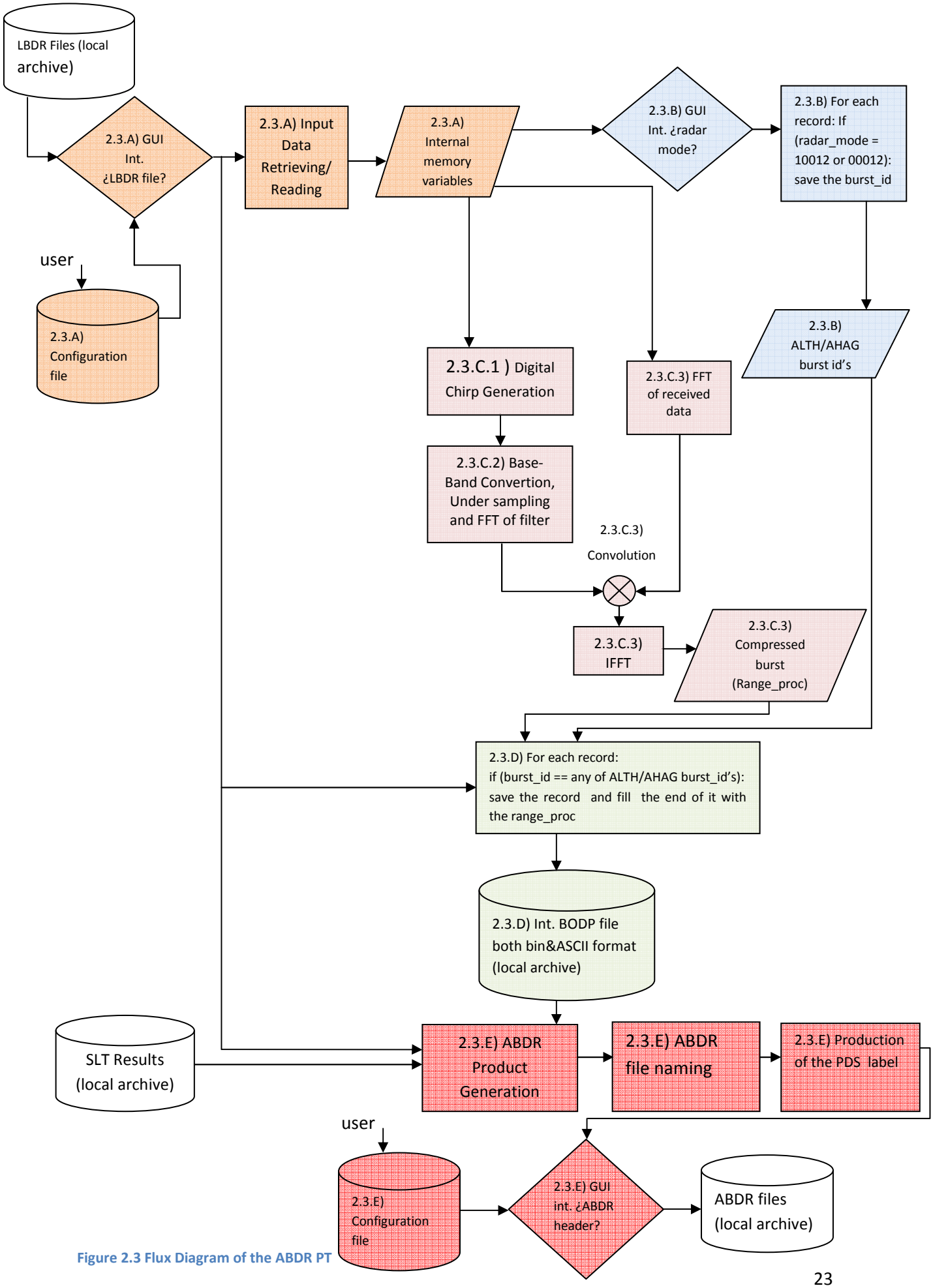

Figure 2.3 Flux Diagram of the ABDR PT

In the following pages will be described the different blocks that need to be commented with more detail:

2.3.A) Input Data Retrieving/Reading.

Starting from the LBDR file selected by user via GUI, this functionality reads all the data fields needed and stores them into the local dedicated workstation in order to be accessed by the following processes. The PT tool allows user to specify the I/O path for reading and saving files by using the configuration file.

To this end, an external function is used within the main program. Moreover, a C algorithm is previously used in order to extract and select the compacted data so that it is possible to create a file, where it will be stored only the data necessary to our processing and finally to obtain a computational "lightening".

Once this file is created the data extraction is performed. Since it is used an external function, it is needed to define those variables to be read and those to be passed:

function [sample_freq, chirp_length, PRI, chirp_start_freq, burst_time,
number_of_pulses, sc_j2000_x, sc_j2000_y, sc_j2000_z,…]=
nomefunction(filename_input, record_start, record_end)

where the variables inside the square brackets are those to be read from the file while those inside the round brackets are those passed from the main to the function, this is the input filename, and the first and the last bursts to be processed respectively.

In order to provide these three parameters to the function the main program requests these variables as input data. To this end, the following windows to introduce such data have been created:

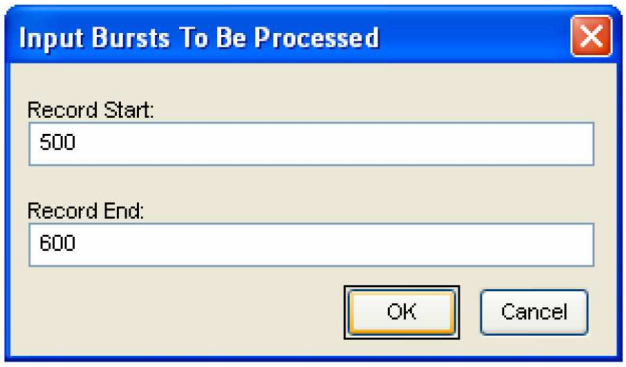

Figure 2.4 Window to select the input bursts to be processed

The figure above figure shows the window used to introduce the *record_start* and the *record_end*, while the following figure shows the window used to select the input file. Each beam has its own file so it is worth noting that, since the Radar in ALT mode utilizes the central, nadir-pointing antenna beam, i.e. the beam nº3, the files involving any of the other beams won't produce remarkable results:

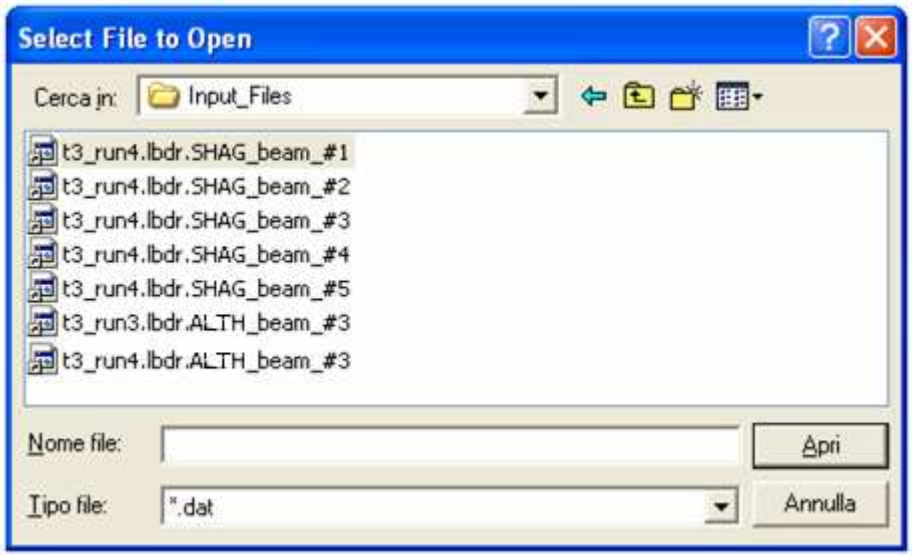

Figure 2.5 Window to select the Input file to be read

The whole inputs/outputs of this function are then listed in the following:

- *Inputs: LBDR file, record_start, record_end*
- *Outputs:*

Variables	Structure	Value/Unit Reference
Rec_echo	[Bi-dimensional Array]	Floating point double precision
activity	[Array]	Short integer non negative value
calibration	[Array]	Short integer non negative value
burst_id	[Array]	Short integer non negative value
radar_mode	[Array]	Short integer
radar_data_lenght	[Array]	Short integer non negative value
sample_freq	[Array]	Floating point double precision [Hz]
chirp_time_step	[Array]	Floating point double precision [s]
num_chirp_steps	[Array]	Short integer non negative value
chirp_length	[Array]	Floating point double precision [s]
chirp_freq_step	[Array]	Floating point double precision [Hz]
PRI	[Array]	Floating point double precision [s]
chirp_start_freq	[Array]	Floating point double precision[Hz]
number_of_pulses	[Array]	Short integer non negative value
rx_window_delay	[Array]	Floating point double precision [s]
sc_j2000_x	[Array]	Floating point double precision [Km]
sc_j2000_y	[Array]	Floating point double precision [Km]
sc_j2000_z	[Array]	Floating point double precision [Km]
TGT_SC_x	[Array]	Floating point double precision [Km]
TGT_SC_y	[Array]	Floating point double precision [Km]
TGT_SC_z	[Array]	Floating point double precision [Km]
rx_effective_pulse	[Array]	Short integer non negative value
act_centroid_longitude	[Array]	Floating point double precision [deg]
act_centroid_latitude	[Array]	Floating point double precision [deg]
reference_SC_clock	[Array]	Floating point double precision [s]
burst_time	[Array]	Floating point double precision [s]
time_from_closest_approach	[Array]	Floating point double precision [s]

transmit_time_offset	*[Array]*	*Floating pt.double precision [s]*
SC_clock	*[Array]*	*Floating point double precision*
ephemeris_time	*[Array]*	*Floating point double precision [s]*
J2000_sc_vel_x	*[Array]*	*Floating point double precision [Km]/[s]*
J2000_sc_vel_y	*[Array]*	*Floating point double precision [Km]/[s]*
J2000_sc_vel_z	*[Array]*	*Floating point double precision [Km]/[s]*
TGT_sc_vel_x	*[Array]*	*Floating point double precision [Km]/[s]*
TGT_sc_vel_y	*[Array]*	*Floating point double precision [Km]/[s]*
TGT_sc_vel_z	*[Array]*	*Floating point double precision [Km]/[s]*
Incidence_angle	*[Array]*	*Floating point double precision [deg]*
active_geometry_time_offset	*[Array]*	*Floating point double precision [s]*
beam_mask	*[Array]*	*Short Integer*
time_from_epoch	*[Array]*	*Floating pt.double precision [s]*

Table 2.2 "Input Data Retrieving/Reading" outputs

In the following each variable is described with more detail:

- *rec_echo*: this variable is basically a Bi-dimensional array containing the active mode time-sampled data as detailed in the previous section. It is used in the subsequent compression with the matched filter.
- *activity*: this variable indicates if the present data corresponds to the active mode operation of the *Cassini* Radar or not.
- *calibration*: The following bit patterns are assigned to the various Calibration Sources: (the three or four character mode name is in parenthesis)
  - 0000_2 = Normal Operation. (norm)
  - 0001_2 = Antenna being used as the Calibration Source. (ant)
  - 0010_2 = Noise Diode being used as the Calibration Source. (diod)
  - 0011_2 = Resistive Load being used as the Calibration Source. (load)
  - 0100_2 = Rerouted Chirp being used as the Calibration Source. (chrp)
  - 0101_2 = Leakage Signal being used as the Calibration Source. (leak)
  - 0110_2 = Radiometer Only Calibration Mode. (rado)
  - 0111_2 = Transmit Only Calibration Mode. (xmto)
  - 1000_2 = Auto-Gain Control. (agc)
  - 1001_2 - 11112 = (reserved by the CTU)
- *burst_id*: array of short integers, coming from the Engineering Data Segment, containing the value that uniquely identifies each burst throughout the mission. minimum_value: 0, maximum_value: 2^{32} -1
- *radar_mode*: This field represents the radar mode, and is defined as follows: (the four character mode name is in parenthesis)
  - 0000_2 = ALTL: Altimeter, Low-Resolution (altl)
  - 0001_2 = ALTH: Altimeter, High-Resolution (alth)
  - 0010_2 = SARL: Synthetic Aperture Radar, Low-Resolution (sarl)
  - 0011_2 = SARH: Synthetic Aperture Radar, High-Resolution (sarh)
  - 0100_2 = Radiometer Only (rado)
  - 0101_2 = Inter-Galactic Object (IGO) Calibration (igoc)
  - 0110_2 = Earth Viewing Calibration (evca)
  - 0111_2 = Bi-Static Operation (bsop)

  - 1000_2 = ALTL with Auto Gain (alag)
  - 1001_2 = ALTH with Auto Gain (ahag)
  - 1010_2 = SARL with Auto Gain (slag)
  - 1011_2 = SARH with Auto Gain (shag)
  - $1100_2 - 1111_2$= (spare)
- *radar_data_length*: this variable is an array containing the number of valid data values in the sampled echo data array after decompression, also coming from the engineering data segment. This number does not have to be constant, and it will be useful if we would like to know if we can trust a concrete value of the sampled echo data or not. maximum value: 32000, minimum value: 0
- *sample_freq*: an array containing the Analog to Digital Converter sampling rate in Hz. This is the rate at which the echo is sampled. Since *Cassini* uses video offset rather than IQ sampling each sample is a real (not complex) value. possible values: 250 kHz, 1.0 MHz, 2.0 MHz, 10.0 MHz
- *chirp_time_step*: array containing the duration in time of each single frequency step. This variable will be needed when we should simulate the transmitted chirp signal as generated by *Cassini* DCG in order to perform the matched filter (section **2.3.C**). possible_values: should always be 666.7 ns.
- *num_chirp_steps*: an array containing the number of chirp steps, this is two different frequencies before and after the step, thus the number of distinct frequencies is one more than the number of steps. This variable will be useful when we should simulate the transmitted chirp signal as generated by *Cassini* DCG. minimum_value: 216, maximum_value: 749
- *chirp_length*: this variable is an array containing the total length of chirp in seconds. This is equivalent to the width (during transmission) of an individual pulse. Will also be useful when we should simulate the transmitted chirp signal as generated by *Cassini* DCG in order to perform the matched filter. minimum_value: 0.144 ms, maximum_value: 0.5 ms
- *chirp_freq_step*: array containing the change in frequency for each chirp step in Hz. Also useful when we should simulate the transmitted chirp signal as generated by *Cassini* DCG. minimum_value: 0 Hz, maximum_value: 117.2 kHz
- *PRI*: array containing the pulse repetition interval in seconds (the time interval between successive transmitted (chirped) pulses). Will be used when the transmitted chirp signal as generated by *Cassini* DCG is simulated at the Range Processing Tool. minimum_value: 0.002 ms, maximum_value: 4.092 ms
- *chirp_start_freq*: array containing the frequency of the first frequency step that forms the chirp. Useful when we should simulate the transmitted chirp signal as generated by *Cassini* DCG in order to perform the matched filter. minimum_value: 0 Hz maximum_value: 30 MHz
- *number_of_pulses*: array of integers containing number of pulses transmitted each burst. Useful when we should simulate the transmitted chirp signal as generated by *Cassini* DCG. minimum_value: 0, maximum_value: 255

- *rx_window_delay*: array containing the received windows delay, measured from the beginning of the first pulse in the first PRI to start of receive window. It includes the PRIs that make up the Transmit Burst and the PRIs between the end of Transmit Burst and the beginning of the Receive Window. The Receive Window Delay will always be an integer number of PRIs. minimum_value: 0, maximum_value: 1023 PRI.
- *sc_j2000_x*: x- component of S/C position in target_centered J2000 inertial coordinate system.
- *sc_j2000_y*: y- component of S/C position in target_centered J2000 inertial coordinate system.
- *sc_j2000_z*: z- component of S/C position in target_centered J2000 inertial coordinate system.
- *TGT_SC_x*: x- component of S/C position in target body fixed (TBF) coordinate system.
- *TGT_SC_y*: y- component of S/C position in target body fixed (TBF) coordinate system.
- *TGT_SC_z*: z- component of S/C position in target body fixed (TBF) coordinate system.
- *J2000_sc_vel_x*: x- component of S/C velocity vector in the J2000 frame.
- *J2000_sc_vel_y*: y- component of S/C velocity vector in the J2000 frame.
- *J2000_sc_vel_z*: z- component of S/C velocity vector in the J2000 frame.
- *TGT_sc_vel_x*: x- component of S/C velocity vector in the TBF. Value is zero if target name is none or calibration.
- *TGT_sc_vel_y*: y- component of S/C velocity vector in the TBF. Value is zero if target name is none or calibration.
- *TGT_sc_vel_z*: z- component of S/C velocity vector in the TBF. Value is zero if target name is none or calibration.
- *rx_effective_pulse*: array containing the number of pulses which were received completely within the echo window. Partial pulses are ignored.
- *act_centroid_longitud*: array containig the longitude of active (two-way) antenna boresight.
- *act_centroid_latitude*: array containing the latitude of active (two-way) antenna boresight.
- *reference_SC_clock*: Reference spacecraft clock count for each burst. The LSB is nearly 1 second but not exactly. For exact time references use t_ephem_time. minimum_value: 0, maximum_value: $2^{32} - 1$.
- *burst_time*: Burst start time expressed as an offset from the reference spacecraft clock count. The precise spacecraft time at the start of the burst is *reference_SC_clock* + *burst_time* in seconds. minimum_value: 0.0 maximum_value: 1.0

- *t_ephem_time*: array that contains the time at start of burst expressed in seconds since 12:00 AM Jan. 1, 2000. Used for exact time references.
- *time_from_closest_approach*: *t_ephem_time – closest_approach_time*.
- *transmit_time_offset*: array containing the time offset in seconds from t_ephem_time at which the leading edge of the first transmit pulse leaves the antenna.
- *SC_clock*: Encoded spacecraft clock time. This value is used by the SPICE software employed by the *Cassini* Navigation Team.
- *Incidence_angle*: array that contains the angle between the antenna look direction and the surface normal halfway between transmission and receipt of the active mode signal.
- *active_geometry_time_offset*: array that contains the time offset in seconds from burst reference time (*t_ephem_time*) for which the active geometry fields were computed. Active mode geometry is computed for the time halfway between the midpoint of the transmission and the midpoint of the active mode receiver window. The full set of measurement geometry for each case includes: the polarization orientation angle, emission/incidence angle, azimuth angle, the measurement centroid, and four points on the 3 dB gain contour of the measurement.
- *beam_mask*: since the *Cassini* Radar is a multimode instrument with up to 5 different beams, a beam mask is needed in order to be able to activate de different beams depending on the radar mode. This variable is an array containing the following bit patterns describing the possible Beam Masks used by the *Cassini* RADAR DSS, minimum_value: 0, maximum_value: 31:
    - 00000_2 = All beams disabled (Used during internal source Calibration modes such as noise diode, resistive load and rerouted chirp).
    - 00001_2 = Beam #1 Only enabled.
    - 00010_2 = Beam #2 Only enabled.
    - 00011_2 = Beams #2 and #1 enabled.
    - 10000_2 = Beam #5 Only enabled.
    - 11010_2 = Beams #5, #4 and #2 enabled.
    - 11111_2 = All Five Beams enabled.
- *time_from_epoch*: *t_ephem_time – epoch_time*. The value of epoch_time is usually the same as the closest approach time but may differ occasionally for logistic reasons.

**two coordinate frames are used to compute spacecraft ephemeris and attitude information: An inertial frame (J2000) centered on the target (typically Titan), and the target body fixed frame (TBF). Although both frames are centered on the target, the orientation of the frames differs. The TBF frame maintains a constant orientation with respect to any point on the surface of the target. For example, if the target were Earth, the TBF coordinates of the point 100 m above the Washington monument would not change with time. The inertial frame coordinate system is the standard J2000 coordinate system translated so that it is centered at the target's (Titan's) center at the*

time of the start of the burst. With these variables we will be able to calculate the distance from the spacecraft to the center of Titan, for each burst.

2.3.B) Radar Mode Reading.

Starting from the variables: radar_mode, and burst_id, from the engineering data segment, this function stores into the local dedicated workstation all burst_id's from those records in which the radar was in altimeter mode:

- radar_mode = 00012 → Altimeter, High Resolution, ALTH.
- radar_mode = 10012 → Altimeter with Auto Gain, AHAG.

depending on previous user selection via GUI. So if radar mode is one of this two the burst_id will be stored in the output of this function.

The whole inputs/outputs of this function are listed in the following:

- *Inputs*: *radar_mode, burst_id*
- *Outputs*: ALTH/AHAG burst id's

2.3.C) Range Processing.

In this section is explained how the received signal is processed in order to achieve an optimal signal waveform that should be taken by the Science Look Tool, to estimate Titan's surface's significant parameters in the most efficient way. A complete description of the Physical concepts of the range processing can be found in **3.1** section.

As detailed on **3.1** the filter that maximizes the SNR (matched filter) is actually the conjugate of signal itself inverted, and the transmitted signal waveform that yields the best distance resolution is the chirp. So in order to perform the matched filtering it is needed to simulate the chirp signal as that generated by *Cassini* DCG.

To this end the chirp is generated at 30MHz and then the Doppler frequency is subtracted see section **3.6**, the resulting signal is undersampled at 10MHz. The matched filter is done in frequency domain by implementing the FFT of both simulated chirp and received data and by doing the convolution of both signals. In the resulting signal all the energy is gathered into a narrow peak in the compressed pulse

The full detailed algorithm is here below reported in terms of pseudocode:

```
1. fc=5*1e6;
2. Np_samples = floor(PRI.*sample_freq/2);
-------------------------------------------------------------------------------
3. t_start = chirp_start_freq./rate_chirp;
4. t_stop = (chirp_start_freq+B)./rate_chirp;
5. for kk=record_start:record_end
6.     td=t_start:1/FC:t_stop;
7.     t=0:1/FC:length(td)/FC-1/FC;
8.     fd=rate_chirp*td;
9.     fased=cumsum(fd)*1/FC*2*pi+rate_chirp*t_start*t_start*pi;
```

2.3.C.1 Digital Chirp Generation

```
10.  f_dop = -chirp_start_freq-B/2+f_cen-fc/4;
11.  filtro=cos(fased).*cos(2*pi*(f_cen-f_dop)*t);
```

```
12.  filtro_f=fft(filtro);
13.  ff=-FC/2:FC/length(filtro):FC/2-1/length(filtro);
14.  i_ff = find(abs(ff)<=f_cen);
15.  filtro_f(i_ff)=0;
16.  filtro=ifft(filtro_f);
17.  filtro_f=fft(filtro(1:floor(FC/fc):length(filtro)));
18.  ff=-fc/4:fc/2/Np_samples:fc/4-fc/Np_samples/2;
19.  i_ff=find(abs(ff)<fc/4-B/2);
```

2.3.C.2) Base-Band Convertion, Under sampling and FFT of filter

---

```
20.  for jj=1:Np
21.      echo_f(jj,:)=fft(echo_f(jj,:));
22.      dati_f=fftshift(echo_f(jj,1:Np_samples).*conj(filtro_f(1:Np_samples)));
23.      dati_f(i_ff)=0;
24.      conv_prova(index,:)=ifft(dati_f);
25.  End
26.End
```

2.3.C.3) FFT of received data, convolution, IFFT and saving the results

---

In the following each sentence is explained with more detail:

1. this is the frequency to undersample
2. this is number of samples of each pulse of the burst
3. here it is calculated the chirp starting time
4. here it is calculated the chirp stopping time
5. this means that is done for all the burst of the record
6. here it is defined the time chirp time reference, we take one sample each 1/FC
7. the same as 6. but starting at t = 0s
8. here it is defined the time chirp frequency reference, we take one sample each FC
9. this is the chirp stepped phase
10. here it is calculated the Doppler frequency to be subtracted from the central frequency in order to compensate the Doppler shifting produced by the spacecraft movement with respect to Titan, see section **3.6**
11. here is performed the chirp in time domain
12. here is performed the chirp in the frequency domain by evaluating the fft (fast Fourier transform)
13. with lines 13 to 15 it is performed a base-band conversion by eliminating the frequencies lower than *f_cen*:

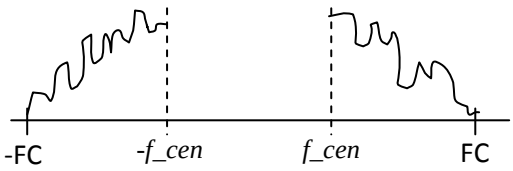

16. here it is performed the filter in time domain shifted in base band by the ifft (inverse fast Fourier transform)
17. here is performed the undersampling by taking one sample each FC/fc

18.with lines 18, 19 and 23 it is performed out-band samples elimination following the same procedure of the base-band conversion
20. this means that this is done for each burst pulse
21.here it is evaluated the fft of the jj_th pulse of the burst of the received echo data
22.here it is performed the convolution of the fft of the jj_th pulse with the matched filter, this is the conjugated of 17.
24.finally it is performed the ifft of 22 in order to obtain and save the range compressed data
The whole inputs/outputs of this function are listed in the following:

- *Inputs*: *PRI, sample_freq, chirp_start_freq, number_of_pulses, rec_echo, B, rate_chirp and FC*.
- *Output: range_proc*

2.3.D) Intermediate files generation

In order to be accessed by the SLT and the MT for internal data processing, this tool generates the intermediate BODP files by saving the data records pertinent to ALTH/AHAG radar operational modes and by filling the end of each record with the range compressed data (range_proc). The final file is saved into the local archive.

In order to achieve it, this tool looks the burst_id of each record of the input LBDR file and saves only those records that match with those in the ALTH/AHAG burst id's stored by the radar mode reading tool.

The whole inputs/outputs of this function are listed in the following:

- *Inputs: range_proc*, input LBDR file, and ALTH/AHAG burst id's
- *Outputs*: Intermediate BODP data files in both binary and ASCII formats.

2.3.E) ABDR file generation, file naming, labeling and saving

Starting from the LBDR selected file and taking into account only the two periods in which the radar was in altimeter mode, this tool fills the end of each record with the range compressed data from the Intermediate BODP file (i.e. altimeter profile). In addition the appropriate data fields in the Science Data Segment are filled with the values obtained from the SLT processing:

- range_to_target: distance from the satellite radar to the observed surface.
- rtt_std: estimated standard deviation of the residual error in the range_to_target measurement.
- altimeter_profile_range_start: a floating point double precision containing the range of the first altimeter profile value in each pulse.
- altimeter_profile_range_step: a floating point double precision containing the difference in range between consecutive range bins in altimeter profile.
- altimeter_profile_length: this is an integer containing the number of valid entries in altimeter profile.

So the final ABDR structure remains the same as the initial LBDR product except for these three differences:

- contains only the records in which the altimeter was in ALTH/AHAG mode.
- contains the altimeter profile from the range compression.
- contains the information of the Science Data Segment from the SLT results.

Moreover the tool produces the filename, the PDS label and allows the user to edit the header of the input ABDR file and to specify the I/O path for reading and saving files by using Configuration File. Finally the final file is saved into the local archive.

Next figure shows the window used to specify the output file:

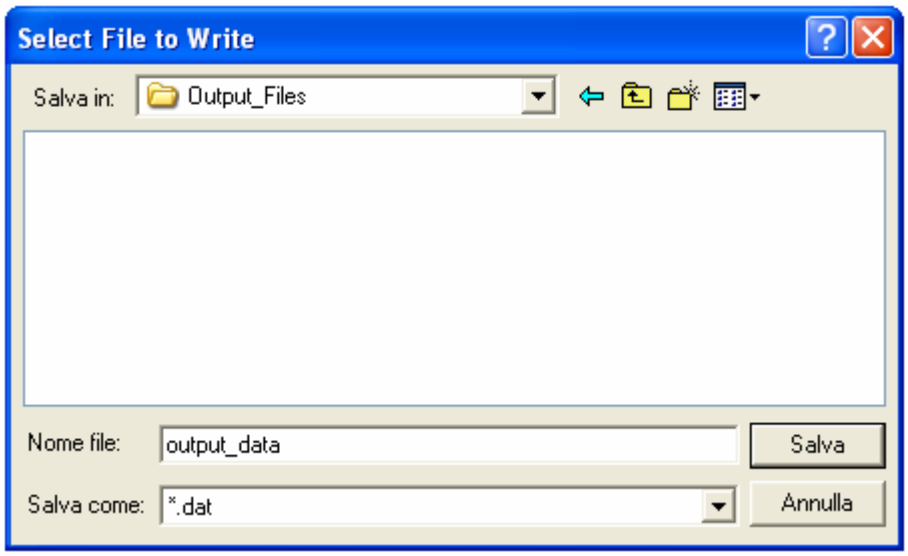

Figure 2.6 Window to select the output file

The whole inputs/outputs of this function are listed in the following:

- *Inputs*: LBDR selected file, SLT results file and Intermediate BODP data file
- *Output*: ABDR file

2.4. PAD Science Look Tool (SLT).

The Science Look Tool is a graphical application of *Cassini* PAD System that includes the procedures and algorithms designed to provide the altimetry profile of Titan surface and to check performances of the *Cassini* Radar in Altimeter when it is operating in high resolution mode.

After interactive selection of the intermediate BODP file by user, the SLT Tool implements an ML estimator that provides statistically optimal values of certain key parameters such as time delay, and surface roughness (σ_h). To this aim the tool uses the range compressed data, produced by the ABDR tool, previously averaged in order to produce a single pulse to be fitted with one of the implemented altimetry models.

After the estimates of centroids positions have been made, the topographic heights are evaluated by subtracting the range derived by taking into account the pulses propagation between transmission and reception of pulses from spacecraft altitude

with respect to the surface (i.e. orbital range-Titan mean radius) satellite orbital range to target.

Moreover, the tool allows the simulation of the performances and the waveform analysis of the *Cassini* Radar Altimeter. The SLT intermediate files and results are stored into the local dedicated workstation where procedure is running, or into the local archive if data shall be shared with other tools.

The SLT results are used subsequently by the ABDR Production Tool to generate the ABDR file. The SLT also generates automatically a text file containing all relevant information on SLT processing outputs and plots of main results, to be stored into the local archive in order to be submitted to the scientific community for further validation of data.

Users may export (i.e. print/save) Plot files containing results produced by SLT, e.g. relevant processing parameters, MLE procedure results, relative elevations of Titan's surface vs. along-track distance (i.e. topographic profiles), altimeter waveforms vs. range bins, ancillary data (e.g. observation geometry and orbital parameters vs. time, instrument data, etc.), surface parameters vs. along-track distance, etc.

The general set of Input/Output Variables of SLT Tool is reported in the following table:

Input	
Name	***Format***
Intermediate data file	*Binary format data file* *ASCII Format Data File*
Output	
SLT file results	*Binary format data file*

Table 2.3 Input and Output variables of the SLT

SLT Results files are automatically produced for both ALTH/AHAG operating modes. In particular, the SLT Results files contain:

- Real/Simulated IR: the real impulse response is that calculated by averaging the range compressed data coming from the intermediate BODP file. The simulated Impulse Response obtained by implementing the models described in **3.3** section
- Pulse Centroid Position estimate: the value of the centroid position obtained by the MLE algorithm explained in the **2.4.D** section
- Titan Surface Roughness estimate: the value of the titan surface roughness (σ_s).
- Surface slope: the value of the surface slope obtained by computing the derivative of the estimated heights

- Topographic profile: the final altitudes computed from values obtained with the MLE algorithm
- Range to target: the final estimated distance from the spacecraft to the Titan's surface
- rtt_std: estimated standard deviation of the residual error in the *range to target* measurement
- Altimeter profile range start
- Altimeter profile range step
- Altimeter profile length

A diagram that contains the main PT functionalities is presented in the following:

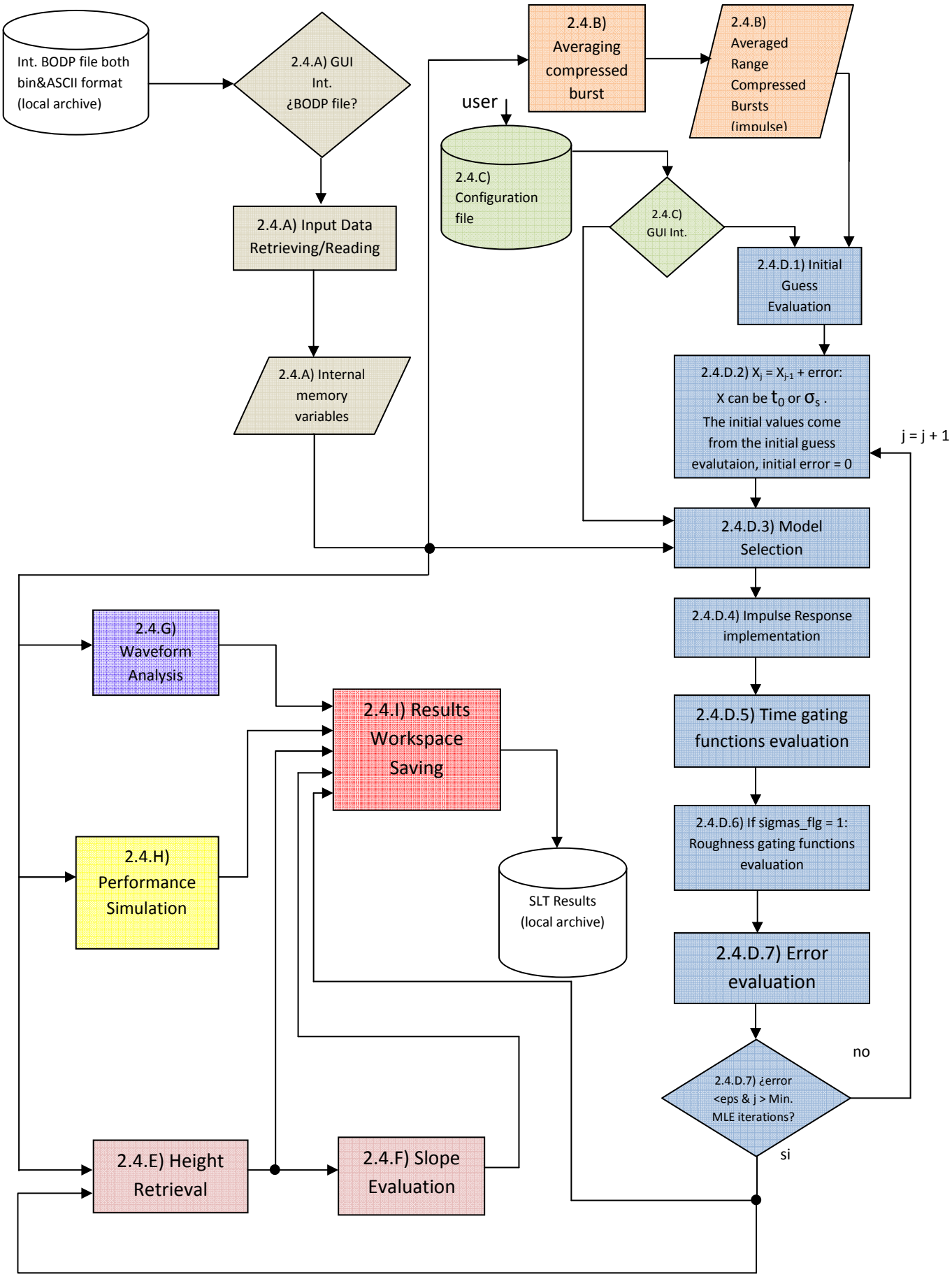

Figure 2.7 Flux Diagram of the SLT

In the following pages will be described the different blocks that need to be commented with more detail:

2.4.A) Input Data Retrieving/Reading

Starting from the intermediate BODP file, produced by the ABDR PT and selected by user, this functionality reads all the data fields and stores them into the local dedicated workstation. The procedure is similar to that of the section **2.3.A.**

The whole inputs/outputs of this function are listed in the following:

- *Input*: Intermediate BODP's data files in both binary and ASCII formats.
- *Outputs*: Internal memory variables (table **2.2**)

2.4.B) Averaging compressed burst

The N_B compressed pulses within the burst are averaged so that each compressed burst becomes an array given by only one averaged pulse-compressed echo. The averaged range compressed burst is stored in an internal memory bi-dimensional array.

The whole inputs/outputs of this function are listed in the following:

- *Input: range_proc*: bidimensional array of floating point double precision containing range compressed burst.
- *Output: data*: an array containing averaged range compressed burst.

The process is performed in the following way:

The acquired samples $\underline{x} = (x_1, \dots, x_N)$, due to the multiplicity of the scattering elements (each acquired sampled is considered as the sum of the contribution of multiple scattering elements), may be approximated, taking into account the central limit theorem, as two complex Gaussian distributed variables: $X_i = Y_i + jZ_i$, and so, as it is commonly known if we calculate:

$$|X_i| = \sqrt{{Y_i}^2 + {Z_i}^2} \quad (2.4.\mathrm{B}.1)$$

the resulting process has a Rayleigh distribution. Now if we do $|X_i|^2 = D_i$, since the radar echo is typically processed after square law detection we obtain, as it is also known, an Exponential distributed process, with mean equal to the i-th sample of the radar averaged impulse response evaluated by using equations **2.4.D.4.2**, **2.4.D.4.3** or **2.4.D.4.4** that will be detailed in the following sections.

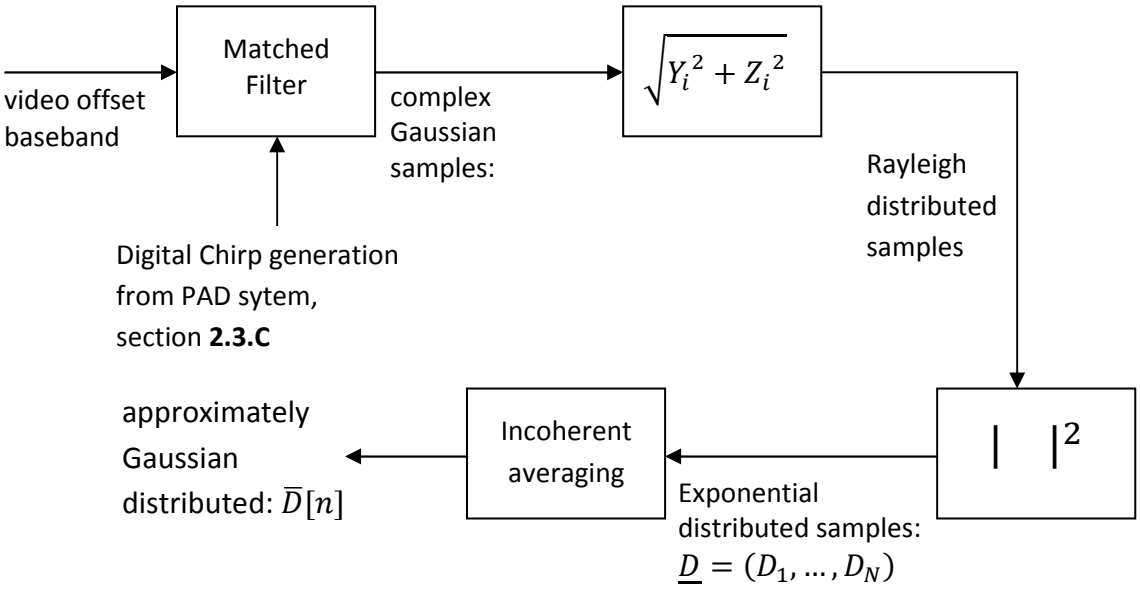

Figure 2.8 Block diagram of the process of the received echo signal in the Cassini PAD System

Each burst of N samples contains N_B pulses (typically 15 for the high resolution altimeter mode) that can be used to obtain a unique single pulse by performing an incoherent summation. This operation that reduces the speckled noise is done in the following way:

$$\underline{D} = (D_1, \dots, D_N) \xrightarrow[M=N/N_B]{\text{The burst is segmented into } N_B \text{ pulses}} \underline{\underline{D_{N_B \times M}}} = \begin{cases} \underline{D}_1 = D_1, \dots, D_M \\ \underline{D}_2 = D_{M+1}, \dots, D_{2M} \\ \vdots \\ \vdots \\ \underline{D}_{N_B} = D_{(N_B-1)M+1}, \dots, D_N \end{cases} \quad (2.4.\text{B}.2)$$

$$\bar{D}[n] = \frac{1}{N_B} \sum_{j=0}^{N_B-1} D_{jM+n} \qquad for\ 1 \le n \le M \quad (2.4.\text{B}.3)$$

As a result of this, the $\bar{D}_i$ averaged sample can be approximately viewed as Gaussian distributed, with:

$$E\{\bar{D}_i\} = E\{D_i\} = IR_i \quad (2.4.\text{B}.4)$$

$$VAR\{\bar{D}_i\} = \frac{VAR\{D_i\}}{N_B} = \frac{IR_i^2}{N_B} \quad (2.4.\text{B}.5)$$

In this way, since the average is performed in an incoherent way, the speckle that is overlapping to received echoes is reduced in a significant way.

The result of the averaging process is showed in the next figure:

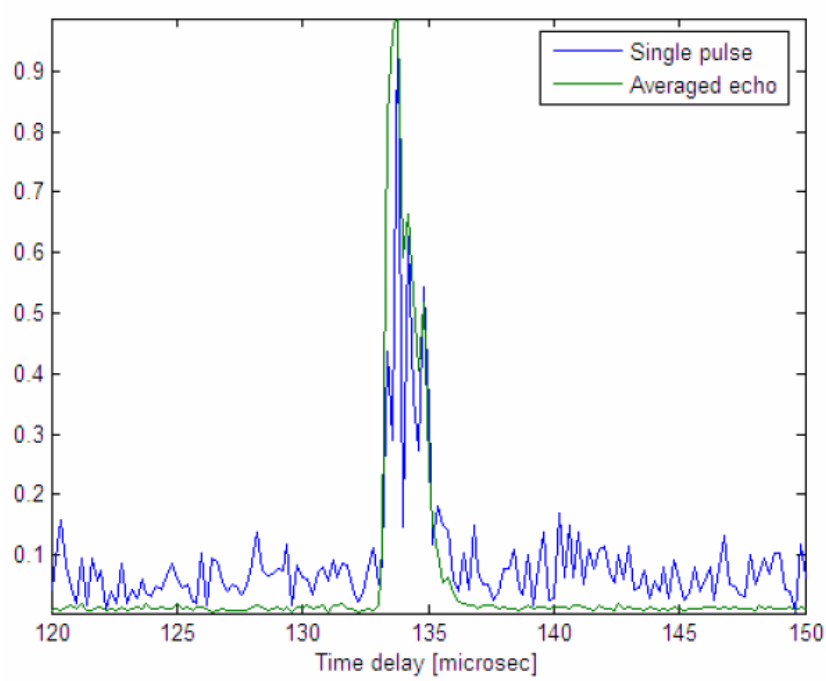

Figure 2.9 Averaged pulse produced for each burst

2.4.C) Configuration file

The SLT tool allows user to specify the default processing parameters by using the Configuration file. In particular the Configuration file will contain:

- Threshold value for off-Nadir angles: the values of the pointing angle on which the MLE estimator is based to switch among the different fitting models.
- Minimum number of MLE iterations: the value of the minimum iterations that the algorithm should perform before stopping
- Method for centroid initial value evaluation: the method selected to evaluate the initial values of the time delay
- Sigmas_flg: the flag used to indicate if the surface roughness estimation must be performed or not

All these parameters will be described in detail in the corresponding paragraphs.

2.4.D) Surface Parameters Estimation

This tool of the SLT provides statistically optimal estimates of the Titan's surface's significant parameters such as time delay (t_0) and roughness (σ_s).

This is achieved using an iterative Maximum Likelihood Estimator algorithm (MLE) by fitting the averaged compressed burst with a theoretical model describing the Radar Impulse Response.

In the following figure is presented the MLE algorithm:

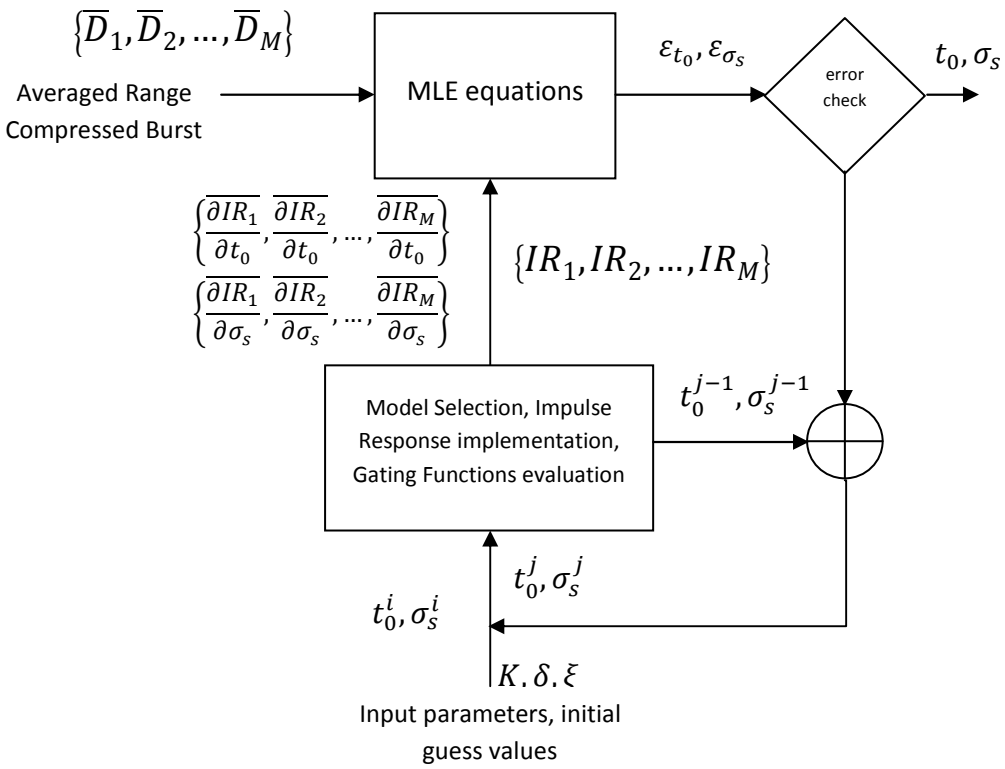

Figure 2.10 Algorithm for actual implementation of MLE

At each iteration the algorithm updates the variables with the errors coming from the previous loop. Then the models and the gating functions are evaluated using current estimated variables. Finally the new errors(*) in the estimation process are evaluated with the appropriate equation and, if they are greater than threshold value, the algorithm is executed once again, if not the algorithm finishes. At first iteration the variable's value come from the initial guess evaluation and the errors are initialized to 0. The process is repeated for each burst.

in the corresponding section **2.4.D.7 it will be explained in detail how it is evaluated the error produced by the estimation algorithm.*

The models, selected depending on the off-nadir value are:

- Nadir Model
- Off-Nadir Model derived by using Brown's asymptotical form of flat surface response
- Off-Nadir Model derived by using Prony's method

In the next paragraphs will be described all the subfunctions of this tool. The MLE concepts and its equations as well as a complete physical explanation of the three models are described in **3.2** and **3.3** annexes respectively.

2.4.D.1) Initial Guess Evaluation

To implement the iterative MLE algorithm is necessary to introduce the initial values of the variables of interest. It is known that the algorithm converges if the first attempt value of the parameter to estimate is close enough to the real value, if not, may converge towards a local or may not converge at all.

The "Method for centroid initial value evaluation" coming from the configuration file, selected by user, is used to allow the algorithm to select between the three different methods.

The whole input/outputs of this function are listed in the following:

- Inputs:
  - *impulse*: a floating point double precision array containing the averaged range compressed burst.
  - method for centroid initial value evaluation (from configuration file)
- Outputs:

Variables	*Structure*	*Value/Unit Reference*
imin		*Floating point double precision non negative value*
imin_i		*Floating point double precision non negative value*
ith		*Floating point double precision non negative value*
dur		*Floating point double precision non negative value*
disp		*Floating point double precision non negative value*
amp		*Floating point double precision non negative value*
impulso	*[Array]*	*Floating point double precision*

Table 2.4 Initial Guess Evaluation outputs

Initial Guess Evaluation Algorithm. Output Variables:

- *imin*: pulse centroid position derived as centre of gravity.
- *imin_i*: pulse centroid position derived by integral formulation.
- *i_th*: pulse centroid position derived by threshold formulation.
- *dur*: pulse duration.
- *amp*: pulse amplitude.
- *disp*: pulse dispersion.
- *impulso*: an array containing the averaged range compressed burst reduced by Noise Estimation Power.

The algorithm that provides the initial values of the estimation is described in the following:

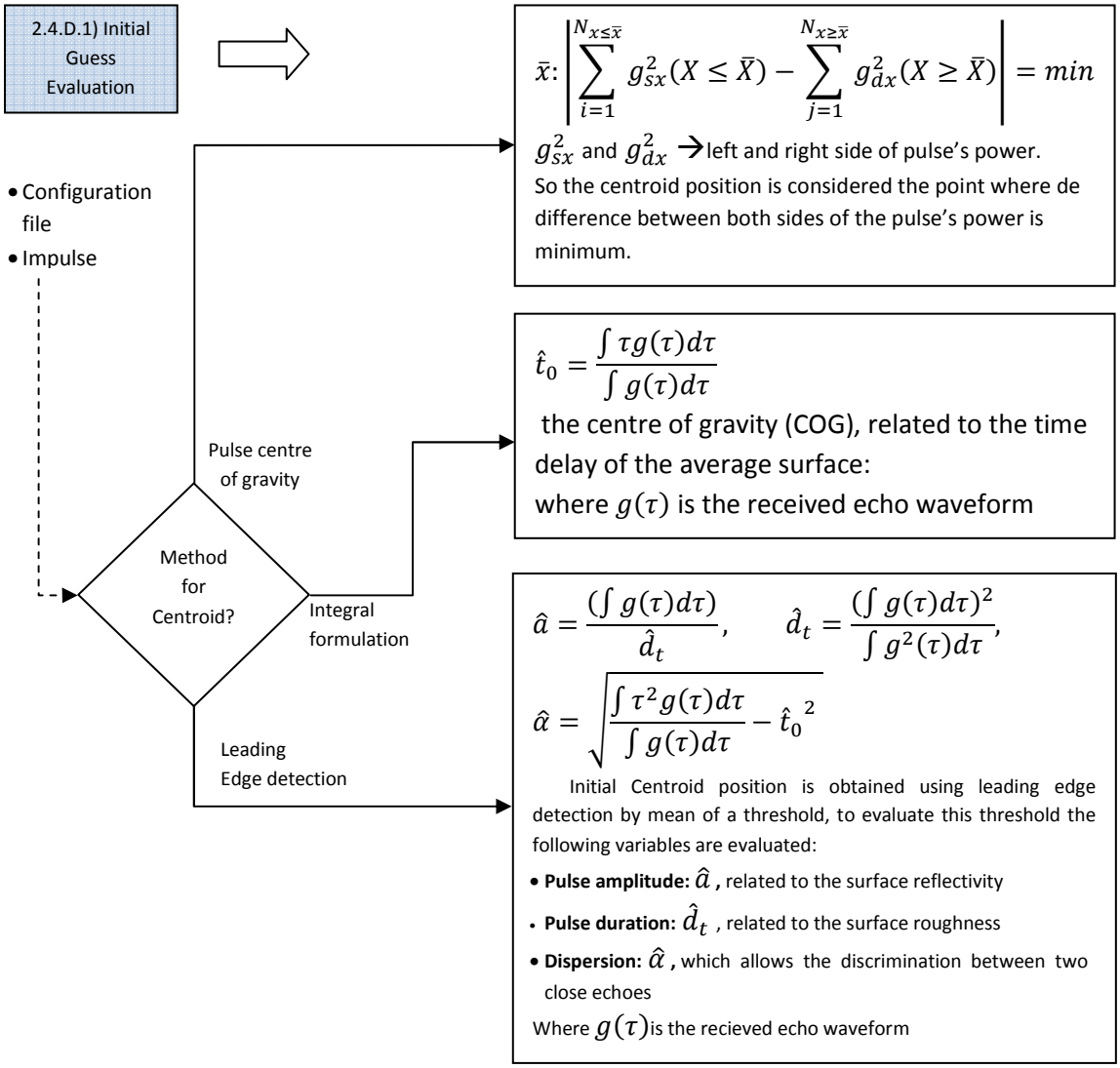

Figure 2.11 Algorithm for actual evaluation of initial guess evaluation

In order to obtain the order of magnitude of the variance in the estimate of the COG position, these subsequent steps have been followed:

- burst #14364 from Ta fly-by has been selected
- simulated waveform has been obtained by adding a white Gaussian thermal noise to the model, see figure **2.12**
- the average of the 15 pulses within the burst has been performed in order to reduce the noise in individual pulses
- the ML estimator has been run N times, see figure **2.13**
- the variance (in pixels) of the N estimates of the centroid position has been evaluated.

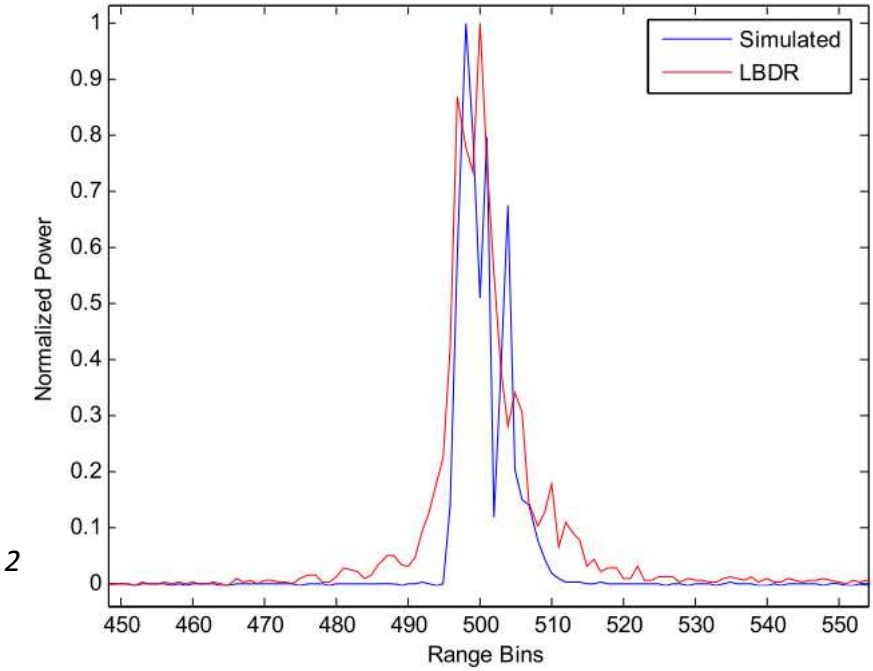

2

Figure 2.12 Fitting between simulated and real echo waveforms (ξ=0.23°, h =5500 km)

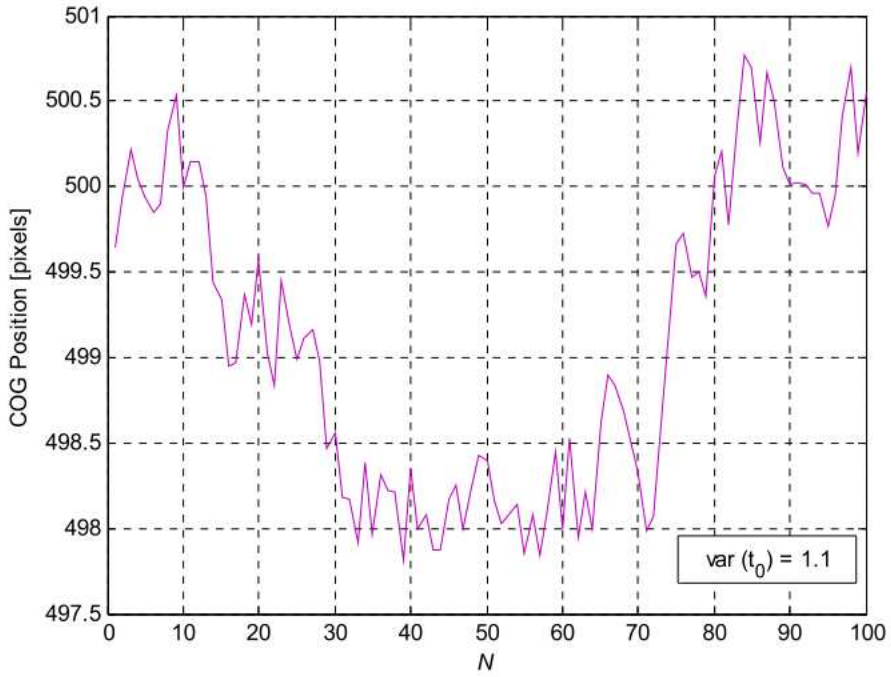

Figure 2.13 Estimations of COG position over N=100 runs (burst # 14364)

2.4.D.3) Model Selection

The best theoretical model to use is selected by reading the off-nadir angle value. Starting from experimental results, threshold values are defined for off-Nadir angle. If the off-Nadir value is between the specified intervals, the algorithm will be able to select one model to fit in the *Cassini* data rather than the others.

In the following will be described the procedure followed to determine the threshold values of each model depending on the mean integral relative error (MIRE), which has

been chosen as the full indicator of the goodness of the model, as a function of off-Nadir angle:

To this aim the errors introduced by the different models with respect to the theoretical impulse response are evaluated. The theoretical impulse response is performed with the convolution of **3.3.1.13** and **3.3.2.4** (see **3.3** annex):

$$IR_{Theo}(\tau) = \int_{0}^{+\infty} P_{FS}(t) P_{HI}(\tau - t) dt \qquad (2.4.\mathrm{D}.3.1)$$

which is computed numerically.

For example, with reference to the main system parameter of the following table:

Frequency	*13,78 GHz*
Antenna beamwidth ($\boldsymbol{\theta_{3dB}}$) *(6.1mrad)*	*0.350 deg*
Sampling frequency ($\boldsymbol{f_c}$)	*5 MHz*
Chirp length ($\boldsymbol{T}$)	*150 μs*
Chirp bandwidth ($\boldsymbol{B}$)	*4.25 MHz*
Range (vertical) resolution ($\boldsymbol{\rho}$)	*35.3 m*

Table 2.5 Main parameters for the Hi-Res Cassini Altimeter

and by considering a 5000 Km spacecraft's altitude and a 0.15° off-nadir angle, next figure shows the corresponding normalized theoretical impulse response:

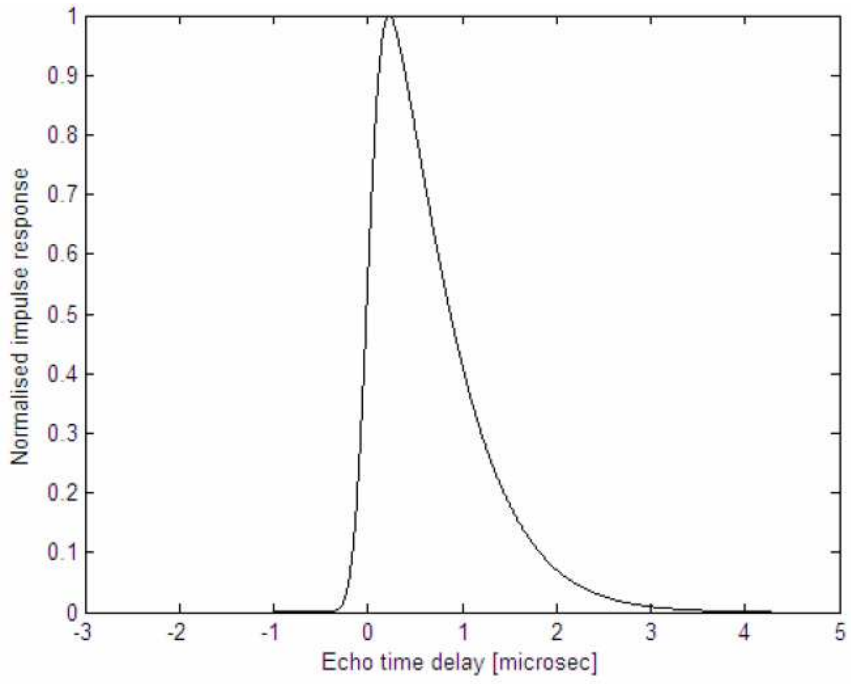

Figure 2.14 Theoretical impulse response (H=5000 Km, ξ=0.15°)

Then the errors introduced by the different models are calculated with respect to the theoretical impulse response. The next figure shows the relative errors, in percentage, for all models:

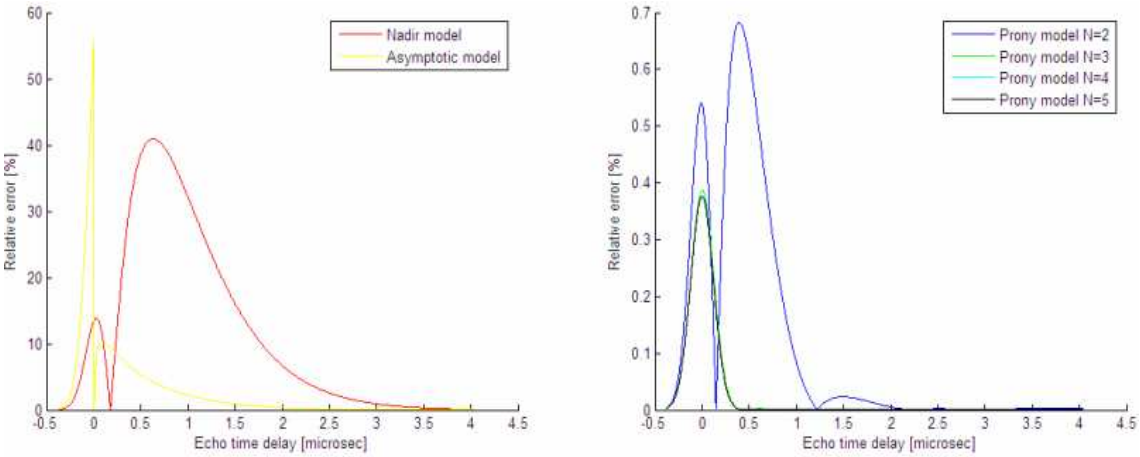

Figure 2.15 Relative errors for all models (H=5000 Km, ξ=0.15°)

This figure proves that even for low values of off-Nadir angle, Nadir model cannot be used while Prony's model gives negligible errors also with few terms (N=2,N=3). Starting with this figure we can plot the MIRE (Mean Integral Relative Error), as a function of off-Nadir angle, for all different models, this is the integral value of the relative errors averaged over the time interval where the theoretical normalized impulse response is significant (>1e-3):

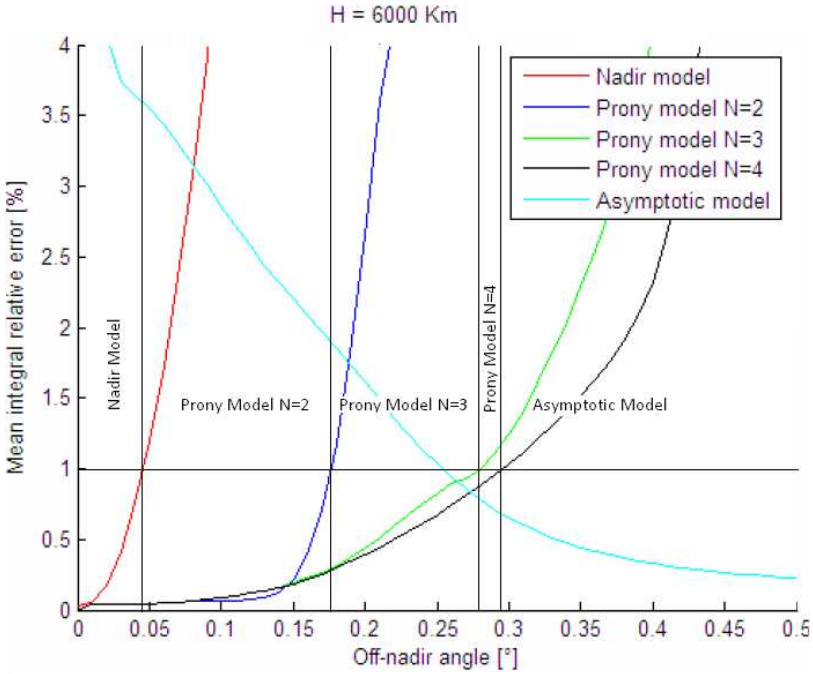

Figure 2.16 Mean integral relative error for all models as a function of off-nadir angle (H=6000 Km)

This figure can be used to fix threshold values for switching among models, by using the crossing point between the different models. In fact the evaluated threshold values and the corresponding model to be used are determined to ensure, in the worst case, a MIRE less than about 1%.

The final selected threshold values are listed in the following table:

Threshold off-nadir angle [deg]	*Model to be used*
$0 < \xi < 0.04$	*Nadir*
$0.04 \leq \xi < 0.16$	*Prony's N=2*
$0.16 \leq \xi < 0.26$	*Prony's N=3*
$0.26 \leq \xi < 0.29$	*Prony's N=4*
$\xi \geq 0.29$	*Asymptotic*

Table 2.6 Threshold values for off-nadir angle and corresponding model for assuring a MIRE < 1 %

Finally it is worth nothing that error's models (MIRE in this case) are almost independent of spacecraft altitude, at least in the *Cassini* altimeter operative range as it shows the next figures:

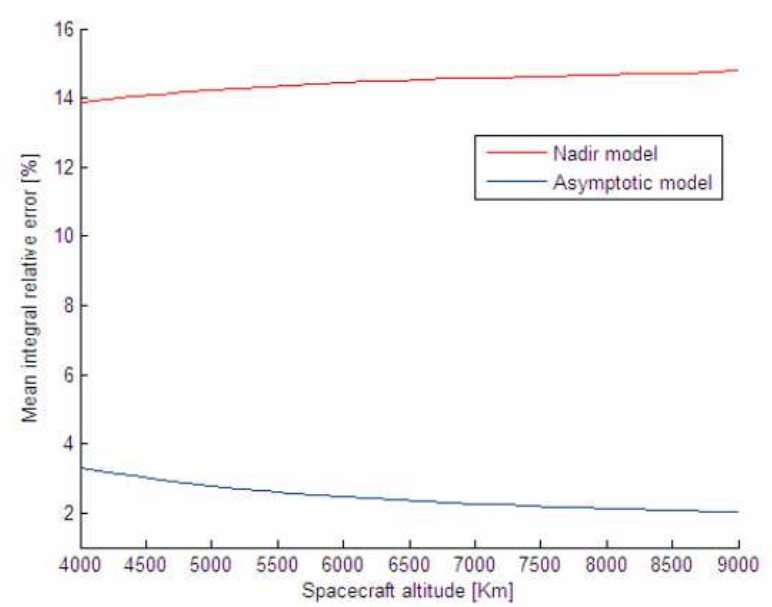

Figure 2.17 Mean integral relative error for Nadir and Asymptotic models as a function of spacecraft altitude (ξ =0.15°)

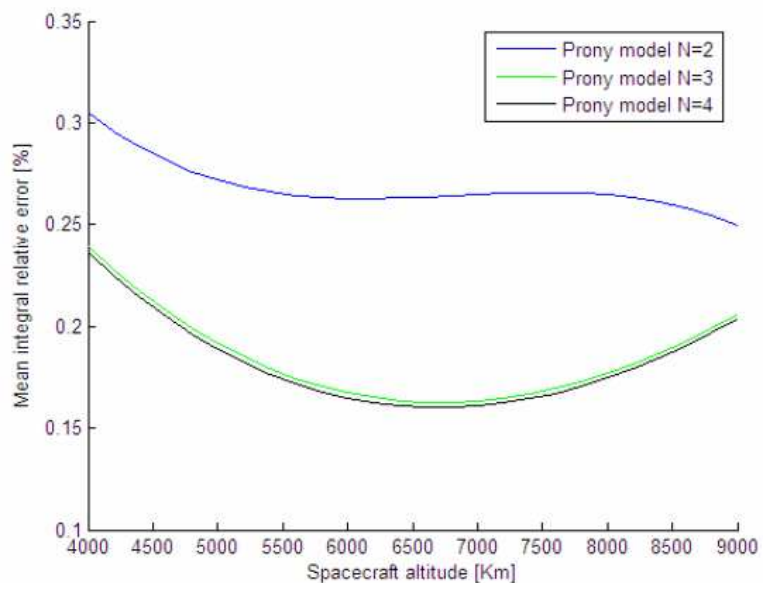

Figure 2.18 Mean integral relative error for Prony's model as a function of spacecraft altitude (ξ =0.15°)

The whole input/outputs of this function are listed in the following:

- *Inputs:*
  - threshold values for off-Nadir values (from configuration file).
  - zita: a floating point double precision (non negative value) containing the off-Nadir angle in rad.
  - nadir_flg: a short integer used to select the model. Value [0,1].
  - prony_flg: a short integer used to select the model. Value [0,1].

- *Outputs*: *modello* (selected theoretical model).

So the procedure followed to select the best theoretical model is described in the following:

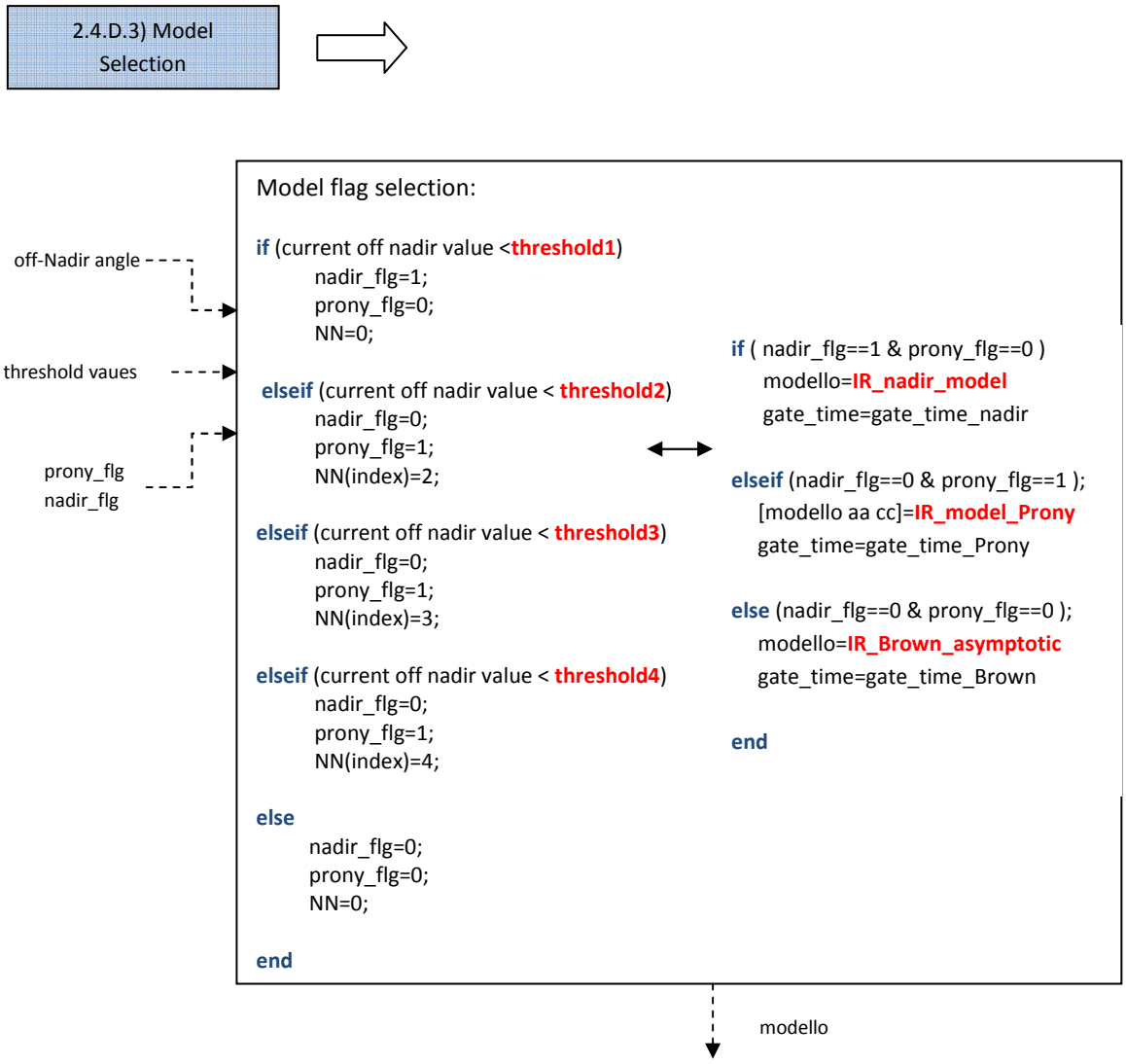

Figure 2.19 Pseudocode used for the Model Selection

2.4.D.4) Impulse Response implementation

The likelihood maximization condition becomes, see section **3.2**:

$$\frac{\partial f\left(\overline{D}[n]\middle|\underline{\theta}\right)}{\partial \underline{\theta}} \equiv \begin{cases} \sum_{i=1}^{M} \frac{\overline{D}_i - IR_i}{IR_i^2} \overline{\frac{\partial IR_i}{\partial t_0}} \\ \sum_{i=1}^{M} \frac{\overline{D}_i - IR_i}{IR_i^2} \overline{\frac{\partial IR_i}{\partial \sigma_s}} \end{cases} \qquad (2.4.\,\mathrm{D}.\,4.1)$$

where IR_i is the analytical impulse response $\overline{D}_i$ the averaged samples and $\underline{\theta}$ the set of parameters to be estimated.

Then the impulse response IR, needed to perform the MLE becomes, depending on the selected model:

Nadir Model: as noted in **3.3.2.7**

$$IR|_{Nadir} = \frac{G_0^2 \lambda^2 c}{2(4\pi)^2 L_p h^3} P_T B T \sigma_p \pi \sigma_0 \frac{1}{2} \exp\left(\frac{\delta^2}{2}\right) \exp\left(-\frac{\delta}{\sigma_c}\tau\right) * \\ * \left[1 + erf\left(\frac{\tau}{\sqrt{2}\sigma_c} - \frac{\delta}{\sqrt{2}}\right)\right] \qquad (2.4.\,\mathrm{D}.\,4.2)$$

starting from the variables in the following table **2.7** the algorithm implements this equation.

Asymptotic Brown Model: as noted in **3.3.3.6**

$$IR|_{Asymp} = \frac{G_o^2 \lambda^2 c}{2(4\pi)^3 L_p h^3} \sigma^0 \exp\left(-\frac{4}{\gamma(1+\varepsilon^2)} (\sin\xi - \varepsilon\cos\xi)^2\right) * \\ * \sqrt{\frac{2\pi}{a+2b}} \sigma_p \left[1 + erf\left(\frac{\tau}{\sqrt{2}\sigma_c}\right)\right] \qquad (2.4.\,\mathrm{D}.\,4.3)$$

starting from the variables in table **2.7** the algorithm implements this equation.

Prony's Method Model: as noted in **3.3.4.6**

$$IR|_{Prony} = K\sigma_0 \frac{1}{2} \exp\left(-\frac{4}{\gamma}\sin^2\xi\right) \sum_{i=1}^{N} C_i \exp\left(\frac{{\delta_i}^2}{2} - \frac{\delta_i}{\sigma_c}\tau\right) * \\ * \left[1 + erf\left(\frac{\tau}{\sqrt{2}\sigma_c} - \frac{\delta_i}{\sqrt{2}}\right)\right] \qquad (2.4.\,\mathrm{D}.\,4.4)$$

starting from the variables in table **2.7** the algorithm implements this equation.

see **3.3 section for comprehensive understanding of the equations exposed above.*

The whole inputs/output of this subfunction are listed in the following:

- *Inputs:*

Variables	*Structure*	*Value/Unit Reference*
t	*[Array]*	*Floating point double precision [s]*
t_0		*Floating point double precision [s]*
H		*Floating point double precision. Non negative value [m]*
Radius		*Short integer. Non negative value [m]*
sigma_h		*[m]*
sigma_p		*Floating point double precision. Constant value [m]*
gamma		*Floating point double precision. Adimensional Constant*
c		*Floating point double precision. Constant value [m]/[s]*
zita		*Floating point double precision. Non negative value[rad]*
B		*Floating point double precision [Hz]*
sigma_c		*Floating point double precision [s]*
NN		*Short Integer Min: 1;Max:4*

Table 2.7 Inputs of the Impulse Response Implementation.

In the following each variable will be described with more detail:

- t: an array containig the time reference, needed when we need to implement the impulse response since $\tau = t - t_0 = t - 2h/c$.
- t_0: Time Delay for propagation Radar-Target-Radar.
- *H:* this value is the Satellite Range to Target.
- *Radius:* The Titan Mean equatorial radius.
- *sigma_h:* In this variable will be stored the value of Titan's surface roughness: $\sigma_h = (c/2)\sigma_s$.
- *sigma_p*: Parameter related to point target 3 dB width. It is needed when we need to implement the impulse response, since ${\sigma_c}^2 = {\sigma_s}^2 + {\sigma_p}^2$. Typically $\sigma_p = T/\sqrt{8\ln 2}$.
- *gamma*: Parameter related to point target 3dB width. Referred as γ in **3.3** section $(\gamma = -2\sin^2(\theta_{3dB}/2)\,/\ln(0.5))$. As can be seen in table **2.5:** $\theta_{3dB} = 0.350 \text{ deg } (6.1\text{mrad})$.
- *c*: speed of light.
- *zita*: This variable stores the value of the off-nadir angle, it is necessary in order to implement the impulse response. Referred as ξ in **3.3** section.
- *B*: Chirp band, needed to implement the impulse response.
- *sigma_c*: Total spreading of the average echo. This value is needed in order to implement the impulse response.
- *NN*: Index of Prony's approximation order, also needed in order to implement the impulse response, minimum_value: 1, maximum_value: 4.

➢ *Outputs:*

Variables	Structure	Value/Unit reference
IR_nadir	*[Array]*	*Floating point double precision*
IR_Brown	*[Array]*	*Floating point double precision*
PFS_Brown_approx	*[Array]*	*Floating point double precision*
IR	*[Array]*	*Floating point double precision*
aa	*[Array]*	*Complex Double Precision*
cc	*[Array]*	*Complex Double Precision*

Table 2.8 Outputs of the Impulse Response implementation.

Where:

- *IR_Nadir*: This variable is an array containing the impulse response for nadir pointing angles. It will be used in the next section to implement the Gating functions.
- *IR_Brown*: This variable is an array containing the impulse response for far off-Nadir mispointing angles. It will be used in the next section to implement the Gating functions.
- *PFS_Brown_approx*: an array containing the Approximate Flat Response obtained by Prony's method.
- *IR:* this variable is an array containing the impulse response for small mispointing angles. It will be used in the next section to implement the Gating functions.
- *aa*: this variable is an array containing the a_i Prony coefficient as explained in annex **3.3**
- *cc*: this variable is an array containing the C_i Prony coefficient as explained in annex **3.3**

2.4.D.5) Time Gating functions evaluation

As can be seen in previous section, in order to perform the MLE algorithm and thus, to estimate the Centroid position, it is necessary to implement the derivative of the chosen model with respect to t_0, this is the time gating function.

The mathematical concepts followed to evaluate the above mentioned time gating functions can be found in **3.4** annex.

In the following is described the procedure followed to implement the time gating functions, in order to evaluate the error in the algorithm's next step. The time gating functions are evaluated every time the algorithm is executed.

The whole inputs/output of this subfunction are listed in the following:

➢ *Inputs*:

Variables	Structure	Value/Unit Reference
t	*[Array]*	*Floating point double precision [s]*
tauzero_ML		*Floating point double precision [s]*
sigma_h		*Short Integer. Non negative value [m]*
B		*Floating point double precision. Non negative value [Hz]*
modello		*Floating point double precision*

gamma	*Floating point double precision. Adimensional Constant*
H	*Floating point double precision. Non negative value [m]*
Radius	*Short Integer. Non negative value [m]*
c	*Floating point double precision. Constant value [m]/[s]*
zita	*Floating point double precision. Non negative value [deg]*
NN	*Short Integer Min: 1;Max:4*
nadir_flg	*Short Integer Value [0,1]*
prony_flg	*Short Integer Value [0,1]*
table 2.8	*Variables listed in **table 2.8***

Table 2.9 Inputs of Time Gating functions evaluation

Where:

- *tauzero_ML*: In this variable the value of the estimated Time Delay for propagation Radar-Target-Radar is stored.
- modello: output variable from **2.4.D.3** Model selection used to choose among the three different models.

**all other variables have already been explained in previous sections.*

- Outputs: *gate_time*: a floating point double precision array containing Time Gating Functions of selected model.

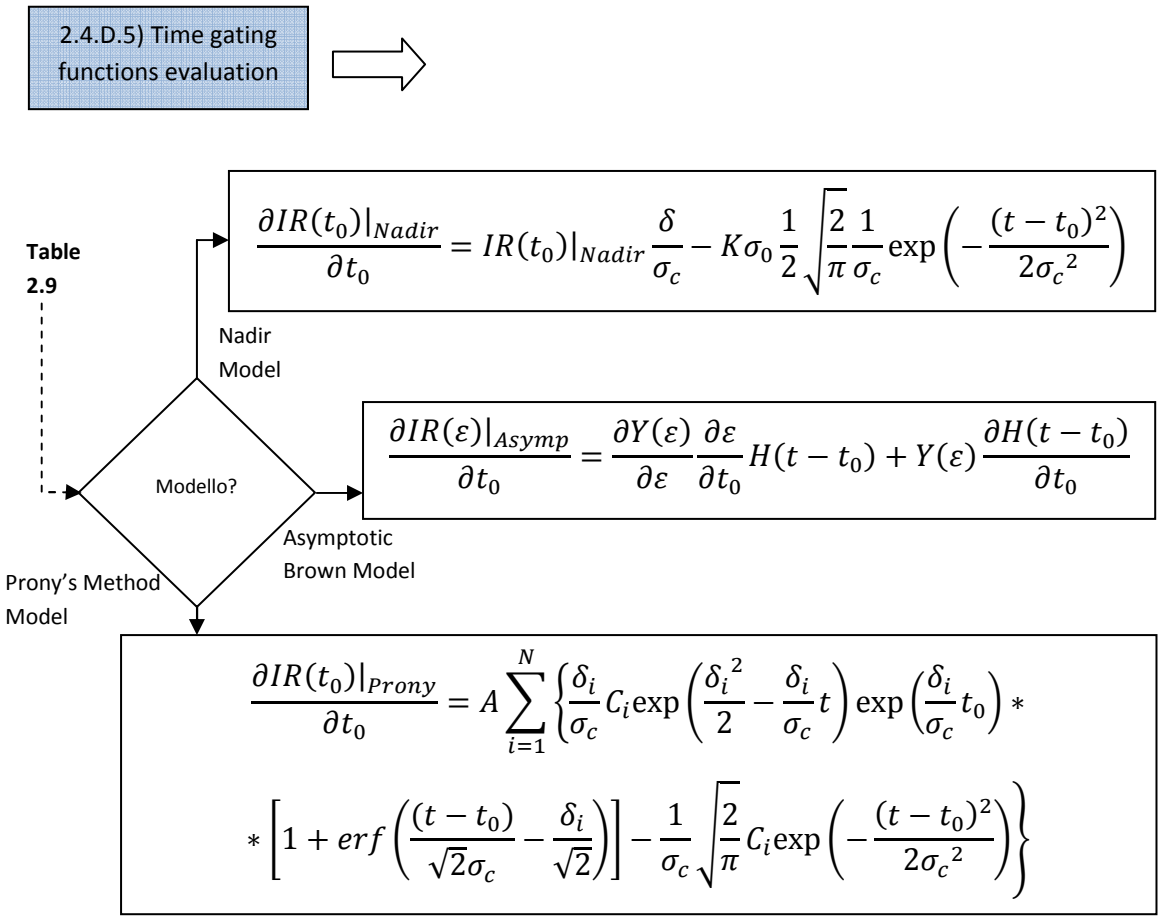

Figure 2.20 Procedure for actual evaluation of Time Gating functions

see **3.4 section for comprehensive understanding of Gating functions exposed above.*

Starting with the variables listed in table **2.9** the algorithms implements one of these functions depending on the value of the variable "modello".

2.4.D.6) Roughness gating functions evaluation

As can be seen in **2.4.D.4**, in order to perform the MLE algorithm and thus, to estimate Titan's surface roughness, it is absolutely necessary to implement the derivative of the chosen model with respect to σ_s, this is the roughness gating function. The mathematical concepts followed to evaluate the above mentioned roughness gating functions can be found in **3.4** annex.

In the following paragraphs is described the procedure followed to implement the roughness gating functions, in order to evaluate the error in the algorithm's next step. The roughness estimation process shall be activated by dedicated flag value, namely *sigmas_flg,* settled by user using the configuration file. Only if sigmas_flg = 1 the roughness gating functions are evaluated

The whole inputs/output of this subfunction are listed in the following:

- Inputs**:** *sigmas_flg*, a short integer containing Roughness flag, Value [0,1], and variables listed in table **2.9**
- Outputs**:** *gate_sigmas*, a floating point double precision array containing Roughness Gating Functions of selected model.

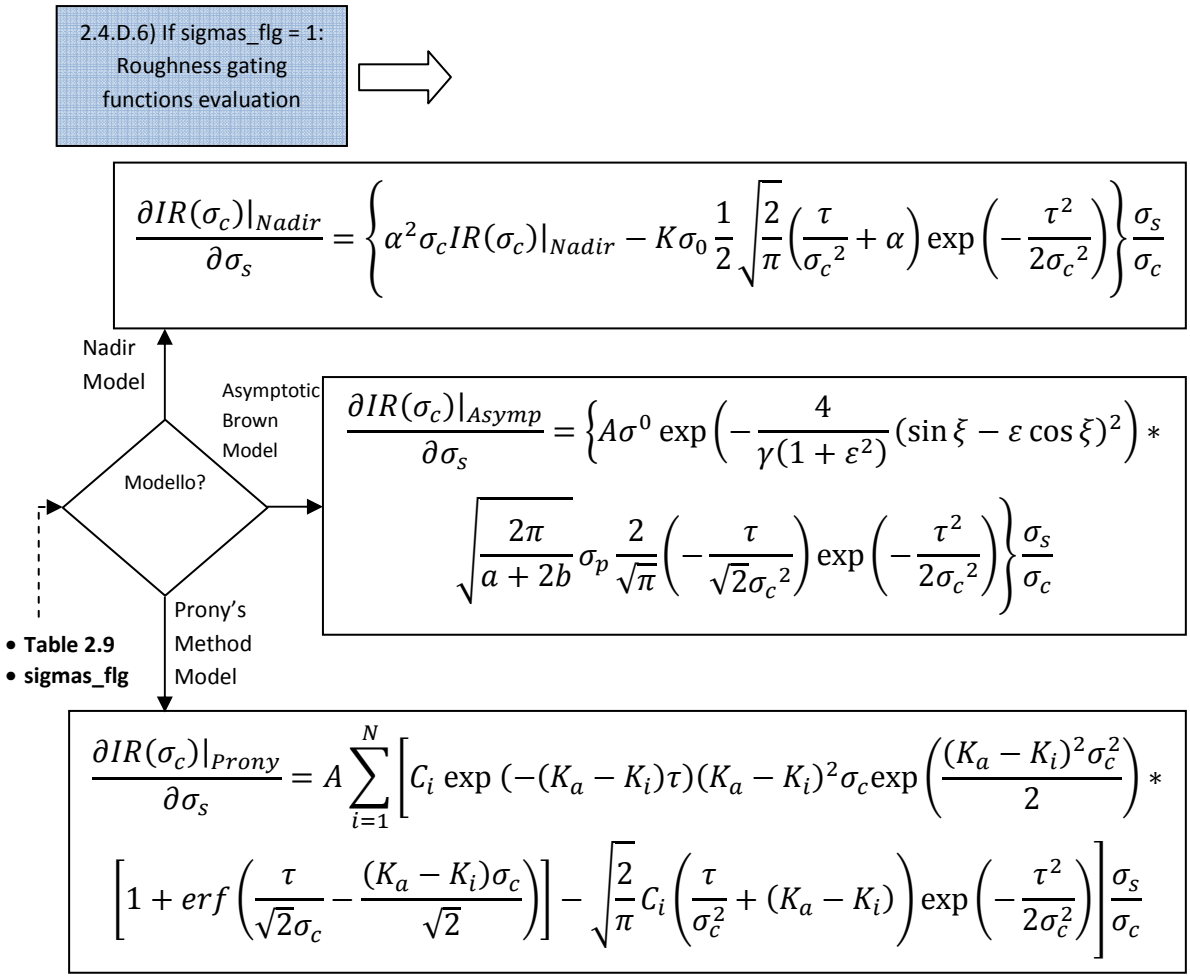

Figure 2.21 Procedure for actual evaluation of Roughness Gating functions

see **3.4 section for comprehensive understanding of Gating functions exposed above.*

Starting with the variables listed above the algorithm implements one of these functions depending on the value of the variable "modello".

2.4.D.7) Error evaluation

As can be seen on **3.2** annex the ultimate goal of the algorithm is to accomplish the following condition (in an ideal case):

$$\frac{\partial f\left(\overline{D}[n]\middle|\underline{\theta}\right)}{\partial \underline{\theta}} \equiv \begin{cases} \sum_{i=1}^{M} \frac{\overline{D}_i - IR_i}{IR_i^2} \overline{\frac{\partial IR_i}{\partial t_0}} \\ \sum_{i=1}^{M} \frac{\overline{D}_i - IR_i}{IR_i^2} \overline{\frac{\partial IR_i}{\partial \sigma_s}} \end{cases} = 0 \qquad (2.4.\mathrm{D}.7.1)$$

or at least to achieve the minimum value as possible. To this end the error is defined as:

2.4.D.7) Error evaluation ⟹

$$error = \begin{cases} \sum_{i=1}^{M} \frac{\overline{D}_i - IR_i}{IR_i^2} \overline{\frac{\partial IR_i}{\partial t_0}} \\ \sum_{i=1}^{M} \frac{\overline{D}_i - IR_i}{IR_i^2} \overline{\frac{\partial IR_i}{\partial \sigma_s}} \end{cases} \qquad (2.4.\mathrm{D}.7.2)$$

where $\overline{\partial IR_i}/\partial t_0$ and $\overline{\partial IR_i}/\partial \sigma_s$ are the time and roughness gating functions respectively, both detailed on **3.4** annex section and used as inputs in this step.

So at each iteration the error is evaluated using the current values of t_0 and σ_s, updated on the first step of the algorithm, and if error is smaller than threshold value and "j" (number of loops executed by the algorithm) is greater than N_iter (minimum number of MLE iterations coming from the configuration file) the algorithm is interrupted and the current values of the variables of the estimation process are stored into an internal memory. If not the algorithm is repeated until both conditions are true (or until the number of iterations is so big that it is assumed that the algorithm won't converge at all), and the new values of t_0 and σ_s are updated using the following method:

$$X_j = X_{j-1} + error \qquad (2.4.\mathrm{D}.7.3)$$

where X can be t_0 or σ_s, the initial values as said previously come from the initial guess evaluation and the initial error = 0.

The whole inputs of the Error evaluation are listed in the following:

- Inputs:
  - *gate_sigmas*: a floating point double precision array containing Roughness Gating Functions of selected model $\left(\overline{\partial IR_i}/\partial \sigma_s\right)$.

- *gate_time*: a floating point double precision array containing Time Gating Functions of selected model $\left(\overline{\partial IR_i}/\partial t_0\right)$.
- *impulse*: a floating point double precision array containing the averaged range compressed burst $\left(\overline{D}[n]\right)$.
- Variables listed in table **2.8**, mainly the impulse response (IR).
- *tauzero_ML*: already detailed
- *sigma_h*: already detailed

The whole outputs of the Surface Parameters Estimation tool are listed in the following:

Variables	*Structure*	*Value/Unit Reference*
tauzero_ML_1step	*[Array]*	*Floating point double precision [s]*
error_min_tau	*[Array]*	*Floating point double precision [s]*
amp_ML_1step	*[Array]*	*Floating point double precision*
error_min_amp	*[Array]*	*Floating point double precision*
modello_fin_1step	*[Array]*	*Floating point double precision*
tauzero_ML_2step	*[Array]*	*Floating point double precision [s]*
amp_ML_2step	*[Array]*	*Floating point double precision*
error_min_amp_2step	*[Array]*	*Floating point double precision*
error_min_tau_2step	*[Array]*	*Floating point double precision [s]*
error_min_sigma_h_2step	*[Array]*	*Floating point double precision [m]*
modello_fin_2step	*[Array]*	*Floating point double precision*
sigmas_ML	*[Array]*	*Floating point double precision [m]*
rtt_std		*Floating point double precision [m]*

Table 2.10 Outputs of the Surface Parameters Estimation Tool

In the following each variable will be described with more detail:

- *tauzero_ML_1step*: a floating point double precision array containing MLE estimated centroid position after 1st loop.
- *error_min_tau:* a floating point double precision array containing MLE convergence errors.
- *amp_ML_1step:* a floating point double precision array containing MLE estimated amplitude after first loop.
- *error_min_amp:* a floating point double precision array containing MLE convergence errors.
- *modello_fin_1step:* a floating point double precision array containing theoretical selected model after first loop.
- *tauzero_ML_2step:* a floating point double precision array containing MLE estimated centroid position after 2nd loop.
- *amp_ML_2step:* a floating point double precision containing MLE estimated amplitude after 2nd loop.

- *error_min_amp_2step:* a floating point double precision array containing MLE convergence errors.
- *error_min_tau_2step:* a floating point double precision array containing MLE convergence errors.
- *error_min_sigma_h_2step:* a floating point double precision array containing MLE convergence errors.
- *modello_fin_2step:* a floating point double precision array containing theoretical selected model after second loop.
- *sigmas_ML:* a floating point double precision array containing MLE estimated roughness
- *rtt_std:* a floating point double precision array containing Estimated standard deviation of the residual error in the range_to_target measurement. This is required for PT ABDR production functionality

2.4.D.8) Parameters estimation: final considerations

An example of fitting of *Cassini* LBDR data from Ta fly-by (burst #14331) with the Prony's Method model described in **3.3.4** is reported in the following. The ML estimator is initialized with the values of COG position (i.e. $\hat{t}_0 * f_c = 500$).

The analytical values used at first attempt ensure the convergence within a limited number of steps.

The results of the iterative cycle are shown in the following figures for the first and the last step of the process, respectively:

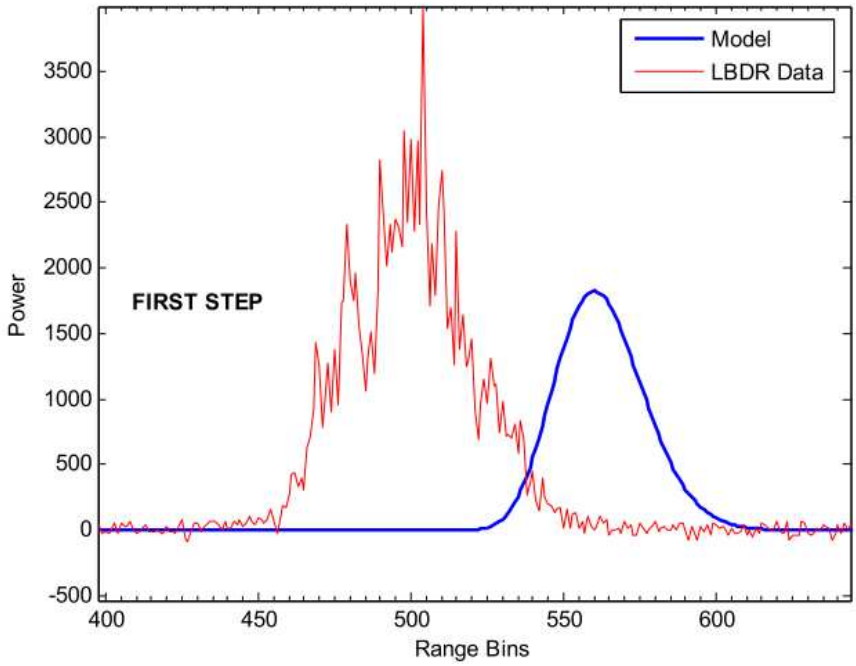

Figure 2.22 MLE first step (ξ=0.8908°, h =5083.2 km)

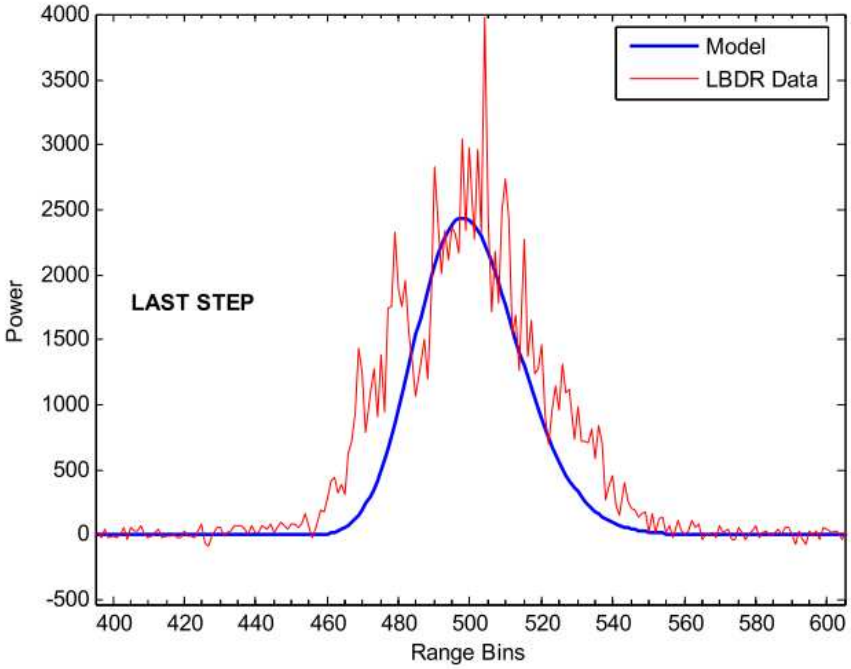

Figure 2.23 MLE last step (ξ=0.8908°, h =5083.2 km)

An example of fitting of real data from Ta fly-by (burst #14364), after the application of the MLE algorithm, with both nadir and off-nadir Prony's method models is reported in next figure, in order to evidence the differences in between:

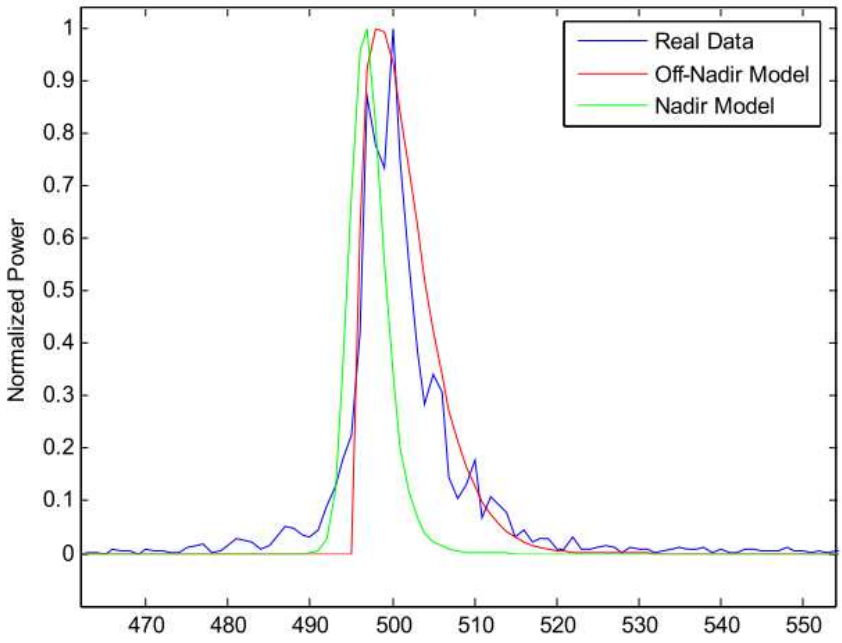

Figure 2.24 Fitting of models with LBDR data (ξ=0.23°, h=5500km)

The errors in best fitting process trend asymptotically to zero, as showed in the following figure, in fact a typical process of convergence requires a number of iterations not greater than 10:

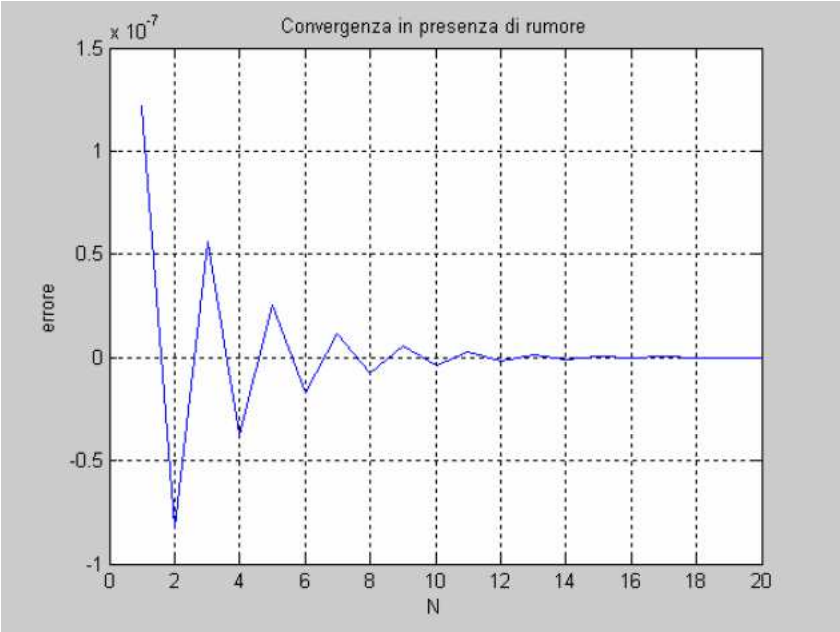

Figure 2.25 MLE Best fitting process: error convergence. (It is evident that at iteration 10th the error is practically zero)

However, sporadically the following anomalies have been identified into the *Cassini* range compressed pulse:

- Echoes spreading (see figure **2.26**)
- Double peaks into the 3dB pulse band (see figure **2.27**)
- Secondary lobes (see figure **2.27**)

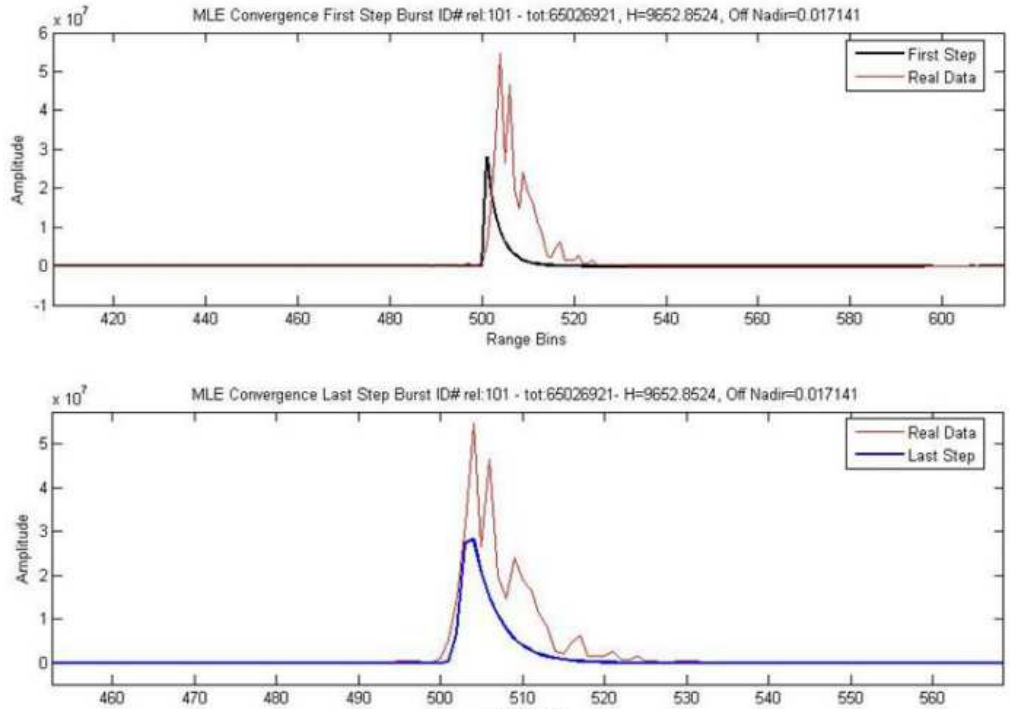

Figure 2.26 Example of fitting impulse spreader. It is possible to note that theoretical models is not able to fit the pulse (which is "larger" than the theoretical one)

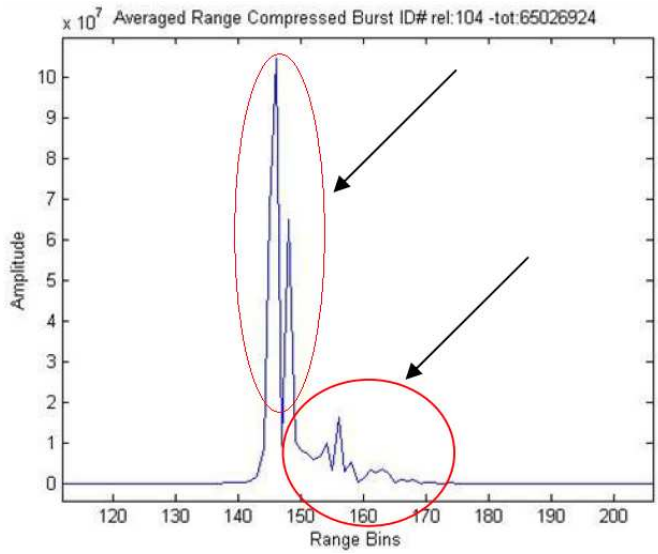

Figure 2.27 Cassini T3 Range Compressed Pulse #65026924. Example of secondary lobes and of double peaks into the band.

The effect of these anomalies on MLE loop is the divergence of the algorithm (see figure **2.28**) and consequentially the propagation of the error in height retrieval estimation (see following section) as can be seen in the peak of figure **2.29**.

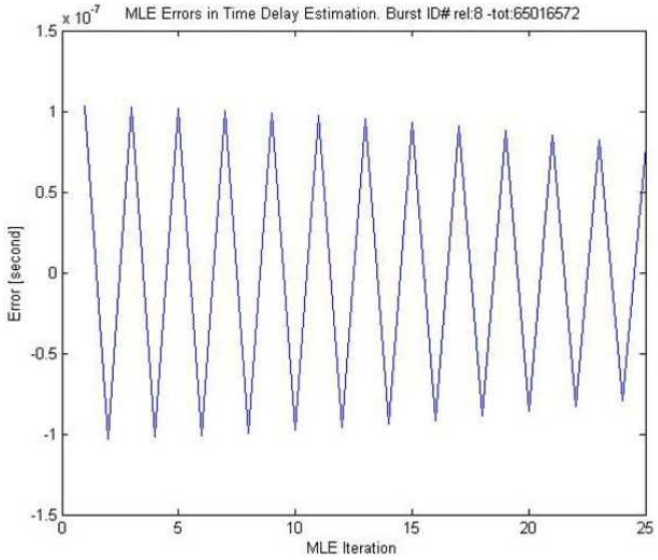

Figure 2.28 MLE Best fitting process: error divergence. It is clear that the model it is not able to fit the real data and the error

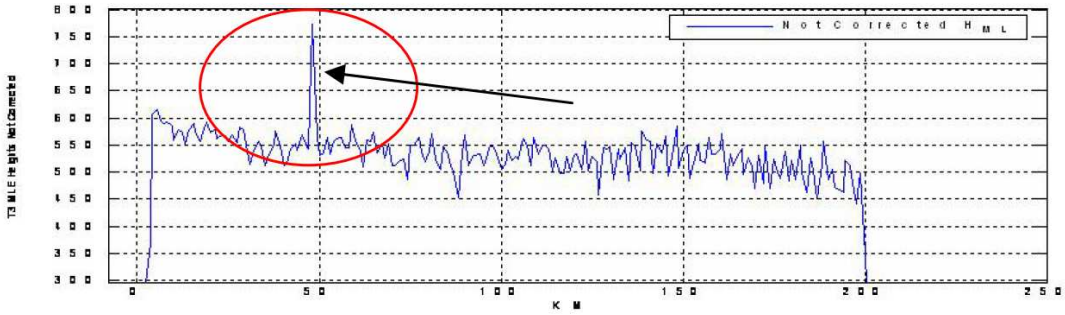

Figure 2.29 The MLE divergence becomes an error in topography estimation as clearly shown in the red box

2.4.E) Height Retrieval

This tool provides the final values to be filled in the fields of the Science Data Segment required for the ABDR production tool.

Starting from Time delay variables, the topographic heights are evaluated by subtracting the range derived by taking into account the time delay pulses propagation time-delay between transmission and reception of pulses from spacecraft altitude with respect to the surface (i.e. orbital range-Titan mean radius) satellite orbital range to target, to finally provide the topographic heights of Titan's surface. The topographic heights are the surface relative elevation respect to Titan mean equatorial radius (*R_Tit*=2575 Km).

In order to synchronize the burst in terms of time delay, it is necessary to know at least one pulse centroid position exactly, i.e. without ambiguity in term of PRIs. For instance, the burst with the minimum number of received pulses must be process first, thus allowing to synchronize all the other positions with respect to it. In other words, the burst with the minimum number of received pulses is used to solve the PRI ambiguity.

The whole inputs/outputs of this function are listed in the following:

- Inputs:

Variables	*Structure*	*Value/Unit Reference*
Tauzero_ML	*[Array]*	*Floating point double precision [s]*
H		*Floating point double precision. Non negative value [m]*
rx_window_delay	*[Array]*	*Floating point double precision [s]*
Radius		*Short Integer. Non negative Value [m]*
Range_proc	*[Bidimensional Array]*	*Floating point double precision.*

Table 2.11 Input variables of Height Retrieval

- Outputs:

Variables	*Structure*	*Value/Unit reference*
H_ML	*[Array]*	*Floating point double precision [m]*
Range_2_target	*[Array]*	*Floating point double precision [m]*
altimeter_profile_length		*Short Integer*
altimeter_profile_range_start		*Floating point double precision*
altimeter_profile_range_step		*Floating point double precision*

Table 2.12 Output variables of Height Retrieval

where:

- *H_ML*: is an array containig the Topographic Profile, i.e. the final altitudes, calculated as can be seen in the following paragraphs.
- *Range_2_target*: this is an array containing the Range S/C to target.
- *altimeter_profile_length:* this is an integer containing the number of valid entries in altimeter profile.
- *altimeter_profile_range_start*: a floating point double precision containing the range of the first altimeter profile value in each pulse.

- *altimeter_profile_range_step*: a floating point double precision containing the difference in range between consecutive range bins in altimeter profile.

The procedure followed to obtain the topographic heights is described in the following:

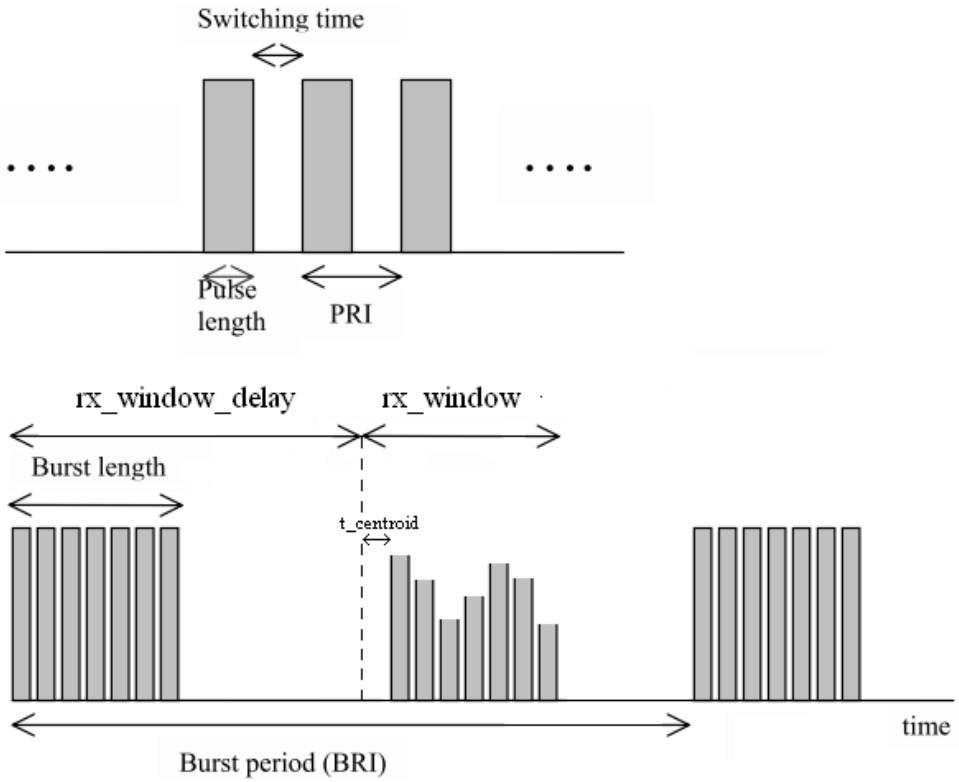

Figure 2.30 Example of burst cycle time

For the altimetry high resolution mode, typically:

- PRI = (1/4700 – 1/5000)s
- Pulse length = 150us
- BRI = 3333ms
- t_0 = rx_window_delay + t_centroid
- nº of pulses = 15

2.4.E) Height Retrieval

Starting with variables of table **2.11** the process starts by calculating the first range, calculated with the burst with the minimum number of received pulses. In this way it is possible to solve the PRI ambiguity since we are able to identify one single burst among all the others present in the intermediate BODP file, and therefore to introduce a time reference from which all other ranges are calculated. The procedure is as follows:

$$H_1 = SC\_radius_1 - RWD_1 \frac{c}{2} - R\_Tit - T_{centroid} \frac{c}{2}$$

where:

- $SC_{radius} = \sqrt{(sc\_j2000\_x)^2 + (sc\_j2000\_y)^2 + (sc\_j2000\_z)^2}$ = Satellite Radius
- RWD = received windows delay, see figure above
- R_Tit = Titan mean equatorial radius = $2575000m$
- $T_{centroid}$ = Pulse centroid position

then for the N_{th} averaged burst:

$$H_N = SC\_radius_N - RWD_N \frac{c}{2} - R\_Tit - T_{centroid} \frac{c}{2} - sg \cdot K \cdot PRI \frac{c}{2}$$

where:

- $K = |H_N - H_1| < PRI(c/4)$
- $sg = sign(H_N - H_{N-1})$

Finally is possible to evaluate the Range to target by performing:

$$Range\_to\_Target = SC\_radius - R\_Tit - H_N$$

It is worth noting that the processing takes also into account the delay due to internal path followed by the transmitted and received signals. This time delay has been evaluated by processing calibration data (rerouted chirp and leakage signal) and it has been found equal to 6 µsec.

Next figure shows the topographic profiles obtained by processing of T13, T16 and T19 fly-bys, where the Titan's height are referred to the mean planet radius:

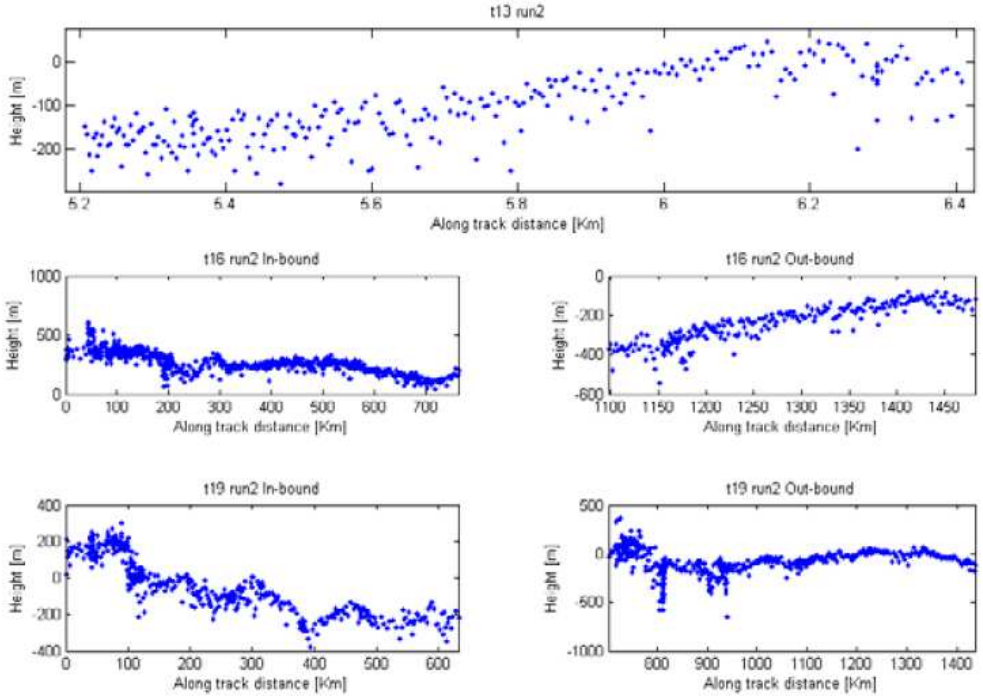

Figure 2.31 Retrieved Titan's surface height as a function of along track distance. The height values are referred to Titan's mean radius of 2575 Km (fly-bys T13, T16 and T19). The distance values are referred to altimetric acquisition start.

2.4.F) Slope Evaluation

This tool allows user to evaluate the bidirectional surface slope in the along track direction starting from H_ML (Topographic Profile), by computing the derivative of the estimated heights expressed in deg. The slope values have been evaluated by taking a linear fit of the height profiles, of course considering the in-bound and out-bound part of the trajectory separately.

The whole input/output of this function is listed in the following:

- *Input: H_ML* (Topographic Profile).
- Output: *slope* (Surface Slope [Array]*,* Floating point double precision [m]).

2.4.G) Waveform Analysis

With this tool the user will be able to visualize the plot of the Radar Impulse Response and the Range Compressed Data by inserting the burst ID in a dedicated edit-box. The waveform analysis can be performed in terms of visual analysis of the shape of the received echo waveforms for the *Cassini* Radar through comparison with relevant processing parameters, on a burst basis. Thus, the SLT also allows user to plot the following parameters:

- Pulse Repetition Interval
- Number of Transmitted/Received Pulses
- Receive Window Delay
- Time from Closest Approach
- Spacecraft Velocity in Target Body Fixed (TBF) coordinate system
- Spacecraft Range
- Off-nadir Angle

- Inputs: *Range_proc* and *IR* (Impulse Response [Array]).

The outputs of this function are on screen diagrams.

2.4.H) Performance Simulation

This tool allows user to simulate, and evaluate by means of the algorithm described in section **2.4.D**, the *Cassini* Radar impulse response (IR) by interactive selection of one implemented model. The SLT allows user to select interactively the parameters to be used for any simulation run, by choosing among:

- Spacecraft Altitude
- Off-nadir Angle
- Surface Roughness
- Surface Topography

User may execute the simulation starting from the list of the above parameters, with current values read from PT internal files, or after setting up of new values, through the GUI interface. This functionality allows user to visualize interactively the simulated IR by using dedicated push-buttons in the SLT GUI interface.

The whole inputs of this function are listed in the following table:

Variables	Structure	Value/Unit reference
t	[Array]	Floating Point Double Precision [s]
t0		Floating Point Double Precision [s]
gamma		Floating Point Double Precision.
zita		Floating Point Double Precision. Non negative value [rad]
H		Floating Point Double Precision. [m]
Radius		Short Integer. Non negative value [m]
sigma_c		Floating Point Double Precision [s]
NN		Short Integer. Min:1 Max:4
sigma_p		Floating Point Double Precision. Constant Value [m]
c		Floating Point Double Precision. Constant value [m]/[s]
B		Floating Point Double Precision. [Hz]

Table 2.13 Inputs of Performance Simulation

The outputs of this function are on screen diagrams.

2.4.I) Results Workspace Saving

This functionality saves all the produced results in a binary format file into the local directory. SLT Results files are automatically produced for both ALTH/AHAG operating modes. The SLT Results file for ALTH/AHAG mode will contain the variables listed in the following table, as noted in the introduction of the present section (**2.4**):

- Inputs:

Variables	Structure	Value/Unit reference
tauzero_ML_1step	[Array]	Floating Point Double precision [s]
error_min_tau	[Array]	Floating Point Double precision [s]
amp_ML_1step	[Array]	Floating Point Double precision
error_min_amp	[Array]	Floating Point Double precision
modello_fin_1step	[Array]	Floating Point Double precision
tauzero_ML_2step	[Array]	Floating Point Double precision
amp_ML_2step	[Array]	Floating Point Double precision
error_min_amp_2step	[Array]	Floating Point Double precision
error_min_tau_2step	[Array]	Floating Point Double precision [s]
error_min_sigma_h_2step	[Array]	Floating Point Double precision [m]
modello_fin_2step	[Array]	Floating Point Double precision
sigmas_ML	[Array]	Floating Point Double precision [m]
H_ML	[Array]	Floating Point Double precision [m]
slope	[Array]	Floating Point Double precision [deg]
Range_2_target	[Array]	Floating Point Double precision [m]
rtt_std		Floating Point Double precision [m]
altimeter_profile_length		Short Integer
altimeter_profile_range_start		Floating Point Double precision
altimeter_profile_range_step		Floating Point Double precision

Table 2.14 Inputs of Results Workspace Saving

The output of this function are the SLT Results files in Binary format data file.

3) ANNEXES

3.0) Altimetry Radar

The altimetry radar is an active sensor that operates in the microwave band. It basically has the function to determinate its distance to the surface “illuminated” by signals sent by the radar itself. It calculates the round trip time to the reflecting surface since a portion of the outgoing radar signal is redirected directly back towards the radar antenna by the target.

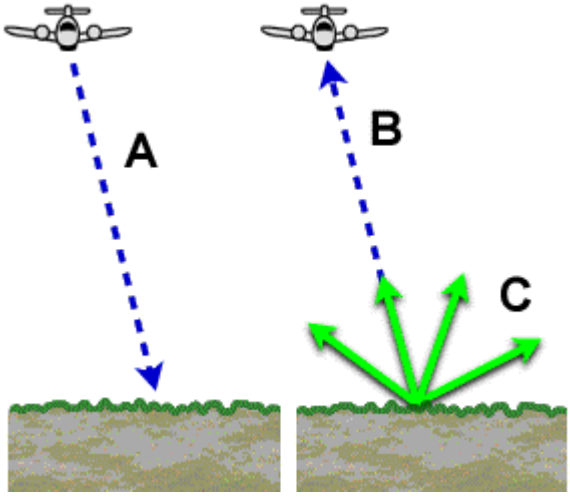

Figure 3.1 Backscattering effect

When a radar system transmits a pulse of energy to the ground (A), it scatters off the ground in all directions (C). A portion of the scattered energy is directed back toward the radar receiver (B), and this portion is referred to as "backscatter".

The accuracy, which is generally on the order of several centimeters or tens of centimeters, depends mainly on the sharpness of the pulse, or signal bandwidth, and the footprint of the radar beam

The backscatter is captured by the antenna, which is connected to the receiver that detects the signal and records it to be later processed. The discrimination of the different backscatters, received from different directions of propagation, can be achieved with different techniques, which involve time discrimination, angular discrimination or discrimination in terms of Doppler deviation.

The components of a radar system are:

- a pulse generator, which sends, with a certain PRF, microwave energy pulses.
- a transmitter.
- a Duplexer, which connects the antenna to the transmitter when we need to send the pulse, and connects the antenna to the receiver when the echo must be received.
- a directive antenna, which focuses the pulse energy into a beam.

- the radar echoes captured by the antenna, which are amplified and processed appropriately.
- a data storage device, for subsequent processing (post processing).

Normally the radar transmits sinusoidal pulses of finite duration. The time between one pulse and the following one is called repetition period $T = 1/PRF$ (Pulse Repetition Frequency).

Let's take a single sinusoidal pulse of duration τ and frequency f_o, which can be expressed as:

$$s(t) = A\cos 2\pi f_o t \quad -\frac{\tau}{2} \leq t \leq \frac{\tau}{2} \qquad (3.0.1)$$

It is possible to demonstrate that the bandwidth of $s(t)$ is $B = 1/\tau$. The pulse duration is usually very short if we compare it with the repetition period, normally τ*PRF=1/1000.

The time interval between the emission and the reception of the echo can be measured with great accuracy and, therefore, if we know the propagation speed of the electromagnetic waves in free space ($\approx c = 3 \cdot 10^8$m/s) we may be able to calculate the distance R from the radar to the observed surface in the following way:

$$R = \frac{c\Delta t}{2} \qquad (3.0.2)$$

since the impulse travels a distance equal to 2R. Obviously the maximum distance that we will be able to detect before the next pulse is transmitted by the radar will be:

$$R_{max} = \frac{cT}{2} \qquad (3.0.3)$$

If two targets are separated by a distance ΔR, two echoes will be received by the antenna (which has sent a single pulse), and will return to the radar with the following temporal separation:

$$\Delta t = \frac{2\Delta R}{c} \qquad (3.0.4)$$

So the pulse duration must be $\tau < 2\Delta R/c$ if we want to distinguish the two targets. Thus we can define the distance resolution as the minimum distance at which two objects can be identified as separate items:

$$R_D = \rho = \frac{c\tau}{2} = \frac{c}{2B} \qquad (3.0.5)$$

This result shows that for good distance resolutions we should transmit pulses of very short duration but on the other hand we also have that for great radar scopes or high SNR's we need long pulse durations since the energy transmitted is directly related to this parameter. This problem will be solved with the pulse modulation technique as we will see in the following section.

The geometry involved in the altimetry radar is shown in the next figure.

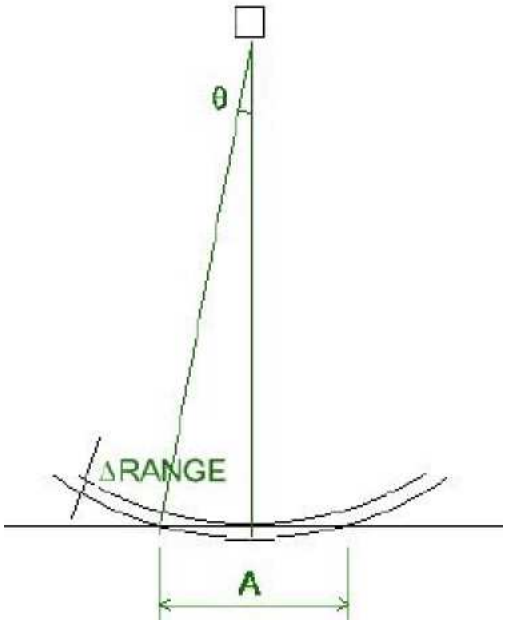

Figure 3.2 Geometry involved in altimetry radar (1)

Δ_{range} is the size of the distance resolution cell, related to the pulse duration. If the beam aperture antenna is greater than + / - θ, which happens when the size of the distance resolution cell is very small, the altimeter is then called pulse-limited, and the incident signal will initially illuminate a circular area of diameter A. Then as long as the wavefront advances the area will no longer be a circle but a ring as shown in the next figure:

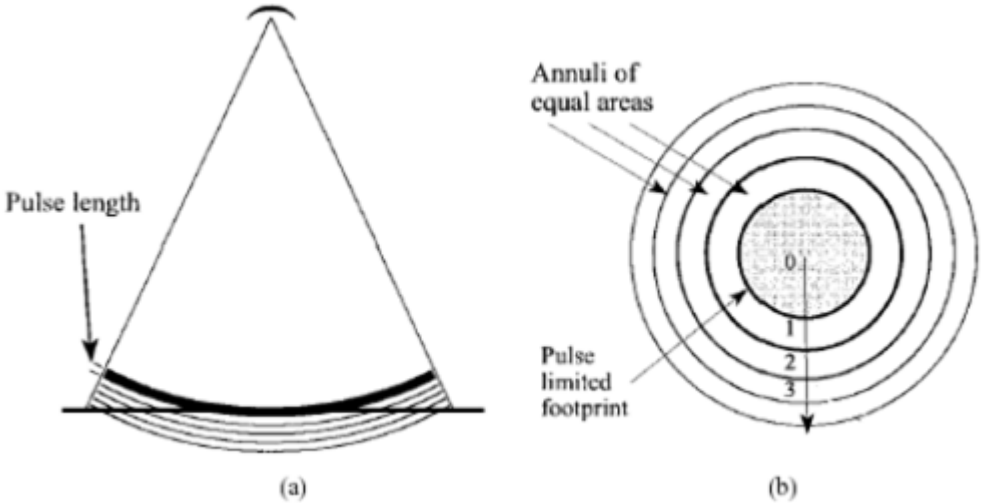

Figure 3.3 Geometry involved in altimetry radar (2)

The first circle will remain as long as $2h/c \leq \tau \leq 2h/c + 2R_D/c$, the second cell resolution, already ring-shaped, will exist while $2h/c + 2R_D/c \leq \tau \leq 2h/c + 2(2R_D/c)$. The first cell resolution will have an area $A_0 = \pi\rho_0^2$ noting that $\rho \ll h$. Where ρ_0, called *pulse-limited circle*, represents the nadir resolution, in ground range, of the altimetry radar and can be written as $\rho_0 = \sqrt{2h\rho} = \sqrt{c\tau h}$.

As can be seen in the next figure, initially the return power increases quickly due to the expansion of the illuminated area from a point to a circle. At that point the return power remains constant since the area of the rings is always the same. Finally it decreases since the ring expands up to the beam limit.

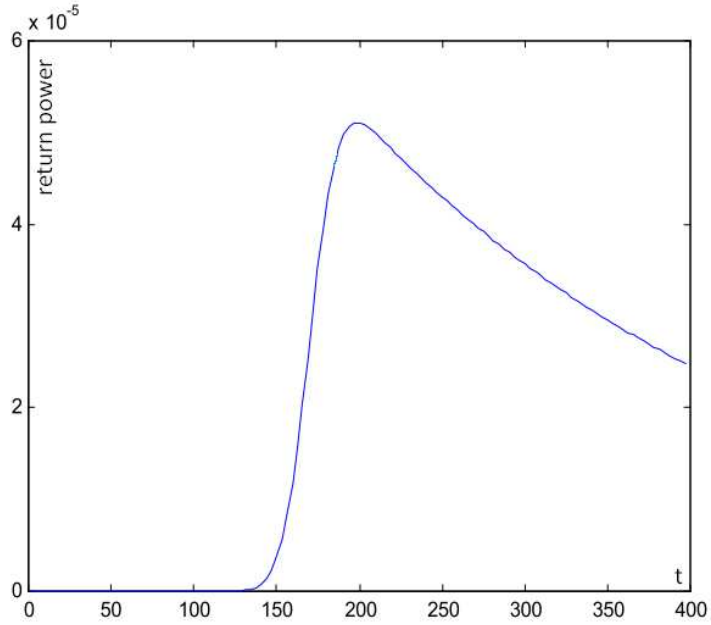

Figure 3.4 Brown's Model: Nadir pointed real Impulse Response of a surface with negligible slope

The radar echo characteristics depend mainly on the physical and geometric properties such as shape, roughness and the dielectric constant of the observed object. In a general way, if we consider oceanic surfaces illuminated by a pulse-limited altimetry radar, with very small incidence angles it can be demonstrated that the return echo, assuming a Gaussian height probability density function of the ocean, can be written as (see Brown's Model **[8]**):

$$P_r(\tau) \approx \begin{cases} \eta P_T P_{FS}(0)\sqrt{2\pi}\sigma_p \dfrac{1}{2}\left[1+\operatorname{erf}\left(\dfrac{\tau}{\sqrt{2}\sigma_c}\right)\right], & \tau < 0 \\ \eta P_T P_{FS}(\tau)\sqrt{2\pi}\sigma_p \dfrac{1}{2}\left[1+\operatorname{erf}\left(\dfrac{\tau}{\sqrt{2}\sigma_c}\right)\right], & \tau \geq 0 \end{cases} \quad (3.0.6)$$

where:

- $\eta = BT$ is the compression ratio of the transmitted pulse.
- P_T is the peak transmitted power.
- P_{FS} is the average backscattered power from a mean flat surface (illuminated by an impulse).
- σ_p=0.4275T and $\sigma_c = \sqrt{\sigma_p^2 + (2\sigma_h/c)^2}$

In section **3.4.1** will be explained in more detail the Brown's model and all its assumptions and characteristics.

Brown's Model has been widely applied to pulse-limited radar altimeters devoted to nadir oceans observations, for Earth observation purposes, in order to map the Earth's geoid, to study oceanic processes, to obtain topographic details of sea surfaces. The

values of the backscattering coefficient of the illuminated surface (σ^0), the surface roughness (σ_h) and the time delay between surface and orbit (t_0) can be obtained by fitting the received echoes with the theoretical Brown's Model. Once we get the value of t_0 we can determine the range to the ocean and if we know the satellite's orbit we can obtain the average height of the observed surface by subtracting the two distances.

In the following figures can be seen the variation of the theoretical impulse response of Brown's Model with respect to σ_h, σ^0, and t_0 respectively

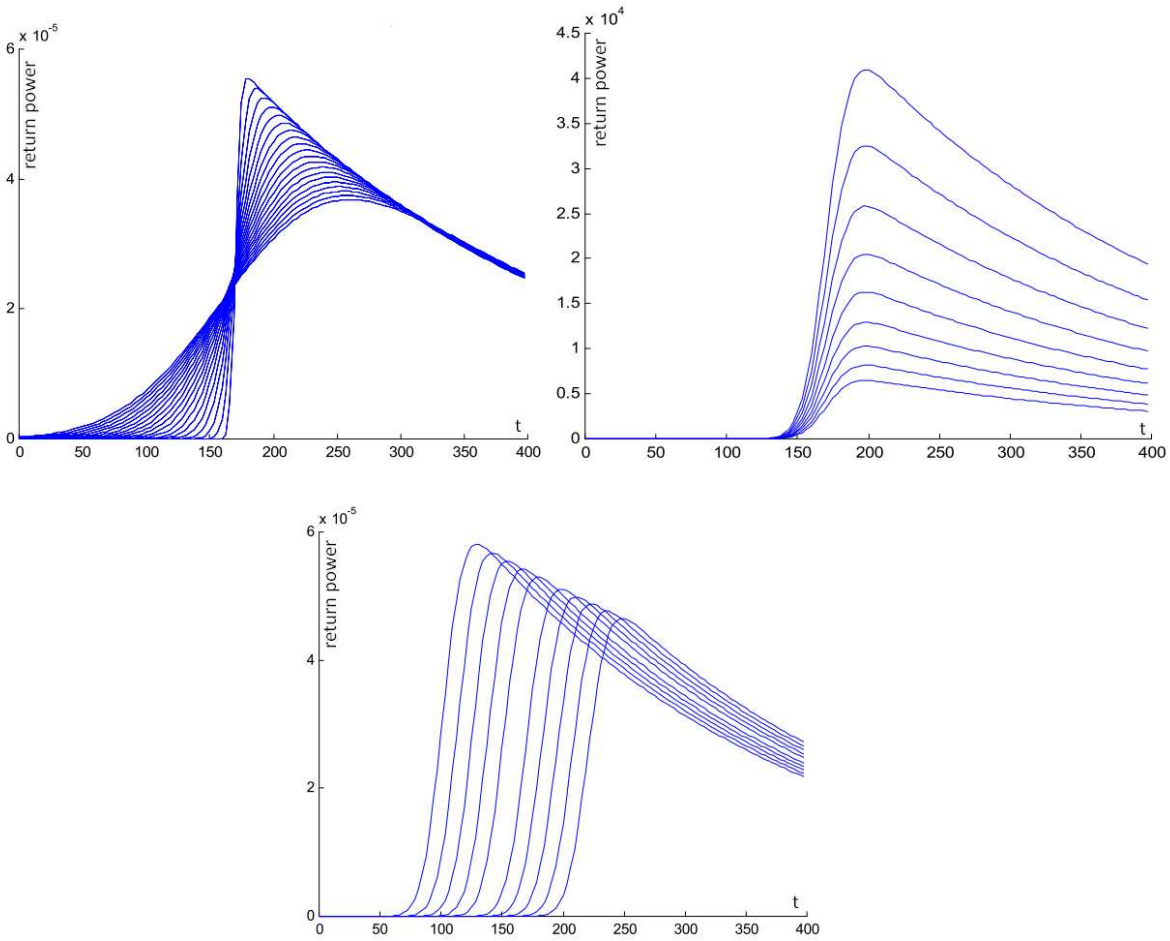

Figure 3.5 theoretical impulse response of Brown's Model with respect to σ_h, σ^0, and t_0 respectively

3.1) Range Processing

Once we have stored the sampled echo data from the LBDR file we need to process it, in order to be able to detect the real echoes from Titan's surface in such a way that we have as few as possible false detections and the distance resolution achieved is as small as possible. In the following paragraphs will be described the physical and mathematical concepts that lead us to choose the more appropriate filter and signal waveform for this purpose.

The problem is then approached from two different points of view. On one hand we are trying to find the optimal linear filter that maximizes the signal to noise ratio (SNR),

and on the other we are trying to find the best transmitted signal waveform in order to achieve the best distance resolution.

3.1.1) SNR Maximization

Here we would like to find the linear filter h(t) that maximizes the SNR (Matched filter). Taking into account the following scheme:

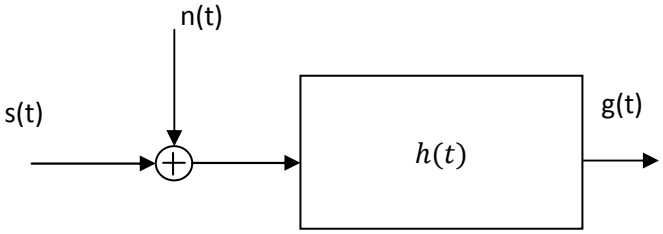

where s(t) is the received signal and n(t) the noise of the whole system. The output signal can be stated (considering the linearity of the system) as:

$$g(t) = \big(s(t) + n(t)\big) * h(t) = \int_{-\infty}^{\infty} \big(s(\tau) + n(\tau)\big)h(t-\tau)d\tau \quad (3.1.1)$$

when $t = t_0$ then:

$$g(t_0) = \int_{-\infty}^{\infty} \big(s(\tau) + n(\tau)\big)h(t_0-\tau)d\tau = g_s(t_0) + g_n(t_0) \quad (3.1.2)$$

so the SNR becomes (since n(t) can be approximated by an additive white Gaussian noise):

$$SNR = \frac{|g_s(t_0)|^2}{E\{{g_n}^2(t_0)\}} = \frac{\left|\int_{-\infty}^{\infty} s(\tau)h(t_0-\tau)dt\right|^2}{\frac{\eta}{2}\int_{-\infty}^{\infty}|h(t_0-\tau)|^2dt} \quad (3.1.3)$$

where, taking into account the Cauchy-Schwarz Inequality:

$$\left|\int_{-\infty}^{\infty} x_1(t)x_2(t)dt\right|^2 \leq \int_{-\infty}^{\infty}|x_1(t)|^2dt\int_{-\infty}^{\infty}|x_2(t)|^2\,dt \quad (3.1.4)$$

the SNR becomes

$$SNR \leq \frac{\int_0^{t_0}|s(\tau)|^2dt\int_0^{t_0}|h(t_0-\tau)|^2\,dt}{\frac{\eta}{2}\int_0^{t_0}|h(t_0-\tau)|^2dt} = \frac{2}{\eta}\int_0^{t_0}|s(\tau)|^2dt \quad (3.1.5)$$

obviously the equality of the function is fulfilled when:

$$h^*(t_0-\tau) = s(\tau)\ or\ h(t) = s^*(t_0-t) \quad (3.1.6)$$

so as it can be seen the filter that maximizes the signal to noise ratio is actually the conjugate of the signal itself inverted and shifted t_0 seconds.

3.1.2) Chirp Pulse Compression

If we use a sinusoidal rectangular pulse, in order to achieve a good distance resolution we need short pulse durations, instead long pulse durations are needed if we want to reach great radar scopes. This problem can be solved, as we will see in the following, with the pulse compression technique.

In fact, as noted in 3.0 if we use:

$$s(t) = \Pi\left(\frac{t}{T}\right)\cos(2\pi f_0 t) \quad (3.1.7)$$

where f_0 is the signal frequency, we have that B = 1/T. As can be seen in 3.0.5 the distance resolution is given by:

$$R_D = \frac{c}{2B} = \frac{cT}{2}$$

On the other hand if we consider a signal such as:

$$s(t) = A\Pi\left(\frac{t}{T}\right)e^{j2\pi f_0 t}e^{j\pi\alpha t^2} \quad (3.1.14)$$

known as chirp pulse, where α is known as chirp rate. The phase and instantaneous frequency of a chirp signal are given respectively by:

$$\begin{cases}\phi(t) = 2\pi f_0 t + \pi\alpha t^2 \\ f(t) = \dfrac{\dot{\phi}}{2\pi} = f_0 + \alpha t\end{cases} \quad -\frac{T}{2} \le t \le \frac{T}{2} \quad (3.1.15)$$

so:

$$\begin{cases}f_{min} = f_0 - \alpha\dfrac{T}{2} \\ f_{max} = f_0 + \alpha\dfrac{T}{2}\end{cases} \quad (3.1.16)$$

and thus we have that:

$$B = f_{min} - f_{max} = \alpha T \quad (3.1.17)$$

In this case the signal bandwidth and the pulse duration are directly proportional and thus the distance resolution is given by:

$$R_D = \frac{c}{2B} = \frac{c}{2\alpha T} \quad (3.1.18)$$

so in this case we can reach good distance resolutions by increasing the pulse duration, which at the same time increases the radar scope.

In the following figures is presented the main structure of the chirp pulse:

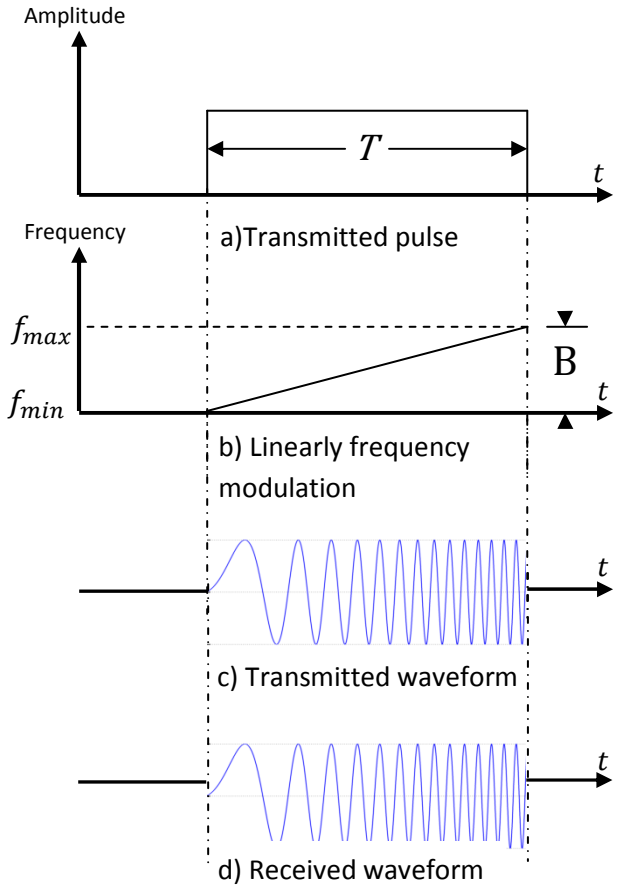

Figure 3.6 Qualitative structure of a chirp signal.

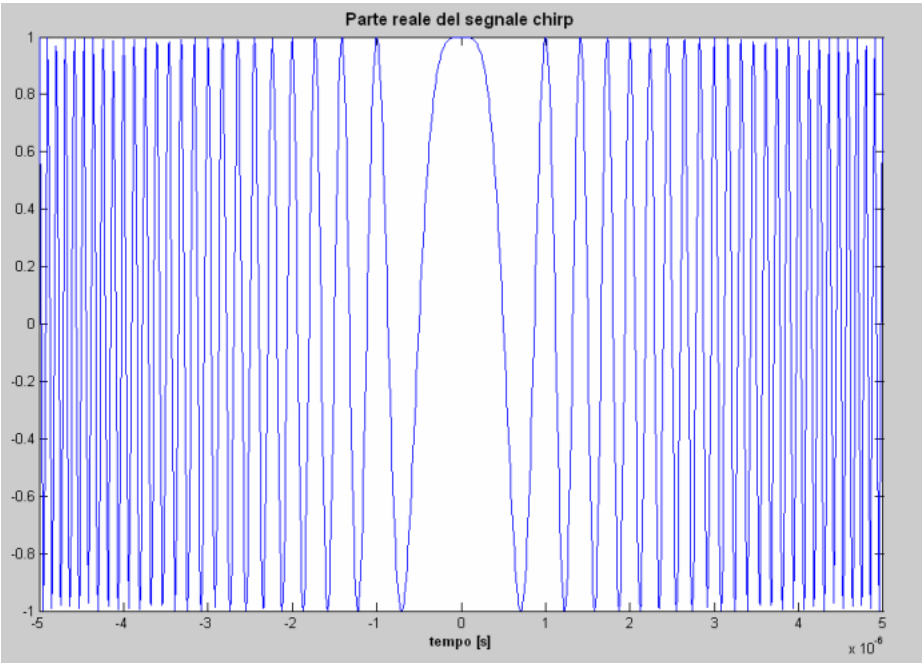

Figure 3.7 Chirp signal as a function of time

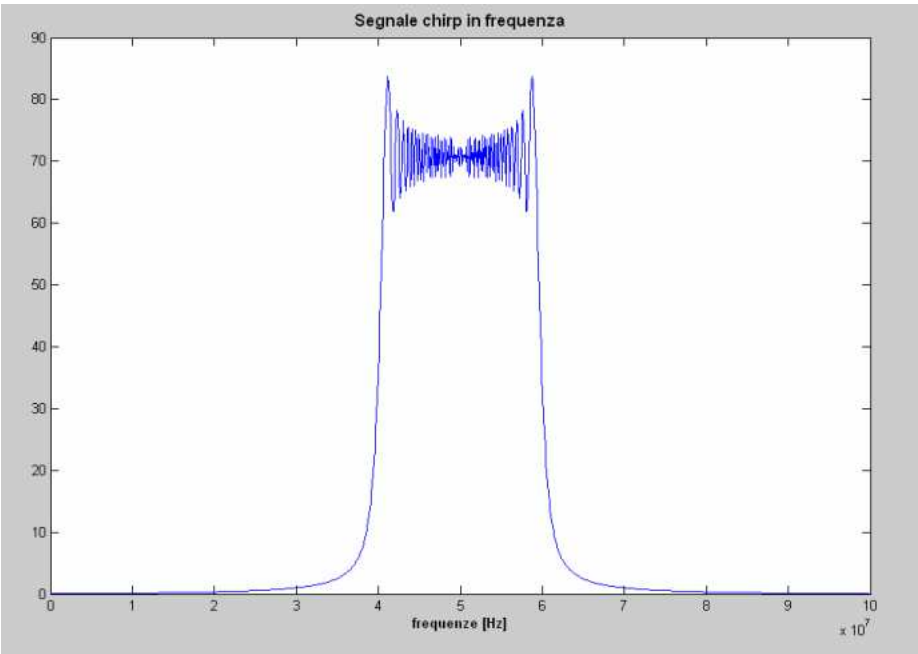

Figure 3.8 Frequency domain chirp spectrum

Let's now make a review of the whole system. The system is, as deduced from the two previous paragraphs, the following:

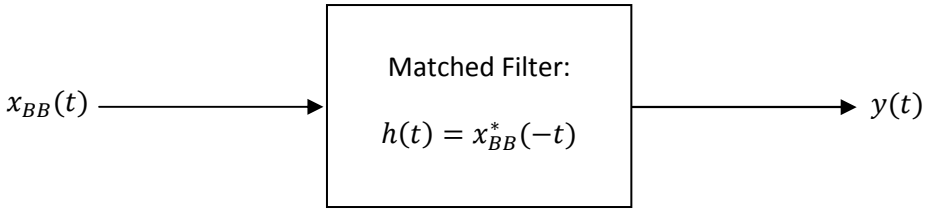

where "BB" indicates Base-Band, this is the signal after the down conversion, and:

$$x_{BB}(t) \approx \Pi\left(\frac{t-t_0}{T}\right) e^{-j2\pi f_0 t_0} e^{j\pi\alpha(t-t_0)^2} \ \ and \ t_0 = \frac{2R}{c} \quad (3.1.19)$$

it can be demonstrated that:

$$X_{BB}(f) \approx \Pi\left(\frac{\bar{t}}{T}\right) e^{j\pi\frac{f^2}{\alpha}} \ with \ \bar{t} = \frac{f}{\alpha} \quad (3.1.20)$$

in that case, the signal output $Y(f)$ will be, since in the frequency domain $H(f) = X_{BB}^*(f)$:

$$Y(f) = X_{BB}(f) \cdot X_{BB}^*(f) = |X_{BB}(f)|^2 \quad (3.1.21)$$

so in the time domain, it can be showed that

$$y(t) \approx BTsinc\big(B(t-t_0)\big) \quad (3.1.22)$$

thus, as it can be noted, we have just obtained from a signal of duration T, a signal (shifted t_0 due to the distance antenna-target-antenna) of duration 2/B .

Since the energy of the signal does not vary during pulse compression, it means that it is now located in the main lobe of the cardinal sine and so the peak power of the compressed pulse has been increased in fact by a factor BT.

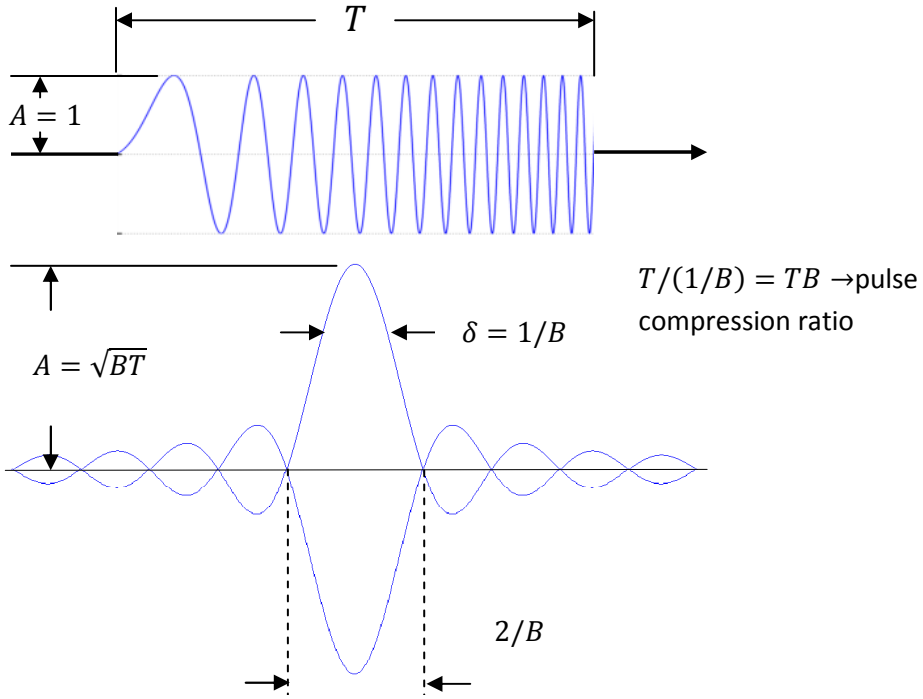

Figure 3.9 Main compression parameters.

As an example we show in the following the case of a real truncated sine of duration T = 1s (in red) of unitary amplitude and $f_T = 10\ Hz$. Two echoes (in blue) come back with a delay of 3 and 5 seconds, respectively, and have an amplitude equal to 0,5 and 0,3; those are just random values for the sake of the example:

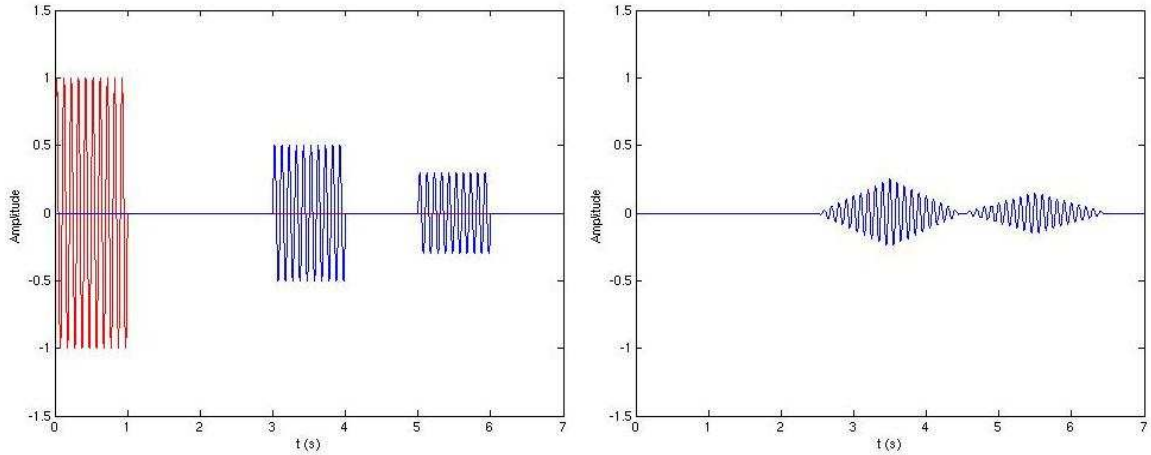

Figure 3.10 Real sine of duration T=1s f_T=10Hz before and after matched filtering, delayed 2 seconds between each other

If two pulses come back (nearly) at the same time, the intercorrelation is equal to the sum of the intercorrelations of the two elementary signals. To distinguish one "triangular" envelope from that of the other pulse, it is clearly visible that the times of arrival of the two pulses must be separated by at least *T* so that the maxima of both pulses can be separated. If this condition is false, both triangles will be mixed together and impossible to separate:

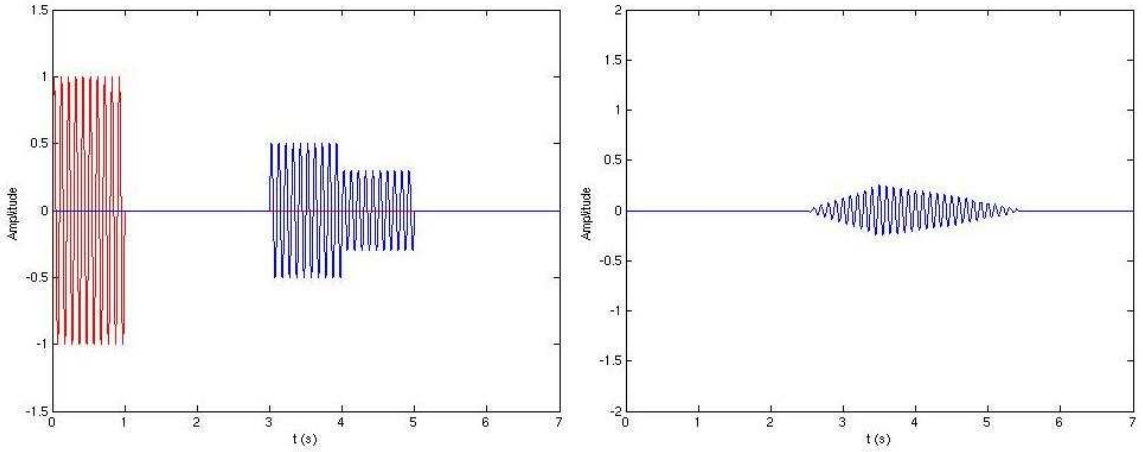

Figure 3.11 Real sine of duration T=1s f_T=10Hz before and after matched filtering, delayed 1 second between each other, before and after matched filtering

On the other hand, if we transmit a chirped pulse (carrier 10 hertz, modulation on 16 hertz, amplitude 1, duration 1 second), we have:

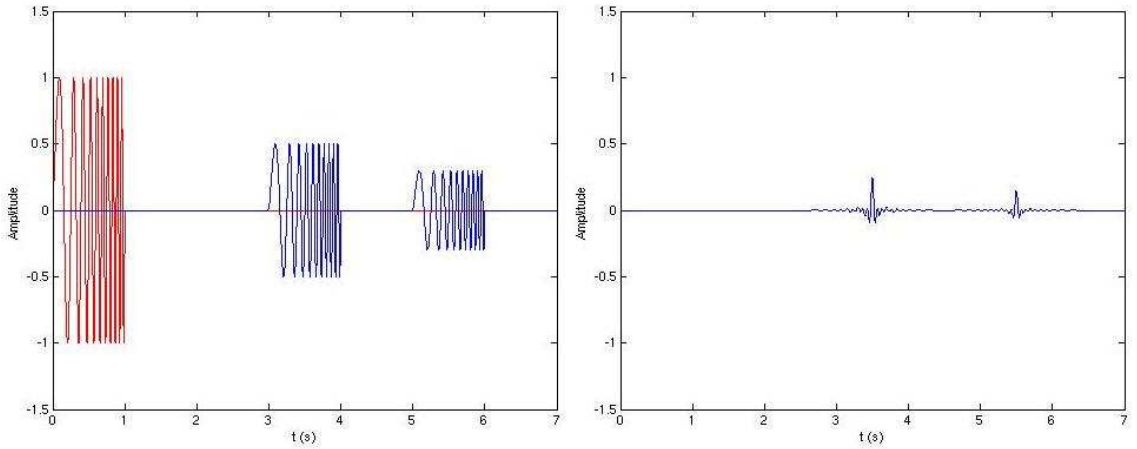

Figure 3.12 Chirped pulse fo=10Hz, B=16Hz, A=1 T=1 before and after matched filtering

3.2) MLE structure

In order to obtain the key parameters of Titan's surface it is needed to fit the received echoes with the theoretical models, so we are dealing now with the problem of estimation of such parameters from real data acquired by the radar, that are affected by thermal noise and, mainly, by speckle.

In the case of *Cassini* PAD system it has been chosen a Maximum Likelihood Estimation (MLE) since this method exhibits several characteristics which can be interpreted to

mean that it is "asymptotically optimal" since it is asymptotically unbiased (its bias tends to zero as the number of samples increases to infinity) and it is asymptotically efficient, i.e., it achieves the Cramér-Rao lower bound when the number of samples tends to infinity **[10]**.

Given observations $\overline{D}[n] = (D_1, \dots, D_M)$ affected by noise with known probability density function and depending on a set of parameters $\underline{\theta} = (\theta_1, \dots, \theta_N)$ the MLE searches for the parameter values that maximize the likelihood function given by:

$$L(\underline{\theta}) = f\left(\overline{D}[n]\middle|\underline{\theta}\right) \quad (3.2.1)$$

As explained on **2.4.B** section, the averaged samples used to perform the MLE can be approximately viewed as Gaussian distributed, so:

$$f\left(\overline{D}_i\middle|\underline{\theta}\right) = \frac{1}{IR_i}\exp\left(-\frac{(\overline{D}_i - IR_i)^2}{2IR_i^2/N_B}\right) \quad (3.2.2)$$

By supposing the samples independent, the likelihood function becomes a product of M Gaussian probability density functions:

$$f\left(\overline{D}[n]\middle|\underline{\theta}\right) = \prod_{i=1}^{M} f\left(\overline{D}_i\middle|\underline{\theta}\right) \quad (3.2.3)$$

it is worth noting that $f\left(\overline{D}_i\middle|\underline{\theta}\right)$ depends actually on the $\underline{\theta}$ parameters (tipycally t_0 and σ_s) since IR_i is that of the equations **2.4.D.4.2**, **2.4.D.4.3** or **2.4.D.4.4**, depending on the selected model.

As is commonly known, it is easier to maximize the logarithm of the likelihood function rather than the function itself since they have the maximum point at the same value:

$$\frac{\partial f\left(\overline{D}[n]\middle|\underline{\theta}\right)}{\partial \underline{\theta}} \equiv \frac{\partial \ln f\left(\overline{D}[n]\middle|\underline{\theta}\right)}{\partial \underline{\theta}} \quad (3.2.4)$$

So we have:

$$\frac{\partial}{\partial\theta_j}\ln\prod_{i=1}^{M} f\left(\overline{D}_i\middle|\underline{\theta}\right) = \frac{\partial}{\partial\theta_j}\sum_{i=1}^{M}\ln f\left(\overline{D}_i\middle|\underline{\theta}\right) = \frac{\partial}{\partial\theta_j}\sum_{i=1}^{M}\ln\frac{1}{IR_i}\exp\left(-\frac{(\overline{D}_i - IR_i)^2}{2IR_i^2/N_B}\right) =$$

$$= \sum_{i=1}^{N}\frac{\partial}{\partial\theta_j}\left(\ln\frac{1}{IR_i} - \frac{(\overline{D}_i - IR_i)^2}{2IR_i^2/N_B}\right) = \sum_{i=1}^{M}\frac{N_B}{IR_i^3}\left(\overline{D}_i{}^2 - \overline{D}_i IR_i\right)\frac{\partial IR_i}{\partial\theta_j} - \frac{1}{IR_i}\frac{\partial IR_i}{\partial\theta_j} =$$

$$= \sum_{i=1}^{M}\frac{N_B\overline{D}_i{}^2 - N_B\overline{D}_i IR_i - IR_i^2}{IR_i^3}\frac{\partial IR_i}{\partial\theta_j} \quad (3.2.5)$$

where θ_j is the generic j-th parameter to be estimated. The solution implemented in the MLE of the *Cassini* PAD system differs from that of the last expression since it

would yield potential instabilities mainly caused by the presence of amplitude terms in the derivative of the model used such as the two-way path loss L_p.

To this end, the $\partial IR_i / \partial \Theta_j$ has been replaced by:

$$\overline{\frac{\partial IR_i}{\partial \Theta_j}} = \frac{\partial IR_i / \partial \Theta_j}{\max\left(\frac{\partial IR_i}{\partial \Theta_j}\right)} \quad (3.2.6)$$

and the IR_i^2 has been neglected in the numerator of **3.2.5** since it is not multiplied by N_B. This sub-optimal strategy yields the actual equations of the implemented MLE:

$$\begin{cases} \sum_{i=1}^{M} \frac{\overline{D}_i - IR_i}{IR_i^2} \overline{\frac{\partial IR_i}{\partial \Theta_1}} \\ \vdots \\ \sum_{i=1}^{M} \frac{\overline{D}_i - IR_i}{IR_i^2} \overline{\frac{\partial IR_i}{\partial \Theta_N}} \end{cases} \quad (3.2.7)$$

It is worth noting that, as can be seen in the following section, for *Cassini* radar system, the IR function mainly depends on surface backscattering, radar round-trip time, off-nadir angle and surface height root standard deviation. This means that MLE can allow, in principle, estimation of all these parameters and not only of the surface height through radar round-trip time, yielding additional useful information for characterizing the planet's surface. This document details only the estimation of t_0 and σ_s, but the normalized backscatter cross-section σ^o can be also estimated with the same procedure with the data obtained from the scatterometer measurement

So in the final step of the MLE algorithm, error is evaluated by implementing the following system of equations with the current values of the t_0 and σ_s variables:

$$\frac{\partial f\left(\overline{D}[n] \middle| \underline{\Theta}\right)}{\partial \underline{\Theta}} \equiv \begin{cases} \sum_{i=1}^{M} \frac{\overline{D}_i - IR_i}{IR_i^2} \overline{\frac{\partial IR_i}{\partial t_0}} \\ \sum_{i=1}^{M} \frac{\overline{D}_i - IR_i}{IR_i^2} \overline{\frac{\partial IR_i}{\partial \sigma_s}} \end{cases} = 0 \quad (3.2.13)$$

3.3) Implemented Models

The information content held by the received echo can be extracted only by obtaining a complete model of the altimeter's echo waveform, since the characteristics of the altimeter waveform are strongly related to surface characteristics (i.e. roughness, rms slope, etc.).

In 1977, G. S. Brown proposed a theoretical model of the average impulse response of a rough surface, the so-called Brown's model, which has been widely applied to pulse-limited radar altimeters devoted to nadir oceans observations but due to mission constraints, the *Cassini* Radar ALT is settled to work in such a way that the pulsewidth-

limited and the beam-limited circles are comparable. Consequently some of the general assumptions at the basis of the conventional models are no longer applicable.

Moreover, the geometry involved, mainly the effective attitude of the *Cassini* orbiter during the hyperbolic Titan fly-bys and the not negligible off-pointing angles (which are expected to be typically up to 0.5 degrees), will affect significantly the waveform shape, and hence the final altimetric measurements. This implies the need for an approximation of the surface impulse response, which incorporates all those effects and admits a friendly closed form solution. Due to the strong dependence of the waveform shape with the pointing angle, one model will be selected from among the three available depending on its value.

In the following is presented a complete review of the physical concepts on which the implemented models are based as well as a detailed review of the three models.

3.3.1) Brown's Model

In 1967 and 1971 some authors **[2]** and **[3]**, starting from the same hypotheses made by Moore and Williams **[1]**, demonstrated that for a rough scattering surface *(a surface appears "rough" to microwave illumination when the height variations become larger than a fraction of the radar wavelength. The fraction is qualitative, but may be shown to decrease with incidence angle)*, the average return power as a function of delay is, when one accounts for the vertical distribution of the surface height and the radar receiver effects, a convolution of the radar system point target response with the average surface impulse response.

The general assumptions at the basis of the convolutional model of near normal incidence rough surface are:

- The scattering surface may be considered to comprise a sufficiently large number of random independent scattering elements.
- The surface height statistics are assumed to be constant over the total area illuminated by the radar during construction of the mean return.
- The scattering is a scalar process with no polarization effects and is frequency independent
- The variation of the scattering process with angle of incidence (relative to the normal to the mean surface) is only dependent upon the backscattering cross section per unit scattering area, σ^0, and the antenna pattern.
- The total Doppler frequency spread $(4V_r/\lambda)$ due to a radial velocity V_r, between the radar and any scattering element on the illuminated surface is small relative to the frequency spread of the envelope of the transmitted pulse *(2/T, where T is the width of the transmitted pulse)*.

The average surface impulse response may, in turn, be represented as a convolution of the probability density function of the height of the specular points on the surface with the quantity defined by Moore and Williams which depends upon σ^0, the antenna gain, and the range from the radar to any point on the scattering surface, referred

from now as $P_{FS}(\tau)$/FSIR (Flat Surface Impulse Response), since it can be considered as the average backscattered power from a mean flat surface (illuminated by an impulse) which has a very small scale of roughness but is characterized by the same backscattering cross section per unit scattering area σ^0 as the true surface.

$$P_{AvIR}(\tau) = P_h(\tau) * P_{FS}(\tau) \quad (3.3.1.1)$$

Since we are dealing with extended target area dependent scatter, $P_{FS}(\tau)$ can be determined from an integration over the illuminated area of the surface, i.e.:

$$P_{FS}(t) = \frac{\lambda^2}{(4\pi)^3 L_p} \int_{illum.\ area} \frac{\delta\left(t - \frac{2r}{c}\right) G^2(\theta, w)\sigma^0(\psi, \phi)}{r^4} dA \quad (3.3.1.2)$$

where:

- λ is the carrier wavelength
- L_p two way propagation loss
- $\delta(t - 2r/c)$ transmitted delta function appropriately delayed in time (c is the speed of light)
- $G(\theta, w)$ antenna gain
- r range from radar to the elemental scattering area dA on the surface

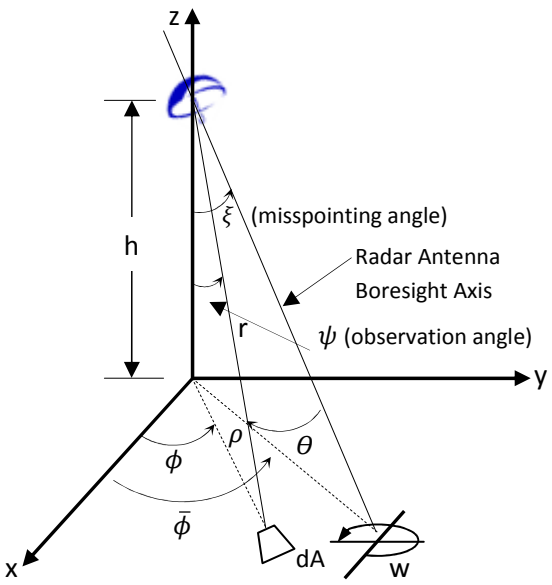

Figure 3.13 Geometry used to evaluate the altimeter echo model

The geometry appropriate to this problem is shown in the figure above, where the xy plane is the flat surface while the z axis corresponds to the line from the radar antenna to the subnadir point on the surface.

The antenna is at a h height above the xy plane. In this case we will assume that the antenna gain is independent of w i.e., a circularly symmetric beam, moreover we shall also assume that the cross section per unit scattering area $\sigma^0(\psi, \phi)$ is independent from ϕ which is nearly valid in the case of typical space borne radar altimeters because of the small pulse widths and narrow antenna beam widths.

Now if we consider that $dA = \rho\, d\rho d\phi$, we just need to determine the θ angle as a function of ρ and ϕ to complete the ϕ-integration in **3.3.1.2.** Using the law of cosines and some trigonometrical identities we find:

$$cos\theta = \frac{\cos\xi + \varepsilon \sin\xi \cos(\bar{\phi} - \phi)}{\sqrt{1+\varepsilon^2}} \quad (3.3.1.3)$$

where $\varepsilon = \rho/h$.

Using a Gaussian approximation to the antenna gain *(generally valid out to the point on the antenna pattern for which there is no appreciable contribution to the backscattered power)*:

$$G(\theta) \approx G_0 \exp\left(-\frac{2}{\gamma}\sin^2\theta\right) \quad (3.3.1.4)$$

where $\gamma = -2\left(\sin^2\left(\frac{\theta_{3dB}}{2}\right)/\ln 0.5\right)$ and with $r = \sqrt{h^2+\rho^2}$, **3.3.1.2** can be written as:

$$P_{FS}(t) = \frac{G_0^2\lambda^2}{(4\pi)^3 L_p}\int_0^\infty\int_0^{2\pi} \frac{\delta\left(t - \frac{2h}{c}\sqrt{1+\varepsilon^2}\right)}{(1+\varepsilon^2)^2}\sigma^0(\psi) *$$

$$* \exp\left\{-\frac{4}{\gamma}\left(1 - \frac{\cos^2\xi}{1+\varepsilon^2}\right) + b + a\cos(\bar{\phi}-\phi) - b\sin^2(\bar{\phi}-\phi)\right\} d\phi\rho d\rho \quad (3.3.1.5)$$

where:

- $a = (4\varepsilon/\gamma)\left(\sin 2\xi/(1+\varepsilon^2)\right)$
- $b = (4\varepsilon^2/\gamma)\left(\sin^2\xi/(1+\varepsilon^2)\right)$

Because of the 2π range of the integration and the form of the integrand, the $\bar{\phi}$ angle can be ignored, thus substituting:

$$\exp(-b\sin^2(\phi)) = \sum_{n=0}^{\infty}\frac{-(1)^n b^n \sin^{2n}\phi}{n!} \quad (3.3.1.6)$$

the equation **3.3.1.5** becomes

$$P_{FS}(t) = \frac{2\sqrt{\pi}G_0^2\lambda^2\sigma^0(\psi_0)}{(4\pi)^3 L_p h^4}\sum_{n=0}^{\infty}\frac{-(1)^n\Gamma(n+1/2)}{\Gamma(n+1)} *$$

$$* \int_0^\infty \left(\frac{2b}{a}\right)^n I_n(a)\exp\left[-\frac{4}{\gamma}\left(1 - \frac{\cos^2\xi}{(1+\varepsilon^2)}\right) + b\right]\frac{\delta\left(t - \frac{2h}{c}\sqrt{1+\varepsilon^2}\right)}{(1+\varepsilon^2)^2}\rho d\rho \quad (3.3.1.7)$$

since:

$$\int_0^{2\pi}\exp(a\cos\phi - b\sin^2\phi)d\phi = 2\sqrt{\pi}\sum_{n=0}^{\infty}\frac{-(1)^n\Gamma(n+1/2)}{\Gamma(n+1)}\left(\frac{2b}{a}\right)^n I_n(a) \quad (3.3.1.8)$$

where $I_n(\cdot)$ are the modified Bessel function of order n, and $\Gamma(\cdot)$ are gamma functions.

Then under a suitable change of variables **3.3.1.7** can be evaluated, and taking into account that for space borne altimetry $c\tau/h \ll 1$, we obtain, in term of the two-way incremental ranging time i.e., $\tau = t - t_0 = t - 2h/c$ (do not confound this τ with that of the **3.0** section):

$$P_{FS}(\tau) = \frac{G_0^2 \lambda^2 c \sigma^0(\psi_0)}{4(4\pi)^2 L_p h^3} \exp\left[-\frac{4}{\gamma}\sin^2\xi - \frac{4c}{\gamma h}\tau\cos 2\xi\right] *$$

$$* \sum_{n=0}^{\infty}\left\{\frac{-(1)^n \Gamma(n+1/2)}{\Gamma(n+1)}\left[\sqrt{\frac{c\tau}{h}}\tan\xi\right]^n I_n\left(\frac{4}{\gamma}\sqrt{\frac{c\tau}{h}}\sin 2\xi\right)\right\} \quad (3.3.1.9)$$

for $\tau \geq 0$ and $P_{FS}(\tau) = 0$ for $\tau \geq 0$.

Now if we rewrite:

$$\sum_{n=0}^{\infty}\{\cdot\} = I_0(Y)\left\{1 + \sum_{n=0}^{\infty}\left(\frac{-(1)^n \Gamma(n+1/2)}{\Gamma(n+1)}\frac{I_n(Y)}{I_0(Y)}\left[\frac{\gamma Y}{8\cos^2\xi}\right]^n\right)\right\} \quad (3.3.1.10)$$

where:

$$Y = \frac{4}{\gamma}\sqrt{\frac{c\tau}{h}}\sin 2\xi \quad (3.3.1.11)$$

we can easily see that for $(\gamma Y)/(8\cos^2\xi) \ll 1$ the series becomes highly convergent due to rapidly decreasing (with n) of $[(\gamma Y)/(8\cos^2\xi)]^n$, so for:

$$\sqrt{\frac{c\tau}{h}}\tan\xi \ll 1 \quad (3.3.1.12)$$

the infinite series in **3.4.1.9** may be truncated at n=0 with no effective loss in accuracy, thus finally:

$$\begin{cases} P_{FS}(\tau) = \dfrac{G_0^2 \lambda^2 c \sigma^0(\psi_0)}{4(4\pi)^2 L_p h^3} \exp\left(-\dfrac{4}{\gamma}\sin^2\xi - \dfrac{4c\tau}{\gamma h} cos\, 2\xi\right) I_o\left(\dfrac{4}{\gamma} sin\, 2\xi \sqrt{\dfrac{c\tau}{h}}\right) & \tau \geq 0 \\ P_{FS}(\tau) = 0 & \tau < 0 \end{cases} \quad (3.3.1.13)$$

where $\tan\psi_0 \approx \sqrt{c\tau/h}$. It is interesting to note that this condition under which **3.3.1.13** is valid, depends on the altitude and the pointing angle but not on the antenna pattern.

As pointed before, in order to obtain the average return power the FSIR must be convoluted with the probability density function of the height of the specular points on the surface and with the radar system point target response:

$$IR(\tau) = P_{FS}(\tau) * P_h(\tau) * P_p(\tau) \quad (3.3.1.14)$$

In the following paragraphs we are going to analyze whether this convolution can be integrated in closed form in all *Cassini* spacecraft attitudes and if it is valid for all ξ pointing angles with which *Cassini* must deal.

The general assumptions at the basis of the development of the *Cassini* altimeter echo model hereafter described are (Brown, 1997):

- presence of very smooth hydrocarbon ocean (lakes) and of icy lands leads to an expected echo which contains either coherent and non coherent scattering contributions
- independent scattering elements on the observed surface;
- rough surface with Gaussian height probability density function;
- variation of scattering process with angle of incidence dependent only upon the backscattering cross section per unit scattering area (0σ) and upon the antenna pattern;
- negligibility of Doppler frequency spreads;
- radar altimeter in ALTH mode the is made working always in pulse limited mode but in any case the pulsewidth limited footprint is never much smaller than the beamwidth limited footprint.

3.3.2) Nadir Model

When dealing with nadir pointing angles, an exact closed form of the impulse response it's still possible since **3.3.1.13** can be rewritten, if we consider $\xi = 0$, as:

$$\begin{cases} P_{FS}(\tau) = \dfrac{G_0^2 \lambda^2 c \sigma^0}{4(4\pi)^2 L_p h^3} \exp\left(-\dfrac{4c}{\gamma h}\tau\right) & \tau \geq 0 \\ P_{FS}(\tau) = 0 & \tau < 0 \end{cases} \quad (3.3.2.1)$$

we can include the spherical effects as described in **[4]** by replacing τ by τ/Λ, being $\Lambda = (1 + h/R_t)$, where R_t is the mean radius of Titan (2575km). Thus we have:

$$\begin{cases} P_{FS}(\tau) = K_{FS} \exp(-\alpha\tau) & \tau \geq 0 \\ P_{FS}(\tau) = 0 & \tau < 0 \end{cases} \quad (3.3.2.1)$$

where:

- $K_{FS} = (G_0^2 \lambda^2 c \sigma^0)/(4(4\pi)^2 L_p h^3)$
- $\alpha = (4c)/(\gamma h \Lambda)$

An example of nadir pointing FSIR evaluation for the *Cassini* Radar Altimeter with varying spacecraft altitude is given in the following figure:

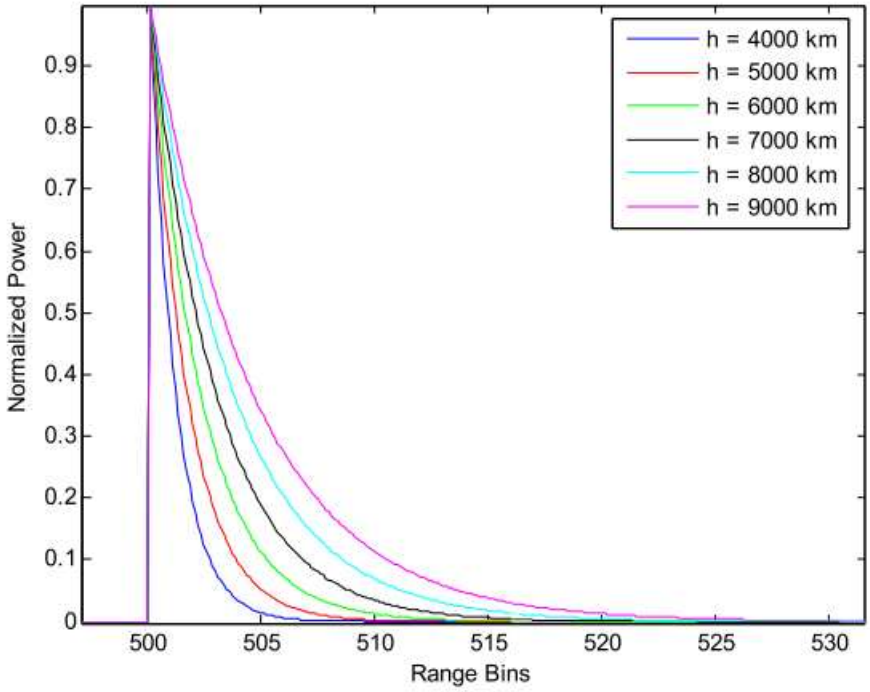

Figure 3.14 Nadir pointing FSIR with varying spacecraft altitude

The width of each waveform sampling gate is 30m, corresponding to the vertical resolution of the Hi-Res Altimeter (ALT) of the *Cassini* Radar, which is given by $c/(2f_c) \approx 30\text{m}$, where f_c is the sampling frequency. In the following t_0 is the reference time, i.e. the instant at which the first echo from the surface within the radar footprint is expected to arrive. Therefore, all the functions will be centered around this value, which at first attempt is settled to be 500 if expressed in range bins ($t_0 * f_c$), as results from LBDR echo data.

The height probability density function and the system point target response, both supposed to be Gaussian, are given by the following expressions:

$$P_h(\tau) = \frac{1}{\sqrt{2\pi}\sigma_h}\frac{c}{2}\exp\left(-\frac{\tau^2}{2\sigma_h^2}\frac{c^2}{4}\right) \quad (3.3.2.2)$$

$$P_p(\tau) = \frac{P_T T}{\sqrt{2\pi}\sigma_p}\exp\left(-\frac{\tau^2}{2\sigma_p^2}\right) \quad (3.3.2.3)$$

where σ_h is the rms height of the specular points relative to the mean surface level, P_T is the peak transmitted power, and σ_p is related to the 37,84 dB width of the transmitted pulse by the following relation: $\sigma_p = T/\sqrt{8\ln 2}$.

The convolution between **3.3.2.2** and **3.3.2.3** can be written as:

$$P_{HI}(\tau) = K_{HI}\exp(-a\tau^2) \quad (3.3.2.4)$$

where:

- $K_{HI} = P_T BT\sqrt{2\pi}(\sigma_p/\sigma_c)$,
- $a = 1/(2{\sigma_c}^2)$
- ${\sigma_c}^2 = {\sigma_s}^2 + {\sigma_p}^2$
- $\sigma_s = \frac{2}{c}\sigma_h$

The total average impulse response is then given by:

$$P_{HI}(\tau) * P_{FS}(\tau) = K_{FS}K_{HI}\exp(-\alpha\tau) * \exp(-a\tau^2) =$$
$$= K_{FS}K_{HI}\exp(-a\tau^2)\int_0^\infty \exp(-2bt)\exp(-at^2)\,dt \quad (3.3.2.5)$$

where $2b = \alpha - 2a\tau$.

Since, as can be seen in **[5]**:

$$\int_0^\infty \exp(-2bt)\exp(-at^2)dt = \frac{1}{2}\sqrt{\frac{\pi}{a}}\exp\left(\frac{b^2}{a}\right)erfc\left(\frac{b}{\sqrt{a}}\right) \quad (3.3.2.6)$$

the total average impulse response can be written as:

$$IR(\tau)|_{Nadir} = P_{HI}(\tau) * P_{FS}(\tau) =$$
$$= K\sigma_0\frac{1}{2}\exp\left(\frac{\delta^2}{2}\right)\exp\left(-\frac{\delta}{\sigma_c}\tau\right)\left[1 + erf\left(\frac{\tau}{\sqrt{2}\sigma_c} - \frac{\delta}{\sqrt{2}}\right)\right] \quad (3.3.2.7)$$

where

- $\delta = \alpha\sigma_c$
- $K = \left[G_0^2\lambda^2 c/\left(2(4\pi)^2 L_p h^3\right)\right]P_T BT\sigma_p\pi$

This equation is not dependent of any condition about the altimeter's operative mode, e.g. pulse-limited or not, and it can be considered as a generalization of the Brown's model.

It is worth noting that if the altimeter operating conditions vary towards a typical pulse-limited mode, then the equation **3.3.2.7** gives back the classical Brown echo, whose validity conditions are met when the parameter δ is small (e.g. δ<<1). In that case we have:

$$\frac{\delta^2}{2} \ll \frac{\delta}{\sigma_c} \; and \; \frac{\delta}{\sqrt{2}} \ll \frac{\tau}{\sqrt{2}\sigma_c}$$

and so equation **3.3.2.7** becomes exactly **that of the section 3.0**.

For the *Cassini* Radar Altimeter, δ varies between 0.5 and 1.1, as shown in the following figure:

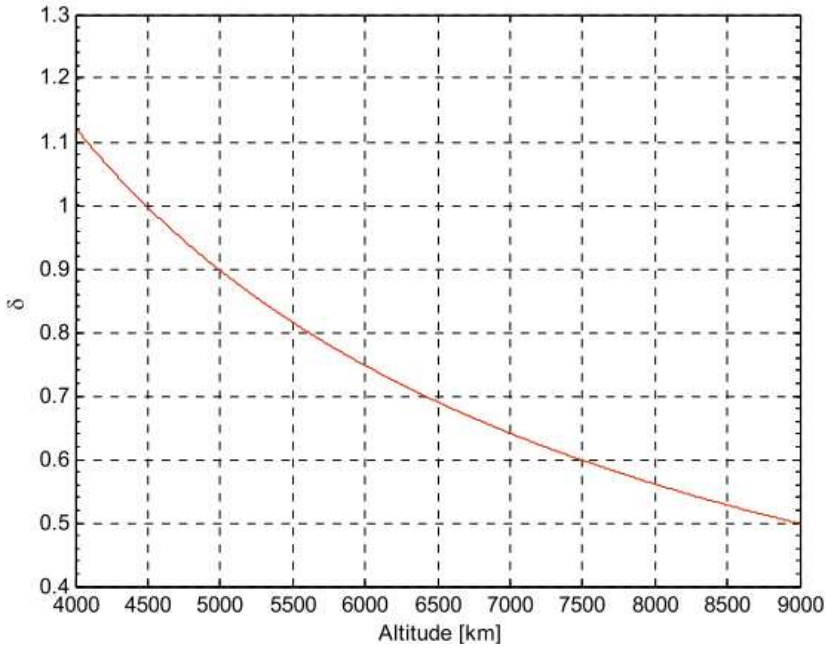

Figure 3.15 Parameter δ versus spacecraft altitude for the Cassini Radar Altimeter

Since $\delta = \alpha\sigma_c$, in general, the condition δ<<1 can be met if:

- $\alpha = f(\gamma^{-1}h^{-1})$ is small, i.e. the spacecraft altitude h increases, given the beamwidth and the pulse duration, and/or the antenna parameter $\gamma = f(\theta_{3dB})$ increases.
- σ_c is small, i.e. the parameter σ_p decreases due to a greater bandwidth B.

Some case studies of echo waveforms with varying δ are shown in the following figure, in order to perform a comparison between the IR model **3.3.2.7** and the Brown's model in case of nadir incidence. For the Skylab S-193 radar altimeter the following parameters have been considered, according to Brown's model: h=435.5km, θ_{3dB}=1.78°, σ_p=29.3ns:

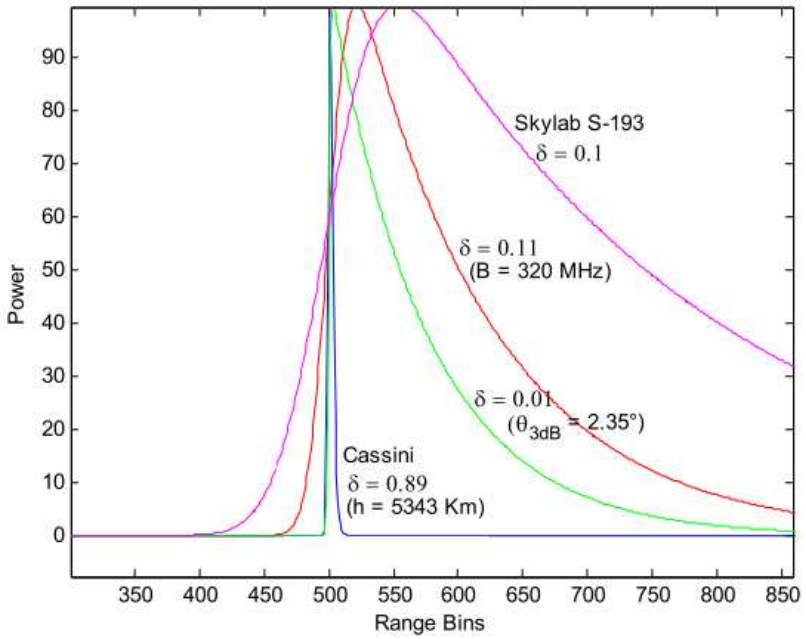

Figure 3.16 Comparison between IR models

An example of nadir pointing impulse response evaluation for the *Cassini* Radar Altimeter is given in the next figure with varying spacecraft altitude:

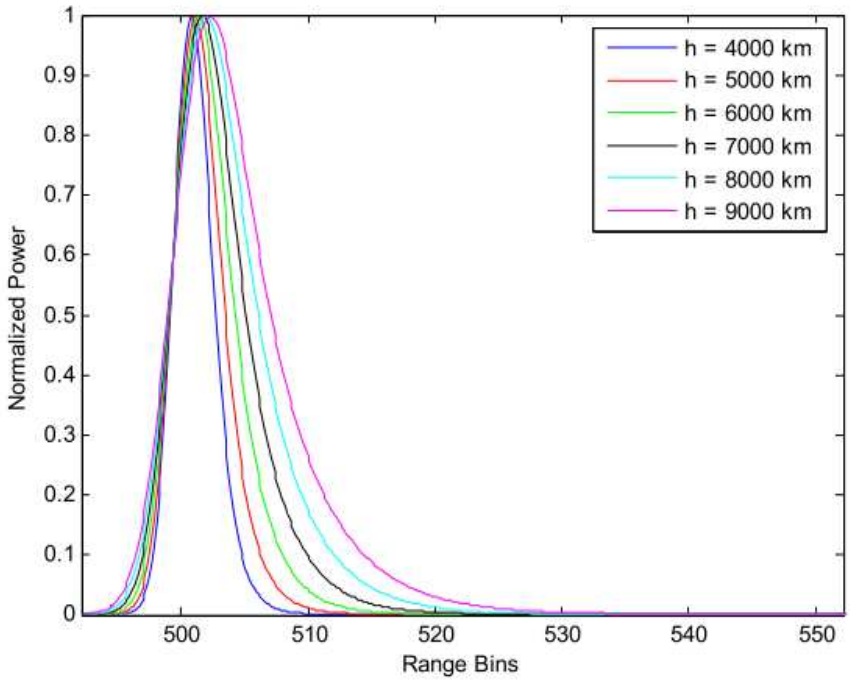

Figure 3.17 Cassini Nadir pointing IR simulation with varying spacecraft altitude (rms=2m)

In the next figure, examples of nadir pointing impulse responses are reported, which have been evaluated for different values of σ_h, the standard deviation:

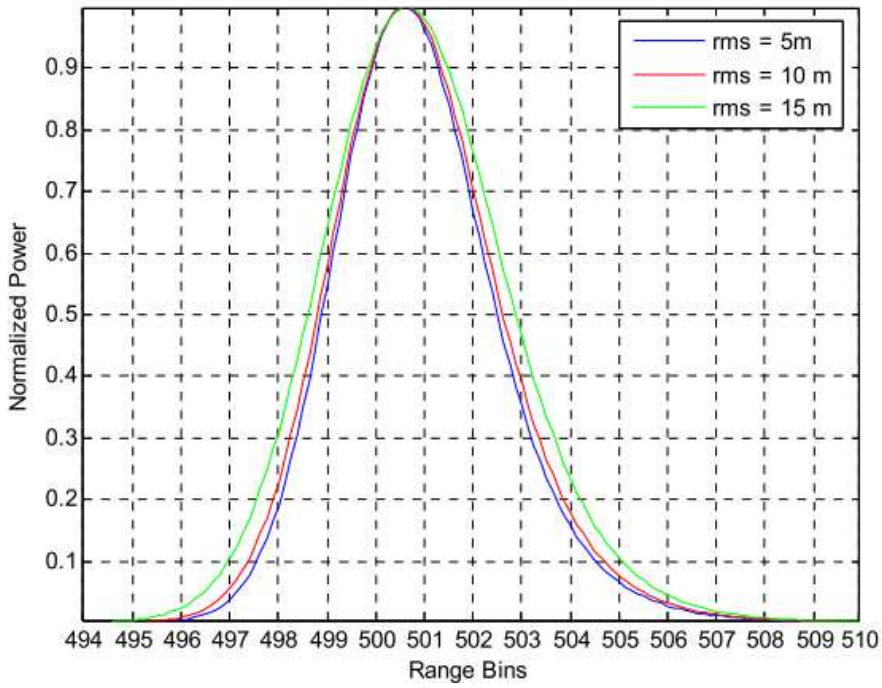

Figure 3.18 Nadir pointing IR for different values of surface rms height

As explained in section **2.4.D.3** this model will be used in case of very low off-nadir pointing angles ($\xi < 0.04$).

3.3.3) Asymptotic Brown Model

When dealing with far ξ off-nadir angles the approximation made in **3.3.1.12** is no longer possible since the argument of the Bessel functions in **3.3.1.9** becomes very large even for relatively small delay times (τ). This large argument requires an alternate expression for the FSIR based on asymptotic methods suggested by Brown in 1989 **[7]**.

If we come back to equation **3.3.1.8**, we see that we can also write:

$$\int_0^{2\pi} \exp(a\cos\phi - b\sin^2\phi)d\phi = \{\sin^2\phi = 1-\cos^2\phi\} =$$

$$= \exp(-b)\int_{-\pi}^{\pi} \exp(a\cos\phi + b\cos^2\phi)d\phi \quad (3.3.3.1)$$

now in the right side of **3.3.3.1** it is clear that the maximum is at $\phi = 0$ so for either a or b or both sufficiently large, **3.3.3.1** can be asymptotically evaluated by Laplace's method **[6]** to finally give:

$$\exp(-b)\int_{-\pi}^{\pi} \exp(a\cos\phi + b\cos^2\phi)d\phi \approx \exp(a)\sqrt{\frac{2\pi}{a\left(1+\frac{2b}{a}\right)}} \quad (3.3.3.2)$$

It is worth noting that in this last result the validity or computability of **3.3.3.2** does not depend on which factor a or b is larger, in contrast to what is taking place with the series in **3.3.1.8** where is easy to compute when $a \gg b$ but difficult when a and b are comparable.

At this point we can substitute **3.3.3.2** back into **3.3.1.5** and complete the ρ-integration to yield:

$$P_{FS}^{Asymp}(\tau) = \frac{G_o^2\lambda^2 c\sigma^0}{2(4\pi)^3 L_p h^3} G(\varepsilon) = A\sigma^0 G(\varepsilon) \quad (3.3.3.3)$$

where:

$$G(\varepsilon) = \exp\left(-\frac{4}{\gamma(1+\varepsilon^2)}(\sin\xi - \varepsilon\cos\xi)^2\right)\sqrt{\frac{2\pi}{a+2b}} \quad (3.3.3.4)$$

in this case the parameter ε has been approximated by $\varepsilon = \sqrt{c\tau/h\Lambda}$.

As can be seen in **[7]** a criterion is provided which, if met, ensures that the error in using the above approximation will be less than 2% of the true value. This criterion can be expressed in the following form:

$$\tau_{min} \geq \frac{h}{c}\left(0.849\gamma\frac{(1+\tan^2\xi)}{\tan\xi}\right)^2$$

which shows how for a given pointing angle ξ, antenna beamwidth (embedded in γ), and radar height h, there is a minimum ranging time τ_{min} for which **3.3.3.3** is accurate to less than 2% error, as indicated in the following figure:

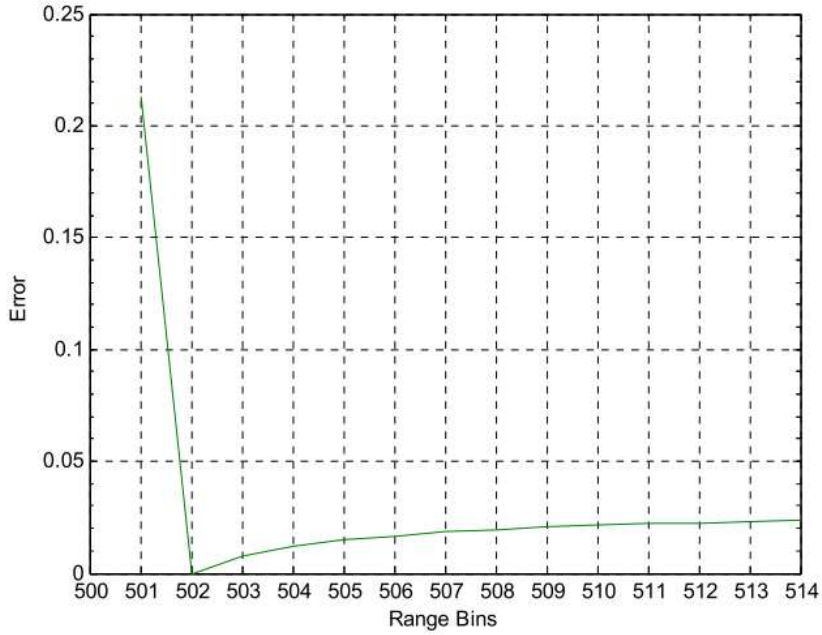

Figure 3.19 Error in using equation 3.3.3.3 (ξ=0.23°, h =4000 km)

However as noted in **2.4.D.3** section the *Cassini PAD System* has developed its own method to establish the range of off-nadir angles where the asymptotic Brown Model can be used.

For the *Cassini* Radar Altimeter, the value of τ_{min} (in range bins) with varying spacecraft altitude and off-nadir angle is given in the following figure. As clearly shown, the error is bounded within the first few pixels:

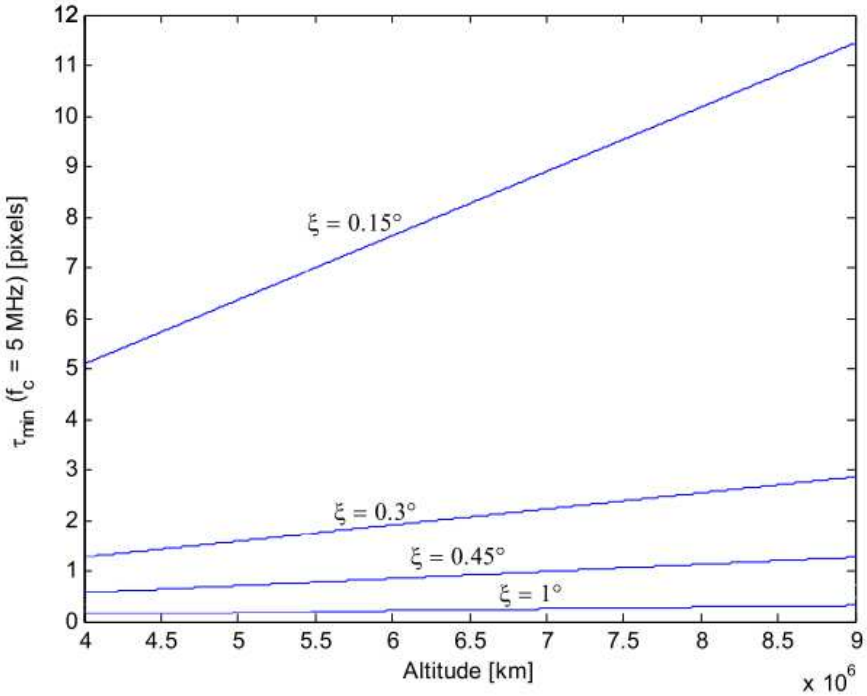

Figure 3.19 Variation of τ_{min} (in range bins) with spacecraft altitude for various off-nadir angles

A comparison between the FSIR evaluated in both nadir and off-nadir case is reported in the next figure:

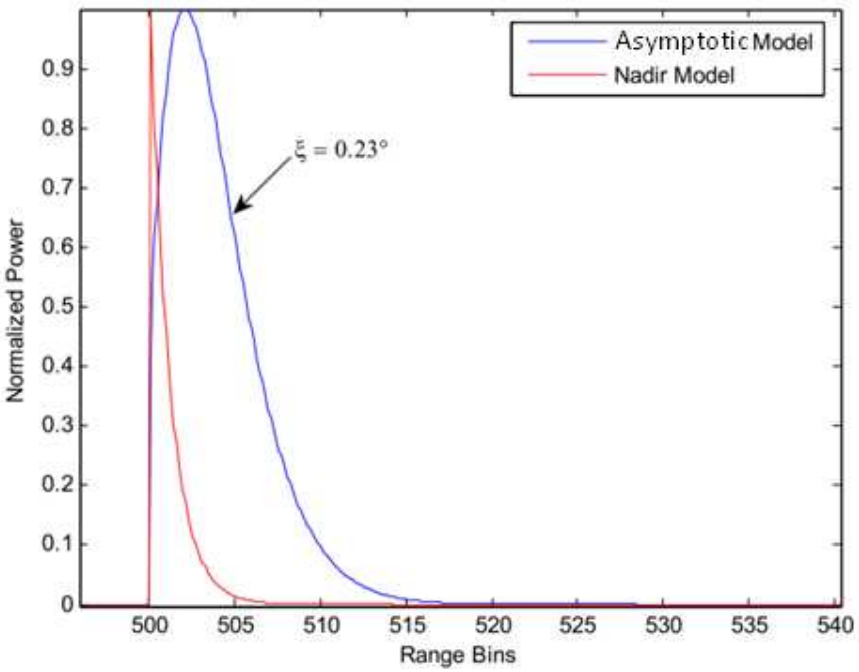

Figure 3.20 Comparison between evaluated FSIR for nadir and Asymptotic Brown model

As in Nadir Model, the system impulse response can be evaluated by the convolution of **3.3.3.3** and **3.3.2.4**, except for the fact that in this case (and also in the following Prony's Model) must be taken into account the time shift of height, given by:

$$\tau_0 = \frac{2(R-h)}{c} \approx \frac{2}{c}\left[(h+R_T)(\cos\xi - 1) + \frac{(h+R_T)^2 \sin^2\xi}{2R_T}\right] \quad (3.3.3.5)$$

as sketched in the following figure:

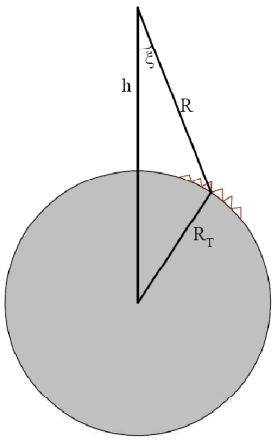

Figure 3.21 Off-nadir altimetry geometry

In the following all the evaluated impulse response functions have to be considered delayed by the previous extra amount of time.

Since for high values of off-nadir angle the P_{FS}^{Asymp} becomes much more wider than the radar point target response and the height probability density function.

Thus the total impulse response can be simply written as the product of the following terms:

$$IR(\tau)|_{Asymp} = P_{FS}^{Asymp}(\tau)\sigma_p\left[1 + erf\left(\frac{\tau}{\sqrt{2}\sigma_c}\right)\right] =$$

$$= A\sigma^0 G(\varepsilon)\sigma_p\left[1 + erf\left(\frac{\tau}{\sqrt{2}\sigma_c}\right)\right] \quad (3.3.3.6)$$

This model is reported in the two following figures, for all likely scenarios in terms of spacecraft altitude and off-pointing angle:

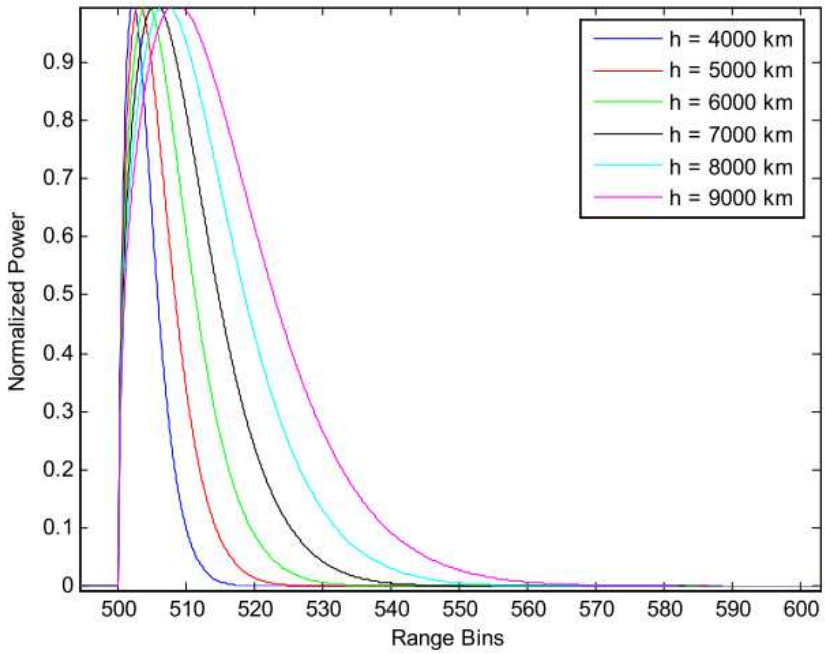

Figure 3.22 Asymptotic model with varying spacecraft altitude (ξ=0.23°)

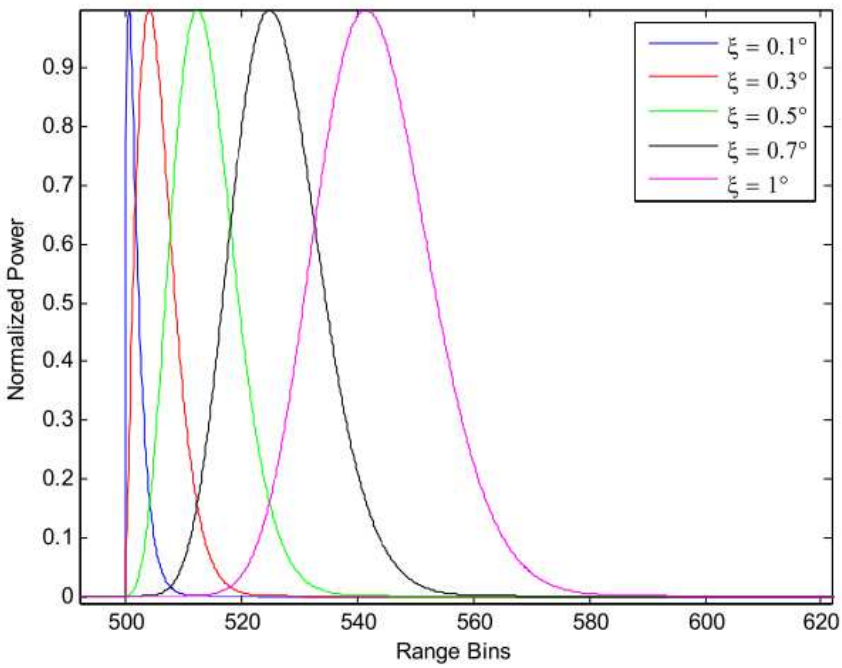

Figure 3.23 Asymptotic model with varying off-nadir angle (h =4000 km)

Due to reasons mentioned above, this model will be chosen when dealing with far off-nadir values.

3.3.4) Prony's Method Model

When dealing with small mispointing angles, we must work in such a way that the approximation made in the previous section is no longer valid since it will produce too big errors to deal with (see ***2.4.D.3*** section). Obviously the equation **3.3.2.1** is not valid since in this case .

In 1977 Brown made some approximations (see **[8]**) that yielded, at the end, with an exact closed form of the equation **3.3.1.14**, this approximations were possible when the pulse-width limited circle is much smaller than the beam-width limited circle. But unfortunately, due to mission constraints, the *Cassini* Radar ALT is settled to work in such a way that the pulsewidth-limited and the beam-limited circles are comparable, so an alternative method was needed in order to manage when dealing with small off-nadir angles.

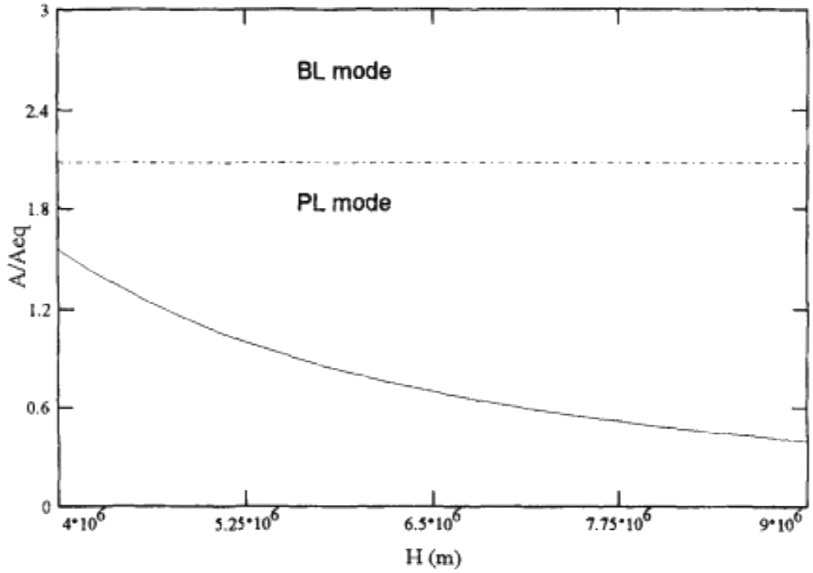

Figure 3.24 Pulsewidth limited to beamwidth limited circle ratio for the case of the high resolution Cassini

The figure above shows that when operating in high resolution altimetry mode the radar operates in the PL region but BL circle and the PL are always comparable. (where , the pulsewidth limited circle and , the beamwidth limited circle)

The method, suggested by Brown in **[8]** and developed by E. Montefredini, F. Morelli, G. Picardi and R. Seu in **[9]** consists in approximating the Bessel function ( ) of the FSIR in **3.3.1.13** by a series of exponentials using Prony's Method see **[6]** and section **3.5**. This method allows closing the convolution integral for each exponential term in the series and yields a simple function of exponentials.

The starting point is the FSIR expression of **3.3.1.13** rewritten as a function of the adimensional parameter :

$$P_{FS}(\varepsilon) = K_{FS} \exp\left(-\frac{4}{\gamma}\varepsilon^2 \cos 2\xi\right) I_0\left(\frac{4}{\gamma}\varepsilon \sin 2\xi\right) \quad (3.3.4.1)$$

After some trade-off (see **[11]**), it has been found that the most convenient way of approximating the Bessel function is the following:

$$I_0\left(\frac{4}{\gamma}\varepsilon \sin 2\xi\right) \cong \sum_{i=1}^{N} C_i \exp(a_i x) \quad (3.3.4.2)$$

where the constants C_i and a_i are evaluated with Prony's method of order N and $x = \sin(2\xi)\varepsilon^2/\gamma$ so the $P_{FS}(\varepsilon)$ can be rewritten as:

$$P_{FS}(\tau) = K_{FS} \exp(-K_a \tau) \sum_{i=1}^{N} C_i \exp(K_i \tau) \quad (3.3.4.3)$$

where:

$$\begin{cases} K_a = \dfrac{4}{\gamma}\cos 2\xi \dfrac{c}{h\Lambda} \\ K_i = \dfrac{4}{\gamma}\sin 2\xi \dfrac{c}{h\Lambda} a_i \end{cases} \quad (3.3.4.4)$$

The final impulse response, using Prony's method can be written as:

$$IR(\tau)|_{Prony} = P_{FS}(\tau) * P_{HI}(\tau) = \sum_{i=1}^{N} IR_i(\tau) \quad (3.3.4.5)$$

where :

$$IR_i(\tau) = K_{FS} K_{HI} C_i \exp(-K_a \tau) \exp(K_i \tau) * \exp(-a\tau^2) =$$
$$= \{\delta_i = (K_a - K_i)\sigma_c\} = K_{FS} K_{HI} C_i \exp(\delta_i \tau) * \exp(-a\tau^2) \quad (3.3.4.6)$$

which is exactly like the **3.3.2.5** except for the C_i term, so we can proceed in an analogous way and finally we have:

$$IR_i(\tau) = C_i K \sigma_0 \frac{1}{2} \exp\left(-\frac{4}{\gamma}\sin^2 \xi\right) \exp\left(\frac{{\delta_i}^2}{2} - \frac{\delta_i}{\sigma_c}\tau\right) *$$
$$* \left[1 + erf\left(\frac{\tau}{\sqrt{2}\sigma_c} - \frac{\delta_i}{\sqrt{2}}\right)\right] \quad (3.3.4.5)$$

so the total impulse response for small mispointing angles calculated with Prony's Method can be stated as:

$$IR|_{Prony}(\tau) = K \sigma_0 \frac{1}{2} \exp\left(-\frac{4}{\gamma}\sin^2 \xi\right) \sum_{i=1}^{N} C_i \exp\left(\frac{{\delta_i}^2}{2} - \frac{\delta_i}{\sigma_c}\tau\right) *$$
$$* \left[1 + erf\left(\frac{\tau}{\sqrt{2}\sigma_c} - \frac{\delta_i}{\sqrt{2}}\right)\right] \quad (3.3.4.6)$$

The values of constants C_i and a_i, calculated with the Prony's method are showed in the following table:

	N=2	N=3	N=4	N=5
C_i	0.4931-3.0089j 0.4931+3.0089j	8.1825-0.0000j -3.5914-0.8860j -3.5914+0.8860j	1.6103-27.0408j 1.6103+27.0408j -1.1103+6.7271j -1.1103-6.7271j	1.3582-17.5134j 1.3582+17.5134j -0.8581+4.2427j -0.8581-4.2427j -2.3922e-5+3.3479e-12j
a_i	52.5318+25.1672j 52.5318-25.1672j	45.3668 31.7576+29.0453j 31.7576-29.0453j	31.5091+8.3585j 31.5091-8.3585j 20.4373+23.3103j 20.4373-23.3103j	34.1407+10.1205j 34.1407-10.1205j 19.7521+25.7877j 19.7521-25.7877j -4.3681e4+9.9049e4j

Table 3.1 Exponential and amplitude factors for Prony's approximation

3.4) Gating Functions

In the following paragraphs will be described the mathematical concepts followed to evaluate the gating functions:

3.4.1) Nadir Model time gating function

The starting point is **3.3.2.7** equation:

$$IR(\tau)|_{Nadir} = K\sigma_0 \frac{1}{2}\exp\left(\frac{\delta^2}{2}\right)\exp\left(-\frac{\delta}{\sigma_c}\tau\right)\left[1 + erf\left(\frac{\tau}{\sqrt{2}\sigma_c} - \frac{\delta}{\sqrt{2}}\right)\right] \quad (3.4.1.1)$$

where $\tau = t - 2h/c = t - t_0$. If we take:

$$B = K\sigma_0 \frac{1}{2}\exp\left(\frac{\delta^2}{2}\right)\exp\left(-\frac{\delta}{\sigma_c}t\right) \quad (3.4.1.2)$$

we can rewrite **3.3.2.7** as:

$$IR(t_0)|_{Nadir} = B\exp\left(\frac{\delta}{\sigma_c}t_0\right)\left[1 + erf\left(\frac{t - t_0}{\sqrt{2}\sigma_c} - \frac{\delta}{\sqrt{2}}\right)\right] \quad (3.4.1.3)$$

By taking the derivative with respect to t_0 and noting that:

$$\frac{\partial \mathrm{erf}\,(z)}{\partial z} = \frac{2}{\sqrt{\pi}}\exp(-z^2) \quad (3.4.1.4)$$

we have:

$$\frac{\partial IR(t_0)|_{Nadir}}{\partial t_0} = B\frac{\delta}{\sigma_c}\exp\left(\frac{\delta}{\sigma_c}t_0\right)\left[1 + erf\left(\frac{t - t_0}{\sqrt{2}\sigma_c} - \frac{\delta}{\sqrt{2}}\right)\right] +$$

$$+B\exp\left(\frac{\delta}{\sigma_c}t_0\right)\frac{2}{\sqrt{\pi}}\exp\left(-\frac{(t - t_0)^2}{2{\sigma_c}^2} - \frac{\delta^2}{2} + \frac{(t - t_0)}{\sigma_c}\delta\right)\left(-\frac{1}{\sqrt{2}\sigma_c}\right) =$$

$$= IR(t_0)|_{Nadir}\frac{\delta}{\sigma_c} - K\sigma_0\frac{1}{2}\sqrt{\frac{2}{\pi}}\frac{1}{\sigma_c}\exp\left(-\frac{(t-t_0)^2}{2{\sigma_c}^2}\right) \quad (3.4.1.5)$$

3.4.2) Asymptotic Brown Model time gating function

The starting point is the **3.3.3.6** equation:

$$IR(\varepsilon)|_{Asymp} = A\sigma^0\exp\left(-\frac{4}{\gamma(1+\varepsilon^2)}(\sin\xi - \varepsilon\cos\xi)^2\right) *$$

$$* \sqrt{\frac{2\pi}{a+2b}}\sigma_p\left[1+erf\left(\frac{\tau}{\sqrt{2}\sigma_c}\right)\right] \quad (3.4.2.1)$$

by taking:

$$H(\tau) = \sigma_p\left[1+erf\left(\frac{\tau}{\sqrt{2}\sigma_c}\right)\right] \quad (3.4.2.2)$$

$$Y(\varepsilon) = A\sigma^0\exp\{F(\varepsilon)\}G(\varepsilon) \quad (3.4.2.3)$$

where:

$$F(\varepsilon) = -\frac{4}{\gamma(1+\varepsilon^2)}(\sin\xi - \varepsilon\cos\xi)^2 \quad (3.4.2.4)$$

$$G(\varepsilon) = \sqrt{\frac{2\pi}{a+2b}} \quad (3.4.2.5)$$

we can express the derivative with respect to t_0 in the following way:

$$\frac{\partial IR(\varepsilon)|_{Asymp}}{\partial t_0} = \frac{\partial IR(\varepsilon)|_{Asymp}}{\partial\varepsilon}\frac{\partial\varepsilon}{\partial t_0} =$$

$$= \frac{\partial Y(\varepsilon)}{\partial\varepsilon}\frac{\partial\varepsilon}{\partial t_0}H(t-t_0) + Y(\varepsilon)\frac{\partial H(t-t_0)}{\partial t_0} \quad (3.4.2.6)$$

where:

$$\frac{\partial Y(\varepsilon)}{\partial\varepsilon} = Y(\varepsilon)F'(\varepsilon) + A\sigma^0\exp\{F(\varepsilon)\}G'(\varepsilon) \quad (3.4.2.7)$$

$$\frac{\partial\varepsilon}{\partial t_0} = -\frac{1}{2\varepsilon}\frac{c}{h\Lambda}, \text{since } \varepsilon = \sqrt{\frac{c(t-t_0)}{h\Lambda}} \quad (3.4.2.8)$$

$$F'(\varepsilon) = -\frac{4}{\gamma(1+\varepsilon^2)^2}[2\varepsilon\cos(2\xi) + (\varepsilon^2-1)\sin(2\xi)] \quad (3.4.2.9)$$

$$G'(\varepsilon) = \frac{G^3(\varepsilon)}{2K}\frac{(\varepsilon^2 - \tan\xi - 1)}{K(1+\varepsilon^2)^2} \quad (3.4.2.10)$$

and remembering, as noted before:

$$\frac{\partial H(t-t_0)}{\partial t_0} \leftrightarrow \frac{\partial \mathrm{erf}\,(z)}{\partial z} = \frac{2}{\sqrt{\pi}}\exp(-z^2) \quad (3.4.2.11)$$

3.4.3) Prony's Method Model time gating function

The starting point is the **3.3.4.6** equation:

$$IR(\tau)|_{Prony} = K\sigma_0 \frac{1}{2}\exp\left(-\frac{4}{\gamma}\sin^2\xi\right)\sum_{i=1}^{N} C_i \exp\left(\frac{{\delta_i}^2}{2} - \frac{\delta_i}{\sigma_c}\tau\right) * \\ * \left[1 + erf\left(\frac{\tau}{\sqrt{2}\sigma_c} - \frac{\delta_i}{\sqrt{2}}\right)\right] \quad (3.4.3.1)$$

which can be rewritten as:

$$IR(t,t_0)|_{Prony} = \\ = \mathrm{A}\sum_{i=1}^{N} C_i \exp\left(\frac{{\delta_i}^2}{2} - \frac{\delta_i}{\sigma_c}t\right)\exp\left(\frac{\delta_i}{\sigma_c}t_0\right)\left[1 + \mathrm{erf}\left(\frac{(t-t_0)}{\sqrt{2}\sigma_c} - \frac{\delta_i}{\sqrt{2}}\right)\right] \quad (3.4.3.2)$$

so the derivative with respect to t_0 can be stated as:

$$\frac{\partial IR(t_0)|_{Prony}}{\partial t_0} = A\sum_{i=1}^{N} C_i \exp\left(\frac{{\delta_i}^2}{2} - \frac{\delta_i}{\sigma_c}t\right)\frac{\partial}{\partial \mathrm{t_0}}\left\{\exp\left(\frac{\delta_i}{\sigma_c}t_0\right) * \right. \\ \left. * \left[1 + erf\left(\frac{(t-t_0)}{\sqrt{2}\sigma_c} - \frac{\delta_i}{\sqrt{2}}\right)\right]\right\} \quad (3.4.3.3)$$

so we can proceed exactly as in the **3.4.1.5:**

$$\frac{\partial IR(t_0)|_{Prony}}{\partial t_0} = A\sum_{i=1}^{N} C_i \exp\left(\frac{{\delta_i}^2}{2} - \frac{\delta_i}{\sigma_c}t\right)\frac{\delta_i}{\sigma_c}\exp\left(\frac{\delta_i}{\sigma_c}t_0\right)\left[1 + erf\left(\frac{(t-t_0)}{\sqrt{2}\sigma_c} - \frac{\delta_i}{\sqrt{2}}\right)\right] - \\ -\frac{1}{\sigma_c}\sqrt{\frac{2}{\pi}} C_i \exp\left(\frac{{\delta_i}^2}{2} - \frac{\delta_i}{\sigma_c}t\right)\exp\left(\frac{\delta_i}{\sigma_c}t_0\right)\exp\left(-\frac{(t-t_0)^2}{2{\sigma_c}^2} - \frac{{\delta_i}^2}{2} + \frac{(t-t_0)}{\sigma_c}\delta_i\right) \quad (3.4.3.4)$$

and the final Time Gating function for Prony's Model becomes:

$$\frac{\partial IR(t_0)|_{Prony}}{\partial t_0} = A\sum_{i=1}^{N}\left\{\frac{\delta_i}{\sigma_c} C_i \exp\left(\frac{{\delta_i}^2}{2} - \frac{\delta_i}{\sigma_c}t\right)\exp\left(\frac{\delta_i}{\sigma_c}t_0\right) * \right. \\ \left. * \left[1 + \mathrm{erf}\left(\frac{(t-t_0)}{\sqrt{2}\sigma_c} - \frac{\delta_i}{\sqrt{2}}\right)\right] - \frac{1}{\sigma_c}\sqrt{\frac{2}{\pi}} C_i \exp\left(-\frac{(t-t_0)^2}{2{\sigma_c}^2}\right)\right\} \quad (3.4.3.5)$$

3.4.4) Nadir Model roughness gating function

The starting point is **3.3.2.7** equation:

$$IR(\tau)|_{Nadir} = K\sigma_0 \frac{1}{2}\exp\left(\frac{\delta^2}{2}\right)\exp\left(-\frac{\delta}{\sigma_c}\tau\right)\left[1 + erf\left(\frac{\tau}{\sqrt{2}\sigma_c} - \frac{\delta}{\sqrt{2}}\right)\right] \quad (3.4.4.1)$$

noting that $\delta = \alpha\sigma_c$ we can rewrite:

$$IR(\sigma_c)|_{Nadir} = K\sigma_0 \frac{1}{2}\exp\left(\frac{\alpha^2{\sigma_c}^2}{2}\right)\exp(-\alpha\tau)\left[1 + erf\left(\frac{\tau}{\sqrt{2}\sigma_c} - \frac{\alpha\sigma_c}{\sqrt{2}}\right)\right] =$$

$$= C\exp\left(\frac{\alpha^2{\sigma_c}^2}{2}\right)\left[1 + erf\left(\frac{\tau}{\sqrt{2}\sigma_c} - \frac{\alpha\sigma_c}{\sqrt{2}}\right)\right] \quad (3.4.4.2)$$

so de derivative with respect to σ_c can be written as:

$$\frac{\partial IR(\sigma_c)|_{Nadir}}{\partial\sigma_c} = C\alpha^2\sigma_c\exp\left(\frac{\alpha^2{\sigma_c}^2}{2}\right)\left[1 + erf\left(\frac{\tau}{\sqrt{2}\sigma_c} - \frac{\alpha\sigma_c}{\sqrt{2}}\right)\right] -$$

$$-\sqrt{\frac{2}{\pi}}\left(\frac{\tau}{{\sigma_c}^2} + \alpha\right)C\exp\left(\frac{\alpha^2{\sigma_c}^2}{2}\right)\exp\left(-\frac{\tau^2}{2{\sigma_c}^2} - \frac{\alpha^2{\sigma_c}^2}{2} + \alpha\tau\right) =$$

$$= \alpha^2\sigma_c IR(\sigma_c)|_{Nadir} - K\sigma_0\frac{1}{2}\sqrt{\frac{2}{\pi}}\left(\frac{\tau}{{\sigma_c}^2} + \alpha\right)\exp\left(-\frac{\tau^2}{2{\sigma_c}^2}\right) \quad (3.4.4.3)$$

finally the Roughness gating function of the Nadir Model can be written as:

$$\frac{\partial IR(\sigma_s)|_{Nadir}}{\partial\sigma_s} = \frac{\partial IR(\sigma_c)|_{Nadir}}{\partial\sigma_c}\frac{\partial\sigma_c}{\partial\sigma_s} \quad (3.4.4.4)$$

where $\partial\sigma_c/\partial\sigma_s = \sigma_s/\sigma_c$ since $\sigma_c = \sqrt{{\sigma_s}^2 + {\sigma_p}^2}$

3.4.5) Asymptotic Brown Model roughness gating function

The starting point is the **3.3.3.6** equation:

$$IR(\sigma_c)|_{Asymp} = A\sigma^0\exp\left(-\frac{4}{\gamma(1+\varepsilon^2)}(\sin\xi - \varepsilon\cos\xi)^2\right) *$$

$$* \sqrt{\frac{2\pi}{a+2b}}\sigma_p\left[1 + erf\left(\frac{\tau}{\sqrt{2}\sigma_c}\right)\right] \quad (3.4.5.1)$$

so de derivative with respect to σ_c can be stated as:

$$\frac{\partial IR(\sigma_c)|_{Asymp}}{\partial\sigma_c} = A\sigma^0\exp\left(-\frac{4}{\gamma(1+\varepsilon^2)}(\sin\xi - \varepsilon\cos\xi)^2\right) *$$

$$* \sqrt{\frac{2\pi}{a+2b}}\sigma_p\frac{2}{\sqrt{\pi}}\left(-\frac{\tau}{\sqrt{2}{\sigma_c}^2}\right)\exp\left(-\frac{\tau^2}{2{\sigma_c}^2}\right) \quad (3.4.5.2)$$

and finally the roughness gating function of the Asymptotic Brown Model can be expressed as:

$$\frac{\partial IR(\sigma_s)|_{Asymp}}{\partial \sigma_s} = \frac{\partial IR(\sigma_c)|_{Asymp}}{\partial \sigma_c}\frac{\partial \sigma_c}{\partial \sigma_s} \quad (3.4.5.3)$$

where $\partial\sigma_c/\partial\sigma_s = \sigma_s/\sigma_c$.

3.4.6) Prony's Method Model roughness gating function

The starting point is the **3.3.4.6** equation:

$$IR(\tau)|_{Prony} = K\sigma_0 \frac{1}{2}\exp\left(-\frac{4}{\gamma}\sin^2\xi\right)\sum_{i=1}^{N} C_i \exp\left(\frac{{\delta_i}^2}{2} - \frac{\delta_i}{\sigma_c}\tau\right) * \\ * \left[1 + erf\left(\frac{\tau}{\sqrt{2}\sigma_c} - \frac{\delta_i}{\sqrt{2}}\right)\right] \quad (3.4.6.1)$$

since $\delta_i = (K_a - K_i)\sigma_c$ we can express the equation as a function of σ_c:

$$IR(\sigma_c)|_{Prony} = A\sum_{i=1}^{N} C_i \exp\left(-(K_a - K_i)\tau\right)\exp\left(\frac{(K_a - K_i)^2\sigma_c^2}{2}\right) * \\ * \left[1 + \mathrm{erf}\left(\frac{\tau}{\sqrt{2}\sigma_c} - \frac{(K_a - K_i)\sigma_c}{\sqrt{2}}\right)\right] \quad (3.4.6.2)$$

the derivative with respect to σ_c results to be

$$\frac{\partial IR(\sigma_c)|_{Prony}}{\partial \sigma_c} = K\sigma_0 \frac{1}{2}\exp\left(-\frac{4}{\gamma}\sin^2\xi\right)\sum_{i=1}^{N} C_i \exp\left(-(K_a - K_i)\tau\right)(K_a - K_i)^2\sigma_c * \\ * \exp\left(\frac{(K_a - K_i)^2\sigma_c^2}{2}\right)\left[1 + \mathrm{erf}\left(\frac{\tau}{\sqrt{2}\sigma_c} - \frac{(K_a - K_i)\sigma_c}{\sqrt{2}}\right)\right] - \\ - \sqrt{\frac{2}{\pi}} C_i \left(\frac{\tau}{\sigma_c^2} + (K_a - K_i)\right)\exp\left(-\frac{\tau^2}{2}\right) \quad (3.4.6.3)$$

and finally the roughness gating function of the Prony's Model, as in the other cases, can be expressed as:

$$\frac{\partial IR(\sigma_s)|_{Prony}}{\partial \sigma_s} = \frac{\partial IR(\sigma_c)|_{Prony}}{\partial \sigma_c}\frac{\partial \sigma_c}{\partial \sigma_s} \quad (3.4.6.4)$$

where $\partial\sigma_c/\partial\sigma_s = \sigma_s/\sigma_c$.

3.5) Prony's Method

Prony analysis is a method of fitting a linear combination of exponential terms to a signal as shown in **3.5.1**. Each term in **3.5.1** has four elements: the magnitude A_n, the damping factor σ_n, the frequency f_n, and the phase angle θ_n. Each exponential

component with a different frequency is viewed as a unique mode of the original signal $y(t)$. The four elements of each mode can be identified from the state space representation of an equally sampled data record. The time interval between each sample is T:

$$y(t) = \sum_{n=1}^{N} A_n e^{\sigma_n t} \cos(2\pi f_n t + \theta_n), \quad n = 1,2,3, \dots, N \quad (3.5.1)$$

Using Euler's theorem and letting t=MT, the samples of $y(t)$ are rewritten as:

$$y_M = \sum_{n=1}^{N} B_n \lambda_n^M \quad (3.5.2)$$

where:

$$B_n = \frac{A_n}{2} e^{j\theta_n} \ and \ \lambda_n = \exp[(\sigma_n + j2\pi f_n)T] \quad (3.5.3)$$

Prony analysis consists of three steps. In the first step, the coefficients of a linear predication model are calculated. The linear predication model (LPM) of order N, shown in **3.5.4**, is built to fit the equally sampled data record $y(t)$ with length M. Normally, the length M should be at least three tines larger than the order N:

$$y_M = a_1 y_{M-1} + a_2 y_{M-2} + \cdots + a_N y_{M-N} \quad (3.5.4)$$

Estimation of the LPM coefficients a_n is crucial for the derivation of the frequency, damping, magnitude and phase angle of a signal. To estimate these coefficients accurately, many algorithms can be used. A matrix representation of the signal at various sample times can be formed by sequentially writing the linear prediction of y_M repetitively. By inverting the matrix representation, the linear coefficients a_n can be derived from **3.5.5**. Am algorithm, which uses singular value decomposition for the matrix inversion to derive the LPM coefficients, is called SVD algorithm,

$$\begin{bmatrix} y_N \\ y_{N+1} \\ \bullet \\ y_{M-1} \end{bmatrix} = \begin{bmatrix} y_{N-1} & y_{N-2} & \bullet & y_0 \\ y_N & y_{N-1} & \bullet & y_1 \\ \bullet & \bullet & \bullet & \bullet \\ y_{M-2} & y_{M-3} & \bullet & y_{M-N-1} \end{bmatrix} \begin{bmatrix} a_1 \\ a_2 \\ \bullet \\ a_N \end{bmatrix} \quad (3.5.5)$$

In the second step, the roots λ_n of the characteristic polynomial shown as **3.5.6** associated with the LPM from the first step are derived. The damping factor σ_n and frequency f_n are calculated from the root λ_n according to **3.5.3:**

$$\lambda^N - a_1\lambda^{N-1} - \cdots - a_{N-1}\lambda - a_N = (\lambda - \lambda_1)(\lambda - \lambda_2) \dots (\lambda - \lambda_N) \quad (3.5.6)$$

In the last step, the magnitudes and the phase angles of the signal are solved in the least square sense. According to **3.5.2**, **3.5.7**, is built using the solved roots λ_n:

$$\underline{Y} = \phi \underline{B} \quad (3.5.7)$$

where:

$$\underline{Y} = [y_0, y_1, \dots, y_N]^T$$

$$\underline{\underline{\Phi}} = \begin{bmatrix} 1 & 1 & \bullet & 1 \\ \lambda_1 & \lambda_2 & \bullet & \lambda_N \\ \bullet & \bullet & \bullet & \bullet \\ \lambda_1^{M-1} & \lambda_2^{M-1} & \bullet & \lambda_N^{M-1} \end{bmatrix}$$

$$\underline{B} = [B_1, B_2, \dots, B_N]^T$$

The magnitude A_n and phase angle θ_n are thus calculated from the variables B_n acording to **3.5.3**. The greatest advantage of Prony analysis is its ability to identify the damping factor of each mode in the signal. Due to this advantage, transient harmonics can be identified accurately.

3.6) Doppler Tracking

Due to the variation of the radial distance between the spacecraft and Titan during each fly-by, the received radar echo will present a Doppler shifting. The Doppler effect is based on the change in frequency observed when there is relative radial movement, this is along the line joining the transmitter and a receiver.

If the distance between the radar and the target is R the number of wavelength within the roundtrip is $2R/\lambda$. Since the phase of the field travels a distance of 2π for each single wavelenght, the total distance ψ "traveled" by the electromagnetic wave of frequency f_0 is $4\pi R/\lambda_0, (\lambda_0 = c/f_0)$. Obviously if there is relative movement between radar and target both R and ψ depend therefore on time and each change in the phase ψ produces an instantaneous frequency f_D which is added to f_0:

$$2\pi f_D = \frac{d\psi}{dt} = -\frac{4\pi}{\lambda_0}\frac{dr}{dt} \quad (3.6.1)$$

This Doppler shift is then directly proportional to the relative radial velocity V_r (i.e. to the component along the line joining the radar-target) and can be expressed in the following way:

$$f_D = \frac{1}{2\pi}\frac{d\psi}{dt} = -\frac{2V_r}{\lambda} \quad (3.6.2)$$

Thus if an impulse is transmitted, the received signal will be frequency-shifted in a quantity proportional to the variation of the distance in the following way:

$$f_D = -\frac{2}{\lambda}\frac{d}{dt}R(t) \quad (3.6.3)$$

The magnitude of this difference depends on the pointing angle, the transmission frequency and on the geometry of the orbit. Assuming that the antenna is pointing towards the centre of Titan, for a certain period of the fly-by, the maximum Doppler deviation Δf will be less than ±600 kHz for a trajectory presenting a range of 1000km in the closest approach taking into account values of range and speed derived from the orbital simulation of the Titan fly-by's.

In the design of the *Cassini* Radar and the chirp signal generated by the Digital Chirp Generator should have a central frequency shifted $-\Delta f$ in order to compensate the Doppler deviation as done in the range processing of the *Cassini* PAD system, see **2.3.C**.

In the following figure it is shown the expected Doppler shifting during each fly-by. The points highlighted in red are the values of the Doppler shifting at the beginning and at the end of the *Cassini* Radar operating in high-resolution altimeter mode:

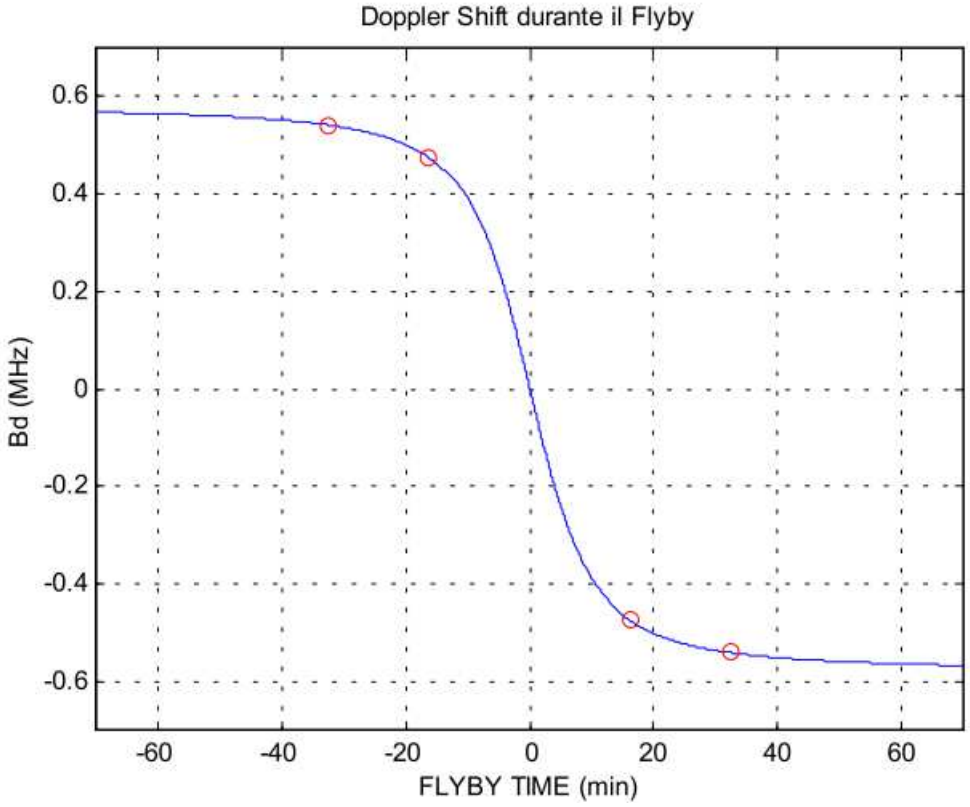

Table 3.25 Doppler shifting during the fly-by

CONCLUSIONS

In this work it has been provided an overview of the *Cassini* Radar Processing Altimetric Data system. It is actually installed and integrated at Thales Alenia Space Italia premises in Rome, funded by Italian Space Agency. It has been presented a review of the main functionalities, in order to show all the potentiality of the system to serve as a useful tool for the scientific community to support the analysis and validation of *Cassini* Radar Altimeter data.

One of the main goals of this work is to present the procedure and physical aspects followed in the derivation of a model for estimating the Radar altimeter performance that could provide good accuracy in any *Cassini* operative conditions. Unlike the previous existing models, with the proposed method, the estimated Impulse Response is independent from the specific operative conditions and instrument characteristics (Pulse Limited or Beam Limited).

In consequence the method developed is able to model the average return waveforms for an altimeter system with no restriction on altitude, antenna beamwidth or transmitted pulsewidth. Models developed up to know had some restrictions in one or more of this parameters which made them incompatible with waveform modeling for high altitude or beamwidth limited altimetry remote sensing.

In fact the proposed models have been implemented and tested and provided simulations demonstrate that equations **3.3.4.6** and **3.3.3.6** are not sensitive with the variation of the pointing angle. The only criterion to take into account is a thresholding selection of the appropriate equation, according to considerations made in section **2.4.D.3**.

Nowadays the evaluation of the performance of models on which is based the *Cassini* PAD system has shown its capability to fit the compressed burst receives from the *Cassini* radar for very different fly-by's and spacecraft attitudes and have allowed to obtain very accurate topographic profiles Titan.

Another improvement of the present model is the possibility to work with analytical models rather than numerical solutions which allows performing a Maximum Likelihood Estimation in order to retrieve statistical information about key parameters of the surface of Titan.

As a result of this, we are able of distinguish the difference between height anomalies due to noise peak and a change in real topography. In fact by analyzing the MLE errors it is possible to mark the anomalous pulses and correct the corresponding time delay estimation in post-processing analysis (when anomalies causes are well understood).

Actual capabilities could be undoubtedly expanded by future system's evolutions since it is not possible yet to identify the real nature of some anomalies such as those explained in section **2.4.D.8**, although it is thought that the nature of double peaks can be related to the speckle distribution

The PAD system is currently in charge of producing standard altimetric *Cassini* products (Altimeter Burst Data records, ABDR) to be archived in PDS nodes. Up to now

the *Cassini* radar operated during several Titan's fly-bys, in addition to the first one done for testing purposes (Ta).

Among these, the high resolution altimetric data was available in most of them and have been processed by the PAD system. The measurements were also made by the spacecraft on the T7 fly-by in September 2005, but the data were lost due to an on-board recorder anomaly.

In next table are summarized the main statistical parameters of the retrieved topographic information:

Pass	Version	Date	# samples	Latitude [°] (start/stop)	Longitude [°] (start/stop)	Height [m]				Slope [m/Km]
						Min.	Max.	Mean	Std	
Ta	Run 6	2004-10-26	458	29.59/22.74	-9.73/-1.51	-158	397	99	65	-0.2
T3-in	run 6	2005-02-15	129	7.91/11.73	-140.61/-133.81	60	338	225	63	-0.9
T3-out			162	14.72/11.03	-2.83/5.91	-330	159	-75	104	1.9
T8-in	run 4	2005-10-28	165	-3.61/0.14	-178.07/178.51	-708	276	102	82	2.1
T8-out			577	-0.79/0.13	51.06/24.92	-840	1398	254	362	3.2
T13	run 2	2006-04-30	268	-0.04/-1.51	-165.63/178.21	-280	48	-106	79	2.0
T16-in	run 2	2006-07-21	648	12.20/29.18	-154.73/-155.84	42	607	270	91	-0.3
T16-out			238	20.77/12.23	25.27/24.77	-543	-79	-245	97	0.8
T19-in	run2	2006-10-09	432	32.74/46.38	-140.80/-135.43	-376	301	-47	155	-0.8
T19-out			479	-1.00/-17.35	29.30/32.55	-656	362	-87	135	0.1
T21	run 2	2006-12-12	444	-14.45/-27.31	57.04/49.23	-237	142	-22	73	-0.3
T23-in	run 2	2007-01-13	685	53.56/62.63	-119.58/-91.89	-861	141	-241	217	-0.7
T23-out			202	-28.01/-34.85	33.24/37.74	-57	288	126	93	0.9
T25	run 1	2007-02-22	57	-35.00/-30.8	-39.50/-38.13	-17	155	55	40	0.3
T28-in	run 1	2007-04-10	853	-26.49/-11.04	-33.30/-27.96	-166	507	83	117	-0.5
T28-out			395	55.07/48.29	125.63/133.19	-437	-213	-291	37	-0.1
T29-in	run 1	2007-04-26	490	-19.26/-4.09	-28.98/-25.24	-209	646	137	167	-0.5
T29-out			161	-49.42/41.44	137.06/141.93	-373	67	-170	101	0.1
T30-in	run 1	2007-05-12	2873	-11.16/68.57	-27.63/1.14	-983	388	99	242	-0.2
T30-out			566	68.62/25.55	1.22/147.82	-889	413	-296	177	-0.1

BIBLIOGRAPHY

[1] R. K. Moore and C. S. Williams, Jr., "*Radar terrain at near vertical incidence*", *Proc*. IRE, vol. 45, pp. 228-238, Feb 1957.

[2] J. K. Schindler, "*Electromagnetic scattering phenomena associated with extended surfaces*," *IEEE Internatl*. *Conv*. Rec., vol. 15. part 2, pp. 136-149, 1967.

[3] L. S. Miller and G. S. Hayne, "*System study of the geodetic altimeter concept*" final rept. on NASA Contract No. NAS6-1829. Research Triangle Institute, March 1971.

[4] Newkirk, M.H., Brown, G.S, "*Issues related to waveform computations for radar altimeter applications*", Antennas and Propagation, IEEE Transactions on, Vol. 40, Issue 12, Dec. 1992, pp. 1478-1488.

[5] Abramowitz, M., Stegum, IA, Eds., "*Handbook of Mathematical Functions*", New York: Dover Publications, 1972.

[6] Bender, C.M., Orzag, S.A., "*Advanced Mathematical Methods for Scientists and Engineers*", New York: Mcgraw-Hill, 1978.

[7] Brown, G.S, "*A useful approximation for the flat surface impulse response*", Antennas and Propagation, IEEE Transactions on, Vol. 37, Issue 6, Jun. 1989, pp. 764-767.

[8] Brown, G.S, "*The average impulse response of a rough surface and its applications*", Antennas and Propagation, IEEE Transactions on [legacy, pre-1988], Vol. 25, Issue 1, Jan. 1977, pp. 67-74.

[9] Montefredini, E., Morelli, F., Picardi, G., Seu, R., "*A non-coherent surface backscattering model for radar observation of planetary bodies and its application to Cassini radar altimeter*", Planet. Space Sci., Vol. 43, No. 12, 1995, pp. 1567-1577.

[10] A. Van Trees, "*Detection estimation and modulation theory*" (part I), John Wiley, 1968.

[11] G. Alberti, L. Festa, C. Papa, G. Vingione, "*A Waveform Model for Near-nadir Radar Altimetry applied to the Cassini Mission to Titan*" CO.RI.S.T.A. Consortium of Research on Advanced Remote Sensing Systems, Naples, Italy.

Alberti G., Papa C., Catallo C., Spataro F., Flamini E., Callahan P. S., Gim Y., Walls S., Del Marmo P. P., Picardi G., Seu R., Orosei R., "Cassini Altimetric Data Processing".

Bryan Stiles, "*Cassini Radar Burst Ordered Data Products SIS*", *Cassini* Radar Instrument Team, Jet Propulsion Laboratory California Institute of Technology NASA, September 27, 2005

G. Alberti, G. Vingione, "*PAD Tools Detailed Processing Model*", *Cassini* Radar Processing Altimetric Data (PAD), CO.RI.S.T.A. Consortium of Research on Advanced Remote Sensing Systems, Naples, Italy.

G. Vingione, "*Radar Altimeter General Waveform Model and Its Application to Cassini Mission*", Department of Aerospace and Mechanical Engineering, Second University of Naples, Aversa, Italy November 2007.

NASA – Home: www.nasa.gov